Renormalization Group Approach to Hot and Dense Matter

Vom Fachbereich Physik
der Technischen Universität Darmstadt

zur Erlangung des Grades
eines Doktors der Naturwissenschaften
(Dr. rer. nat.)

genehmigte

Dissertation

von
Dipl.-Phys. Borislav Stokić
aus Olten (Schweiz)

Referent: Prof. Dr. B. Friman
Korreferent: Prof. Dr. J. Wambach

Tag der Einreichung: 01.12.2008
Tag der Prüfung: 22.12.2008

Darmstadt 2008
D17

Посвећено мојим драгим родитељима

Abstract

The chiral quark-meson model, being an effective low-energy realization for spontaneous chiral symmetry breaking of QCD at intermediate momentum scales, is often used to study various properties of strongly interacting matter. In this thesis we employ this model to investigate the critical behavior of hot and dense matter with two degenerate light flavors. Using the method of the functional renormalization group, we derive the flow equation for the scale dependent thermodynamic potential at finite temperature and chemical potential in the presence of an explicit symmetry breaking term. We explore the scaling behavior of various observables and confront our results with the Widom-Griffiths form of the equation of state. The focus of our study are especially the scaling properties of the order parameter and its transverse and longitudinal susceptibilities for small, but finite values of the external field when approaching the critical point from the symmetric as well as from the broken phase.

We also explore the thermodynamics and the phase structure of strongly interacting hot and dense matter. Apart from the renormalization group formalism, here we also employ the mean field approximation in order to investigate thermodynamic observables sensitive to the phase transition. As an effective model, we use the Polyakov loop extended two flavor chiral quark-meson model in order to connect the chiral and confining properties of QCD. The gluon dynamics is included by coupling quarks with the Polyakov loop and by introducing an effective Polyakov loop potential. We discuss the properties of the net quark number fluctuations in the vicinity of the QCD chiral phase transition. Our main focus of exploration is the ratio of the fourth- to second- order cumulants (kurtosis) and the compressibility. The sensitivity of both observables to the values of the pion mass near the chiral phase transition is also discussed. Within the renormalization group approach, the thermodynamics and the phase structure of the Polyakov loop extended quark-meson model is the main focus of our study. We propose an extended truncation of the effective average action with quarks coupled to background gluonic fields and derive

the corresponding flow equation for the scale dependent thermodynamic potential.

A full RG treatment of all fields is very complex and thus while solving the flow equation for the quark and meson fields we use the mean field results obtained previously for the Polyakov loop and its conjugate. Thus, within this scheme we determine the phase structure of the model and employ the Taylor expansion coefficients of the thermodynamic pressure in order to locate the position of the critical end point in the phase diagram. Due to the inclusion of fluctuations, we observe a change of the phase diagram compared to that obtained in the mean field approximation. In the end we also briefly discuss the cutoff effect present in the renormalization group method.

Zusammenfassung

Das chirale Quark-Meson Modell, das eine effektive Realisierung der spontan gebrochenen chiralen Symmetrie der QCD bei kleinen Energien darstellt, wird zur Untersuchung verschiedener Eigenschaften stark wechselwirkender Materie verwendet. In dieser Arbeit benutzen wir dieses Modell um das kritische Verhalten heißer und dichter Materie mit zwei Flavors zu untersuchen. Mit Hilfe der funktionalen Renormierungsgruppe haben wir die Flußgleichung für das effektive thermodynamische Potenzial sowohl bei endlicher Temperatur und Dichte als auch in der Präsenz eines explizit symmetriebrechenden Terms hergeleitet. Wir untersuchen das Skalenverhalten verschiedener Observablen und vergleichen unsere Ergebnisse mit der Widom-Griffiths Zustandsgleichung. Im Mittelpunkt unserer Untersuchung steht das Skalenverhalten des Ordnungsparameters und seiner transversalen und longitudinalen Suszeptibilität bei kleinen Werten des externen Feldes während man sich dem kritischen Punkt sowohl von der symmetrischen als auch von der symmetriegebrochenen Seite annähert.

Außerdem untersuchen wir die Thermodynamik und die Phasenstruktur heißer und dichter stark wechselwirkender Materie. In diesem Fall verwenden wir neben der RG Methode auch die Mean-Field Näherung um thermodynamische Observablen am Phasenübergang zu untersuchen. Als das effektive Modell benutzen wir das Polyakov Loop erweiterte Quark-Meson Modell um die chiralen und Confinement-Eigenschaften der QCD zu verknüpfen. Das Polyakov Loop Potenzial wird eingeführt, und die Quarks werden mit dem Polyakov Loop gekoppelt um einen entsprechenden gluonischen Hintergrund zu schaffen. Wir erörtern die Eigenschaften der Quark Fluktuationen in der Nähe des chiralen Phasenübergangs. Der Schwerpunkt unserer Untersuchung liegt auf dem Verhältnis des vierten und zweiten Kumulants (auch Kurtosis genannt) und auf der Kompressibilität. Weiterhin wird die Abhängigkeit der beiden Observablen von der Masse des Pion-Feldes in der Nähe des chiralen Phasenübergangs diskutiert. Im Rahmen des Renormierungsgruppenzugangs ist die Thermodynamik und die Phasenstruktur des Polyakov Loop erweiterten Quark-

Meson Modells im Mittelpunkt unserer Studie. Wir führen eine erweiterte Trunkierung der effektiven gemittelten Wirkung ein, in der Quarks mit einem gluonischen Hintergrund gekoppelt sind, und leiten die entsprechende Flußgleichung für das effektive thermodynamische Potenzial her.

Aufgrund der großen Komplexität, die einen vollständigen Renormierungsgruppenzugang erheblich erschwert, benutzen wir für den Polyakov Loop die Ergebnisse die wir mittels der Mean-Field Näherung erhalten haben, um die Flußgleichung lösen zu können. Infolgedessen wird durch dieses Schema die Phasenstruktur des Modells bestimmt, und mit Hilfe der Taylor-Entwicklung des thermodynamischen Drucks der kritische Endpunkt im Phasendiagramm lokalisiert. Aufgrund der Einbeziehung von Fluktuationen bemerken wir eine Änderung des Phasendiagramms im Vergleich zu dem Phasendiagramm, das wir früher mittels der Mean-Field Näherung berechnet haben. Letztendlich wird auch der Effekt, verursacht durch den Abschneideparameter, der in jedem Renormierungsgruppenzugang zu finden ist, kurz untersucht.

Contents

Chapter 1

Introduction

The quest for understanding the underlying laws of Nature has always been present in physics. Altough this is a very difficult and formidable task, without any warranty to find (and maybe to comprehend) all the answers, physicists have been working industriously over the last centuries in order to find the key to how and why various phenomena in Nature occur. Theorists as well as experimentalists have furnished tools, techniques and data to improve and extend our understanding of Nature. In the last century, physicists were especially successful in uncovering many secrets of Nature, whereas by saying this we do not want to depreciate the work of their predecessors in any way.

What is so special about the achievements in the 20th century physics and what topics still arouse our interest today? First, during the last 100 years, the special theory of relativity and quantum mechanics, apart from bringing a groundbreaking novelty in the perception of space and time, also had an immense impact on theoretical physics, and led to the formulation of quantum field theories. In the aftermath of an amazing interplay between physics and mathematics, quantum gauge theories and the general theory of relativity came to light. The important concepts of symmetry and later, unification entered physics and the quest for the connection between the four fundamental interactions (two of them, the electromagnetic force and gravity, were known before 1901) began. All these efforts finally resulted in what we know today as the *Standard Model* of particle physics that represents a theory of the electromagnetic, weak and strong interaction [1].

The wish to unravel Nature's still unsolved puzzles has never diminished, and the possibilities open today are probably unmatched due to powerful computers and laboratory equipment available. One interaction in particular, namely the strong

[1] For reasons that we do not yet understand, gravity does not fit into the framework of quantum field theories and hence it is not a part of the Standard Model.

interaction, was in the last fifty years a highly investigated area in physics and still is a subject of great interest. It is believed that in the early Universe, i.e. at the time of the Big Bang, primordial matter built of elementary particles (quarks) and carriers of the strong interaction (gluons) existed. During the expansion, the Universe cooled down and various phase transitions took place. Today, we have evidence for what happened at that time through the cosmic microwave background[2] (CMB). By measuring the temperature anisotropy of the CMB, the Wilkinson Microwave Anisotropy Probe (WMAP) mission was able to map out the 13.7 billion year old temperature fluctuations of the Universe. An analysis of the WMAP connects these fluctuations to inhomogeneities of the matter in the early Universe some 300000 years after the Big Bang.

The thermal history of the Universe can be roughly divided into several, important phases [1]

- Early epoch ($T > 1$ GeV)
- Quark gluon plasma ($T > 170$ MeV)
- QCD phase transition ($T \sim 170$ MeV)
- Neutrino decoupling ($T \sim 1$ MeV)
- Recombination ($T \sim 4000$ K)
- Photon decoupling ($T \sim 2700$ K)
- Cosmic background radiation ($T \ll 2700$ K)

One of the most interesting stages in the evolution of the Universe is the quark gluon plasma stage where the main components are the mediators of the strong and electromagnetic interaction as well as quarks and leptons. The quarks and gluons form the so-called quark gluon plasma. It is believed that this stage in the thermal history of the Universe can be simulated and investigated in relativistic heavy ion collisions. Especially the quest for a new state of matter conjectured to be built out of quarks and gluons and the possible existence of a (tri)critical endpoint in the phase diagram of strongly interacting matter have attracted a lot of interest in recent years.

Many theoretical approaches have been developed, ranging from solutions of QCD on the lattice (lattice gauge theory) to phenomenological models in order to provide answers to the questions concerning the physics of hot and dense matter. All these

[2] Apart from the cosmic microwave background, there are also two more statements usually used to underpin the Big Bang theory, namely the Hubble's law and the scenario of primordial nucelosynthesis that predicts a mass fraction of ^{4}He to the total baryon masses.

studies should also contribute to a better understanding of the nature of the strong interaction.

Apart from various theoretical studies, there are also quite a few experiments that have already been undertaken or are planned in the near future. These experimental investigations are expected to be able to access different regions of the phase diagram we are interested in. Several projects have been launched (or are under development, such as the future Facility for Antiproton and Ion Research (FAIR) at GSI) to fulfil this important and foremost interesting task.

For instance, the famous Large Hadron Collider (LHC) at CERN represents a project which is expected to provide valuable insight into the phase structure of hot and dense matter and information on the properties of nuclear matter under extreme conditions[3]. It is expected that from the experiments that are going to be performed one can learn more about nuclear matter under extreme conditions.

Another issue that is intimately related to the equation of state of hot and dense matter is the existence of the critical endpoint, and if it exists, also its location. The existence of the critical endpoint in the phase diagram of strongly interacting matter is still under debate [2]. This critical endpoint of QCD has attracted a lot of attention among physicists because if it exists, it is a landmark of the QCD phase diagram, and because of the possibility to explore the critical endpoint in experiments[4]. Thus, the character of this critical point can reveal the nature of the phase transitions in nuclear matter under extreme conditions.

However, this is a subtle issue since the order of the phase transition is not unique and it depends on the current quark masses and also on the number of degrees of freedom (color and flavor). Apparently the phase diagram of hot and dense matter has a rich structure with different phases depending on the temperature and chemical potential. Some progress has already been made concerning the exploration of the phase diagram. In experiments done at the Relativistic Heavy Ion Collider (RHIC) at BNL and at the Super Proton Synchrotron (SPS) at CERN some regions of high temperatures and densities have been successfully reached and investigated. These results are of utmost importance for future, experimental and theoretical, studies. However, here one has to be careful since, the heavy ion experiments also have their limitations. Due to the finite time and volume of the ultrarelativistic heavy ion collisions the hot matter created in the collisions may not reach thermal equilibrium (see e.g. [4] and references therein). As a consequence, this complicates the analysis of different regions of the phase diagram. Thus, altough we have a

[3]Being the worlds largest particle accelerator, there are quite a few experiments to be undertaken at LHC. One expects to get answers to various questions and puzzles, in the first place about the Higgs boson, the nature of dark matter and dark energy, about supersymmetry and possible extra dimensions.

[4]One speaks of the critical endpoint as the point in a phase diagram where the line of the first order phase transition ends. On the other hand, the tricritical point marks the transition from a first order phase transition to the one of second order.

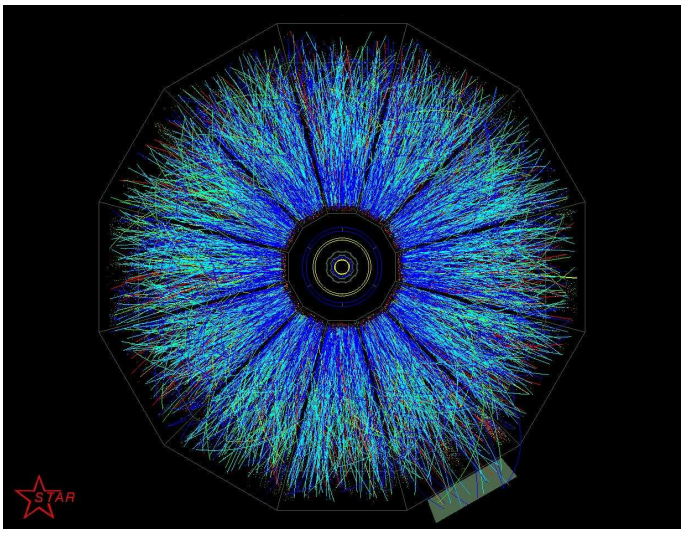

Figure 1.1: First gold beam-beam collision events at RHIC at 100+100 GeV/c per beam recorded by STAR [3].

theory that describes the strong interaction, as we will show later in Chapter 2, our present knowledge about the thermodynamics and phase structure of strongly interacting matter under extreme conditions (i.e. high temperatures and densities) is still inadequate and incomplete.

One of the reasons for this is the quite complex nature of strongly interacting matter at high temperatures and densities. Due to the pronounced nonperturbative nature of strong interactions at certain length scales, calculations within some theoretical methods and techniques (e.g. perturbation theory), are not feasible. Lattice gauge theories, using Monte Carlo techniques, represent one possible choice to tackle the problem of nonperturbative effects, limited to small baryon densities, that are beyond the scope of perturbation theory. However, there is another promising approach that is able to cope with the problems that arise in investigating strong interactions.

The method of the renormalization group poses a very promising tool in addressing phenomena that occur in exploring the thermodynamics and the phase structure of strongly interacting matter. This approach has already shown significant success in various areas of physics. The renormalization group method was pioneered by Murray Gell-Mann and Francis E. Low in their seminal paper [7] discussing the asymptotic behavior of Green's functions in quantum electrodynamics. Later, Kenneth G. Wilson (who was a PhD student of Murray Gell-Mann) applied the idea of the renormalization group to critical phenomena and received the Nobel Prize in physics in 1982. Since then, this method has been successfully applied in the theory of critical phenomena and phase transitions. Within these investigations one has

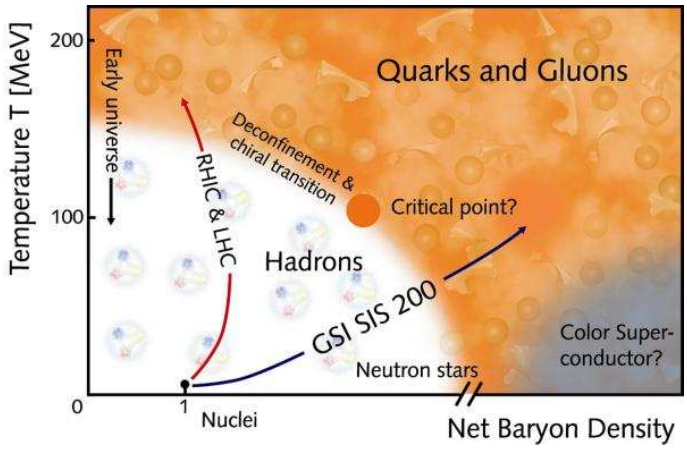

Figure 1.2: A schematic phase diagram of QCD [6].

focused on universal quantities such as critical exponents, for instance.

In the last fifteen years, a "reformulated" version of the renormalization group approach appeared, combining the functional method used in quantum field theory with Wilson's ideas [34, 35, 36, 37, 38]. Within this approach also various non-universal quantities (such as e.g. susceptibilities) can be calculated. The method of the functional renormalization group is based on the effective average action in close analogy to the standard effective action. The only difference is that an infrared cutoff is implemented in the functional integral. In other words, fields that are present in some theory are separated into high- and low-momentum modes, in close analogy with Wilson's coarse graining approach. As a consequence, short range fluctuations are integrated out of the problem. We discuss the basic ideas and features of the functional renormalization group in detail in Chapter 3.

This powerful method has also been applied to the physics of strongly interacting many-body systems where different phase transitions occur. In order to describe them, the renormalization group approach seems to be a natural choice. The successful use of the method in statistical physics where various scaling relations and critical indices have been calculated opens the perspective for a functional renormalization group approach to critical phenomena and (possible) phase transitions in strongly interacting hot and dense matter.

Overview of the thesis

We start our study by presenting the theory and models relevant for our investigation. An overview concerning theoretical foundations and effective models used to describe the physics we are interested in, is presented in Chapter 2. Here we give a short summary of the main and most important features of strong interactions. We

then continue by defining the effective models we use in our study, the chiral quark-meson model and the Polyakov loop extended quark-meson model. The motivation for using these models is also discussed as well as their main characteristics.

In Chapter 3 we introduce and discuss the renormalization group method. As this will be our main tool throughout the thesis, we focus on its main features and characteristics. We also give a short overview of advantages of the renormalization group method. In particular, we introduce and define the functional renormalization group method. The most important part, namely the flow equation for the effective average action is derived and its main features are explained.

First results of our study we present in Chapter 4. Here we investigate, within the functional renormalization group method, the critical behavior of the chiral quark-meson model. The main focus of our study in this chapter is the critical scaling behavior of the order parameter, its transverse and longitudinal susceptibilities as well as the correlation lengths near the chiral phase transition. Furthermore, we explore the scaling properties of these observables at a non-zero external field when approaching the critical point both, from the symmetric and the broken phase. As a tool throughout this chapter we employ the flow equation for the scale dependent thermodynamic potential at finite temperature and density in the presence of an external magnetic field.

In Chapter 5 are presented results regarding hot and dense matter. Here we investigate the thermodynamics and the phase structure of both, the chiral quark-meson model and the Polyakov loop extended quark-meson model. The analysis is based on the mean field approximation as well as on the functional renormalization group approach. Especially, we discuss the influence of quantum fluctuations and of the background gluon field on the properties of the net quark number density fluctuations and their higher moments. The flow equation for the scale dependent thermodynamic potential derived in Chapter 4 is extended by introducing a new truncation of an effective action with quarks coupled to gluonic background fields.

In Chapter 6 we summarize the results presented in this thesis and conclude with an outlook on work in progress as well as on further envisaged research.

Chapter 2

Physics of strongly interacting matter

The properties and behavior of strongly interacting matter pose a vast and very intriguing research area in physics for both, theoreticians and experimentalists today. Unsolved puzzles, still present in the Standard Model of particle physics push forward the fundamental research and give rise to various mathematical models and concepts. The purely academic interest (that is fortunately in science, especially in physics, always present), gave rise to quite a few theoretical and phenomenological models developed during the years to venture on a difficult task of understanding the laws of Nature i.e. the principles and features of the Standard Model and also strong interactions, being a part of the Model.

The physics of the early universe, new states of matter, astrophysics of neutron stars, and heavy ion collisions represent some of the topics that have attracted an immense interest during recent years. Especially, the QCD transition in the early universe represents a topic that has triggered a strong interest in the properties of strongly interacting matter at high temperatures and/or densities. One of the primary objectives in these investigations (theoretical/phenomenological and experimental) is to explore and map out the accessible region of the QCD phase diagram. It has also been conjectured that a new phase of matter, dubbed the quark-gluon plasma, might be experimentally produced in relativistic heavy-ion collisions. This phase should represent a chirally restored and confined phase where the system ends up after undergoing a phase transition starting from the hadronic phase. Further, new phases are expected at low temperatures and high densities, such as the two-flavor or color-flavor locked color superconducting phase. One expects that a better understanding of the properties of QCD phase transition will enable us to have a better overall picture of QCD itself. In light of these investigations, one expects that especially the non-perturbative properties of QCD and the chiral symmetry could be better understood. Also different issues concerning astrophysical and cosmological

phenomena could be addressed and answered.

There is, however, one subject (or better to say, a whole research area) that represents the most distinct challenge in the research concerning the QCD phase diagram and its main features. The topic that puzzles physicists over years is the existence of the critical endpoint (CEP) in the QCD phase diagram. Consequently, if there is a CEP, the next logical question to be answered is: "Where is this CEP ?". The search for the position of the CEP represents one of the most interesting and challenging topics in hot and dense QCD nowadays. In the case that the location of the CEP is experimentally accessible it might be discovered at the Relativistic Heavy Ion Collider (RHIC) at BNL, the Super Proton Synchrotron (SPS), Large Hadron Collider (LHC) at CERN or the future Facility for Antiproton and Ion Research (FAIR) at GSI. One hopes that by studying the so called event-by-event fluctuations in heavy-ion collisions at these facilities, various information related to the phase transition could be extracted and understood.

All these problems and issues mentioned above, clearly justify todays increased interest in the physics of strongly interacting matter. An elaborative investigation of QCD with the combination of various methods and techniques, will give a more transparent picture of the phase structure and thermodynamics of strongly interacting matter.

In this chapter we will give a short overview of the most important features of QCD, a theory that is believed to govern strong interactions. Further, we will introduce an effective model for low-energy QCD, the so called chiral quark-meson model and we also extend this model by including new degrees of freedom. Here, these new degrees of freedom are the gluons coupled via the Polyakov loop to the quarks. This enables us to study the chiral symmetry breaking and deconfinement effects in a simple framework and our study is expected to provide input for the phenomenology of relativistic heavy-ion collisions.

2.1 Quantum chromodynamics

One of the four fundamental interactions in nature is the strong interaction with quarks and gluons as the elementary degrees of freedom. The relativistic quantum field theory, developed to describe the interaction of a massive fermionic field with massless bosonic gauge field is known as *Quantum Chromodynamics* (QCD) with the color $SU(3)$ group being the relevant symmetry group for QCD[1]. This theory is an example of *non-Abelian* gauge theories[2].

[1]For a general non-Abelian gauge theory, $SU(N)$ represents the relevant symmetry group. This is the so called *special unitary group*. Elements of the $SU(N)$ group are $N \times N$ unitary matrices $\mathcal{U} \in SU(N)$ with the property $\det \mathcal{U} = 1$.

[2]The theory of weak interactions that describes among others, the well known nuclear β-decay process: $n \to p + e^- + \bar{\nu}_e$, is another example of a non-Abelian gauge theory with $SU(2)$ being

On the other hand, *Quantum Electrodynamics* (QED) is an *Abelian* gauge theory. It describes the interaction of electrons with photons and has been developed to describe the Compton effect, electron-electron scattering, pair creation and Bremsstrahlung, just to name a few. This quantum field theory is based on the $U(1)$ gauge group with the following local gauge transformation for the field $\psi(x)$

$$\psi(x) \rightarrow \psi^{'}(x) = e^{-i\alpha(x)}\psi(x)\,, \tag{2.1}$$

and for the electromagnetic field $A_\mu(x)$

$$A_\mu(x) \rightarrow A^{'}_\mu(x) = A_\mu(x) - \partial_\mu\alpha(x)\,, \tag{2.2}$$

that leave the QED Lagrangian invariant. Here, the local gauge transformation means that the phase factor $\alpha(x)$ is a function of spacetime (accordingly, for global symmetry transformation this factor is constant).

In the case of non-Abelian gauge theories there are also different gauge groups that leave the appropriate Lagrangian of the theory invariant. The difference between Abelian and non-Abelian gauge theories and the relevant symmetry group for strong interactions is discussed in the following part of this section.

According to the usual practice, we start with the Lagrangian of QCD, that is given in the following general form

$$\mathscr{L}_{\mathsf{qcd}} = \bar{\psi}\left(i\not{D} - \hat{m}\right)\psi - \frac{1}{4}G^a_{\mu\nu}G^{\mu\nu}_a. \tag{2.3}$$

The compact and rather elegant form of Eq. (2.3) should not give the impression that QCD represents a finished and fully understood theory.

One of the elementary constituents of the QCD, the quark field, is represented with ψ and carries $N_c = 3$ color and $N_f = 6$ flavor (u, d, s, c, b, t) degrees of freedom. Generally speaking, quarks are fermions and classified as spin-1/2 particles. The corresponding quark mass matrix in flavor space is given by

$$\hat{m} = \mathrm{diag}_f\left(m_u, m_d, m_s, m_c, m_b, m_t\right). \tag{2.4}$$

The relevant symmetry group for QCD is the $SU_c(3)$ group with a set of eight linearly independent 3×3 matrices. These matrices (known as Gell-Mann matrices) are generators of the $SU_c(3)$. Vector fields belonging to the adjoint representation of $SU_c(3)$ gauge group are gluons. The gluon field A^a_μ is related to the covariant derivative in Eq. (2.3) in the following way ($\not{D} = \gamma^\mu D_\mu$)

$$D_\mu = \partial_\mu - i\tilde{g}\frac{\lambda^a}{2}A^a_\mu, \tag{2.5}$$

the relevant symmetry group.

where $\tilde{g}$ is the QCD coupling constant and λ^a are the Gell-Mann matrices. Gluons represent an octet **8**, and mediate the strong interaction. The number of gluons is given by the dimension of the corresponding adjoint representation. For $SU_c(3)$ group the number of dimension is 3^2-1, thus there are 8 gluons present in QCD. Different then photons, that mediate the electromagnetic interaction and are uncharged, gluons do carry color charge and hence selfinteract. This is the most prominent feature that distinguishes Abelian from non-Abelian gauge theories. In QED there are no photon self-coupling terms (i.e. photons do not selfinteract) but in QCD one has three- and four-gluon vertices. The QCD Lagrangian given in Eq. (2.3) is invariant under local $SU_c(3)$ gauge transformations. The non-Abelian structure of the $SU_c(3)$ gauge group is encoded in the definition of the gluon field strength tensor $G^a_{\mu\nu}$ that reads

$$G^a_{\mu\nu} = \partial_\mu A^a_\nu - \partial_\nu A^a_\mu + \tilde{g} f^{abc} A^b_\mu A^c_\nu, \tag{2.6}$$

where f^{abc} is the antisymmetric structure constant of the $SU_c(3)$ gauge group. The appearance of an extra non-linear term in (2.6) causes the aforementioned gluon self interaction.

One of the most striking features of QCD is the *asymptotic freedom* [3]. For the discovery of asymptotic freedom in the theory of the strong interaction David J. Gross, H. David Politzer and Frank Wilczek received the Nobel Prize in physics in 2004. In order to shed some light on this issue, let us again make a comparison with QED. The strength of the electromagnetic interaction in QED is characterized by a coupling called the fine structure constant α_{qed} that has a numerical value of

$$\alpha_{qed} = 1/137.035999679(94). \tag{2.7}$$

This coupling constant is small, thus one can use, with high accuracy, perturbation theory in QED calculations. Theoretical predictions for the values of the anomalous magnetic moments of electron and muons agree with experiments within ten decimals. This prominent example is often used to stress the validity of quantum field theories.

However, in QCD the situation is different (here we mean the coupling, not the validity, altough the latter is also sometimes disputed). The strong interaction becomes weaker at short distances and quarks behave as free particles at very high momenta (short distances). Consequently, the strong coupling constant will increase

[3] Another prominent phenomenon of QCD is *confinement*. We will briefly address this issue in the following section.

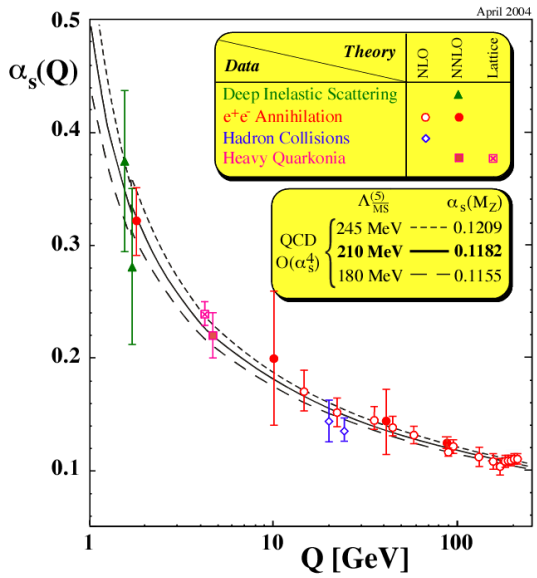

Figure 2.1: The QCD running coupling α_s [10].

with distance. In the leading order the QCD coupling[4] is given by [8, 9]

$$\alpha_s(Q^2) = \frac{\tilde{g}(Q^2)}{4\pi} = \frac{4\pi}{\beta_0 \log(Q^2/\Lambda^2_{qcd})}, \qquad \beta_0 = \left(\frac{11}{3}N_c - \frac{2}{3}N_f\right) \tag{2.8}$$

where $\Lambda_{qcd} \simeq 200$ MeV.

For very high momenta one has $Q^2 \to \infty$ and it follows directly from Eq. (2.8) that the QCD coupling α_s goes to zero. On the other hand, for temperatures $T \simeq \Lambda_{qcd}$ the system is strongly coupled and perturbative calculations are not feasible (one can not for instance describe hadrons with masses below 2 GeV i.e. their mass spectrum or scattering lengths by means of perturbative QCD). This actually means that with a decrease of the energy scale, the perturbation theory fails in giving an accurate and quantitative correct picture of low energy physics. Hence, in this regime non-perturbative effects are dominant and call for appropriate tools and techniques (or effective theory models) that can yield valid and reliable results. In the sections below we present an effective low-energy model, constructed in the

[4]Here we have to stress the fact that α_{qed} is also scale dependent. The one-loop beta-function (shows how a coupling parameter of some theory depends on the energy scale) in QED is given in terms of the fine structure constant α_{qed} as

$$\beta_{qed}(\alpha_{qed}) = \frac{2\alpha^2_{qed}}{3\pi} + \mathcal{O}(\alpha^3_{qed}).$$

expectation of being capable to incorporate some features of the strong interaction i.e. QCD. Further, in Chapter 3 we will introduce a technique that is able to cope with difficulties arising from non-perturbative effects.

2.2 The chiral quark-meson model

A chirally invariant model that describes the interaction of pions and nucleons was first introduced by Gell-Mann and Levy [11]. This model, at that time also known as the *linear sigma model*, was based on the assumption that chiral symmetry represents one of many QCD symmetries. Today we know that chiral symmetry, whose possible existence was indicated from the study of the nuclear beta decay, is an exact symmetry only in the limit of vanishing quark masses. In the light (up/down) sector the chiral symmetry can be considered to be an exact symmetry since one can treat up/down quarks as massless. However, once the strangeness is included the chiral symmetry becomes only an approximate symmetry due to the large mass of the strange quark. Still, chiral symmetry is of great importance in QCD since the low energy regime can be successfully described in terms of this symmetry. One of the most interesting issues regarding chiral symmetry is that it is not only broken spontaneously but also explicitly. This explicit symmetry breaking is due to the finite current quark masses that can be thought of as some external magnetic field. An important advantage that the linear sigma model incorporates is its renormalizability on the perturbative level. If one replaces nucleons by two lightest quarks, the linear-sigma model is the chiral *quark-meson model*.

Before we give a description of the model itself, let us first consider some important aspects of chiral symmetry. Chiral symmetry represents only an approximate (not exact!) symmetry of QCD and as we have already pointed out, this symmetry is exact only in the massles case i.e. for N_f massless fermions. To see what is actually going on, we follow a good theoretical tradition, and consider a simple model for free and massless fermions, described by the following Lagrangian

$$\mathscr{L}_{\mathsf{simple}} = \bar{\psi} i \partial\!\!\!/ \psi. \tag{2.9}$$

Now we can introduce the left-handed and right-handed fields (quarks) in the following way

$$\psi_L = \frac{1}{2}\left(1-\gamma_5\right)\psi, \qquad \psi_R = \frac{1}{2}\left(1+\gamma_5\right)\psi\,. \tag{2.10}$$

This transforms the Lagrangian (2.9) into

$$\mathscr{L}_{\mathsf{simple}} = \bar{\psi}_L i \partial\!\!\!/ \psi_L + \bar{\psi}_R i \partial\!\!\!/ \psi_R\,. \tag{2.11}$$

Having defined this simple Lagrangian, all what we need is a global symmetry transformation that will leave (2.9) i.e. (2.11) invariant. In the following we confine ourselves to the two-flavor case $N_f = 2$ in anticipation of the definition of the model

we introduce below. Thus, a global symmetry that leaves the Lagrangian (2.11) invariant[5] is

$$U_L(2) \times U_R(2)\,, \tag{2.12}$$

and represents left- and right-handed rotations in flavor space. This symmetry group can be further decomposed into

$$SU_L(2) \times SU_R(2) \times U_V(1) \times U_A(1)\,. \tag{2.13}$$

The $U_V(1)$ symmetry is related to the baryon number, whereas $U_A(1)$ does not represent a symmetry on a quantum level (this phenomenon is in the literature know as the *axial anomaly*). The Lagrangian (2.11) with massless quarks is invariant under the $SU_L(2) \times SU_R(2)$ chiral rotation. However, the chiral condensate, $\langle \bar{q}q \rangle$ defined by

$$\langle \bar{q}q \rangle = \langle \bar{q}_L q_R \rangle + \langle \bar{q}_R q_L \rangle\,, \tag{2.14}$$

is not invariant under the same symmetry transformation. Consequently, the thermal expectation value of the chiral condensate $\langle \bar{q}q \rangle$ is considered as an order parameter for the chiral symmetry breaking. Here, one says that the $SU_L(2) \times SU_R(2)$ global symmetry group is spontaneously broken in a QCD vacuum. However, there is one symmetry remaining in vacuum, namely the symmetry group $SU_L(2) \times SU_R(2)$ is broken spontaneously to $SU_V(2)$ the so called vector symmetry. Let us now define the vector transformation as

$$SU_V(2): \quad \psi \longrightarrow e^{-i\frac{\vec{\tau}}{2}\vec{\Theta}}\psi \tag{2.15}$$

and also the vector-axial transformation

$$SU_A(2): \quad \psi \longrightarrow e^{-i\gamma_5\frac{\vec{\tau}}{2}\vec{\Theta}}\psi, \tag{2.16}$$

where $\vec{\tau}$ are Pauli matrices and $\vec{\Theta}$ represents a constant vector used to specify the transformation angle. The set of transformations rules given above for ψ (and $\bar{\psi}$ accordingly) can be Taylor expanded

$$e^{-i\frac{\vec{\tau}}{2}\vec{\Theta}} \simeq 1 - i\frac{\vec{\tau}}{2}\vec{\Theta}\,, \qquad e^{-i\gamma_5\frac{\vec{\tau}}{2}\vec{\Theta}} \simeq 1 - i\gamma_5\frac{\vec{\tau}}{2}\vec{\Theta} \tag{2.17}$$

and afterwards it is straightforward to check that $\mathscr{L}_{\mathsf{simple}}$ is indeed invariant under global vector and axial-vector transformation. After introducing a mass term into (2.9), the $\mathscr{L}_{\mathsf{simple}}$ is not invariant under axial-vector transformation $SU_A(2)$ anymore, thus $SU_A(2)$ is not an exact symmetry for finite masses. However, in QCD the masses of lightest quarks are much smaller than Λ_{qcd} and hence $SU_A(2)$ can be considered as an approximate symmetry of QCD. In this context, the chiral symmetry is then referred to as the $SU_V(2) \times SU_A(2)$ symmetry.

[5] We could have included the gluonic part in the Lagrangian (2.11) as well since it is also invariant under the global symmetry group (2.13).

We can now proceed and introduce a QCD-inspired effective theory model. The chiral quark-meson model represents an effective low-energy realization for dynamical spontaneous chiral symmetry breaking at the intermediate momentum scale $4\pi f_\pi \approx 1$ GeV. One can view this model as an effective model of QCD, where the gluon degrees of freedom have been integrated out. As a consequence, this model is not suitable for describing the confinement-deconfinement phase transition. However, we will try to circumvent this drawback in the following section, by including some aspects of gluon dynamics.

The Lagrangian density of the chiral quark-meson model is given by

$$\mathscr{L}_{\mathsf{qm}} = \frac{1}{2}\left(\partial_\mu \phi\right)^2 + \bar{q} i \partial\!\!\!/ q - g \bar{q} M q - U(\sigma, \vec{\pi}), \tag{2.18}$$

where the $O(4)$ representation of the meson fields is $\phi = (\sigma, \vec{\pi})$. The corresponding $SU(2)_L \times SU(2)_R$ chiral representation is given by

$$M = \sigma + i\vec{\tau} \cdot \vec{\pi}\gamma_5 \,, \tag{2.19}$$

where the pion field $\vec{\pi}$ is a triplet **3** belonging to the adjoint representation of $SU(2)$

$$\vec{\pi} = (\pi^0, \pi^+, \pi^-) \,. \tag{2.20}$$

In this way one has $N_f^2 = 4$ mesonic degrees of freedom coupled to $N_f = 2$ flavors of constituent quarks q. The mesonic field σ is a scalar and $\vec{\pi}$ is an isovector i.e.

$$\sigma = \bar{\psi}\psi \,, \qquad \vec{\pi} = i\bar{\psi}\vec{\tau}\gamma_5\psi \,. \tag{2.21}$$

Since we are only interested in the chiral properties of the model, we consider the simplest mesons of the model i.e. σ and $\vec{\pi}$. In order to obtain a realistic description of scattering processes, one would need to include ρ and a_1 mesons in the chiral quark-meson model as well.

The mesonic potential of the model $U(\sigma, \vec{\pi})$ is given by

$$U(\sigma, \vec{\pi}) = \frac{1}{2} m^2 \phi^2 + \frac{\lambda}{4}\phi^4 - c\sigma. \tag{2.22}$$

For $m^2 > 0$ and without an explicit symmetry breaking term ($c = 0$), the potential (2.22) has a minimum at $\sigma = 0$ and $\vec{\pi} = 0$. In the vacuum, the $O(4)$ symmetry of the Lagrangian (2.18) is broken spontaneously to $O(3)$ for $m^2 < 0$. This leads to a nonvanishing scalar condensate $\langle\sigma\rangle = f_\pi$. In the case of spontaneously broken chiral symmetry, pions are considered to be the Goldstone bosons. Here, one has to be careful, since Goldstone bosons are massless, while pion has a small, but still finite mass ($m_\pi \simeq 138$ MeV). Nevertheless, the interpretation of pions as Goldston bosons is reasonable, since the chiral symmetry is not an exact symmetry and the pion mass is small compared to other particles in QCD. The small pion mass reflects

the explicit symmetry breaking through the two lightest quarks i.e. up and down quark.

Here we want to stress the fact that the scalar condensate is closely related to the quark condensate $\langle\bar{q}q\rangle$ and for small values of $\langle\sigma\rangle$ the two condensates are proportional in the chiral limit. At this point it is also interesting to emphasize that chiral symmetry resembles a typical spin system known from statistical physics.

The explicit symmetry breaking term $c\sigma$ in the potential provides the mass m_π to the pions. At the tree level, the expression

$$c_0 = f_\pi m_\pi^2 \tag{2.23}$$

yields the physical pion mass in vacuum. For convenience we introduce a dimensionless parameter

$$h = \frac{c}{c_0} \tag{2.24}$$

as a measure for for the strength of the symmetry breaking term. The physical value at tree level is $h = 1$. We will make use of this parameter later in Chapter 4. In a medium, the chiral symmetry of the Lagrangian is restored leading to a vanishing chiral condensate at some critical temperature and/or density.

Closely connected with the chiral quark-meson model are the following, very important and useful relations. However, we refrain from going into details concerning their derivation and just quote them. The origin of their importance lies in the fact that knowing them, we can connect the parameters of the model with actual physical observables. The first relation, that relates the constituent quark mass m_q to the pion decay constant f_π is the Goldberger-Treiman relation

$$g_A m_q = g f_\pi, \tag{2.25}$$

where g is the Yukawa coupling and $g_A \simeq 1.25$. In other words, this relation connects the minimum of the mesonic potential with f_π. On the other hand the Gell-Mann-Oakes-Renner relation is given by

$$m_\pi^2 f_\pi^2 = \frac{1}{2}\left(m_u + m_d\right)\langle\bar{q}q\rangle = \tilde{m}_c\langle\bar{q}q\rangle. \tag{2.26}$$

Here we can relate the pion mass m_π to the chiral condensate $\langle\bar{q}q\rangle$ and the current quark mass $\tilde{m}_c$.

2.3 The Polyakov quark-meson model

As we have already mentioned in the previous section, the chiral quark-meson model is often used as an effective realization of the low-energy sector of QCD, which belongs to the $O(4)$ universality class. It should however be emphasized that the low

energy properties of QCD are captured only incompletely since confinement effects are not properly taken into account. Clearly, any description of the QCD chiral phase transition within the quark-meson model also has some drawbacks and limitations. Furthermore, due to the replacement of the local $SU(N_c)$ gauge invariance by a global symmetry one can not address the deconfinement phenomena in QCD. The lack of understanding the deconfinement phenomena is one of the most important issues encountered in such an analysis. One possibility to circumvent this problem is to incorporate gluons and their dynamics into the existing chiral model. By doing so, confinement effects can be included, at least approximately. The importance of including gluons is obvious, since their contribution to the bulk thermodynamics of hot and dense matter is significant, as we will show in Chapter 5. Thus, the need for having an appropriate model where gluonic degrees of freedom are included is obvious.

Before we give a closer description of the model itself, let us briefly and schematically address the issue of confinement. Mesons and baryons represent the well known and at the same time the most observed states in nature. On a more elementary level they consist of either quark/antiquark pair (mesons) or three quarks (baryons)[6]. The quarks interact via the exchange of gluons. Due to this interaction quarks/antiquarks are bound, i.e. confined, and thus not observed as free particles. In other words, quarks and gluons appear as free particles only at small distances. As a consequence, quarks can only be studied as constituents of hadrons.

Now we proceed with the question how one can address, and later incorporate in some given effective model, the effect of confinement. Here we follow the arguments given in Refs. [13, 14]. An $SU(N)$ non-Abelian gauge theory (with quarks included), as we have seen previously, is invariant under local $SU(N)$ symmetry transformation. This implies that the covariant derivative (2.5) and field ψ transform as

$$D_\mu \to \mathcal{U}^\dagger D_\mu \mathcal{U}, \qquad \psi \to \mathcal{U}^\dagger \psi\,, \tag{2.27}$$

where the symmetry transformation $\mathcal{U} \in SU(N)$. However, one can define another symmetry transformation of the form

$$\mathcal{U}_c = e^{i\vartheta}\,\mathbb{I}\,, \tag{2.28}$$

where $\mathbb{I}$ represents the unit matrix. On the other hand, $\mathcal{U}_c$ belongs to the $SU(N)$ group, hence it satisfies

$$\det \mathcal{U}_c = 1, \qquad \mathcal{U}_c^\dagger \mathcal{U}_c = \mathcal{U}_c \mathcal{U}_c^\dagger = \mathbb{I}\,. \tag{2.29}$$

From this requirement, one deduces that the phase factor in Eq. (2.28) must read

$$\vartheta = \frac{2\pi n}{N}\,, \qquad n = 0, 1, \ldots (N-1)\,. \tag{2.30}$$

[6]The most prominent baryons are proton (2 up and 1 down quark) and neutron (2 down and 1 up quark).

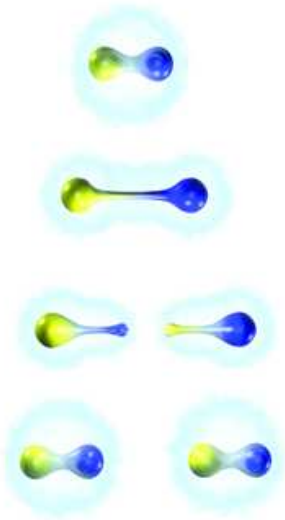

Figure 2.2: An artist's view of confinement [5]. In nature there are no free quarks and any attempt to separate a pair of quarks will result in the production of quark-antiquark pairs, yielding again color neutral objects, hadrons.

Thus, this symmetry transformation is not a continuous one, and hence it defines a global $Z(N)$ symmetry transformation.

In a general case of an $SU(N)$ non-Abelian gauge theory at finite temperature, Polyakov and 't Hooft [12, 13] conjectured that there is a gauge invariant operator that can be identified as an order parameter. In the case of three colors ($N_c = 3$) the corresponding global symmetry transformations belong to the $Z(3)$ group. This group is the center group of $SU_c(3)$ and from the mathematical point of view it is a *cyclic* group. The order parameter for the $Z(3)$ symmetry group is constructed using the *Polyakov loop* [7]. The Polyakov loop represents one of the most important observables in QCD at finite temperatures. It is represented as a matrix in color space given by:

$$L(\vec{x}) = \mathcal{P} \exp\left(i \int_0^\beta d\tau A_0(\vec{x}, \tau) \right) , \tag{2.31}$$

where $\mathcal{P}$ stands for path ordering and $\beta = 1/T$. In the heavy quark limit the deconfinement phase transition is well defined and QCD has the $Z(3)$ center symmetry which is spontaneously broken in the high temperature phase. The order parameter

[7] Some authors introduce an order parameter for the $Z(N)$ symmetry via the so-called thermal Wilson line. The Polyakov loop is then defined as a trace of the timelike Wilson line.

of the $Z(3)$ symmetry in this case is the thermal expectation value of the trace of the Polyakov loop

$$\ell = \frac{1}{N_c}\langle \mathrm{Tr}_c L(\vec{x})\rangle, \quad \ell^* = \frac{1}{N_c}\langle \mathrm{Tr}_c L^\dagger(\vec{x})\rangle. \tag{2.32}$$

Under a global $Z(3)$ transformation ℓ transforms by an overall phase factor

$$\ell \to \exp\left(\frac{2\pi i n}{3}\right)\ell, \qquad n = 0, 1, 2. \tag{2.33}$$

In the absence of dynamical quarks, i.e. in the heavy quark limit of QCD, the expectation value of the Polyakov loop indeed serves as an order parameter for the deconfinement phase transition. As a consequence of the confinement/deconfinement phase transition, the Polyakov loop acquires a nonzero expectation value. Thus, we have

$$\ell = 0 \longrightarrow \text{confined phase} \quad (T < T_d)$$
$$\ell \neq 0 \longrightarrow \text{deconfined phase} \quad (T > T_d),$$

where T_d is the deconfinement temperature. It is interesting to note that, contrary to the $O(4)$ symmetry, the $Z(3)$ symmetry is broken at high and not at low temperatures. Thus, in contrast to other symmetry breaking phase transitions, the high temperature phase is the ordered phase and consequently, the low temperature phase the disordered one in the $Z(3)$ symmetry.

In general, the fields ℓ and ℓ^* are different at non-zero quark chemical potential. For the $SU_c(3)$ color gauge group the Polyakov loop matrix L satisfies the following rules

$$LL^\dagger = 1 \qquad \text{and} \qquad \det L = 1, \tag{2.34}$$

and can be written in diagonal form

$$L = \mathrm{diag}\left(e^{i\varphi}, e^{i\varphi'}, e^{-i(\varphi+\varphi')}\right) \tag{2.35}$$

in the Polyakov gauge.

It should be noted that in the presence of dynamical quarks the $Z(3)$ symmetry is explicitly broken and there is no order parameter which characterizes the deconfinement phase transition in this case. Nevertheless, the Polyakov loop remains a useful concept also for dynamical quarks, an indicator of a rapid crossover transition towards confinement.

The Polyakov quark-meson model was first introduced in Ref. [33] as a new method to extend the 2-flavor chiral quark-meson model by coupling it with the Polyakov loop. In this model, it is possible to address both, the chiral and confining properties of QCD and investigate them on a mean field level.

The Lagrangian of the PQM model is given by

$$\mathscr{L}_{\mathsf{pqm}} = \bar{q}\left(i\not{D} - g(\sigma + i\gamma_5\vec{\tau}\vec{\pi})\right)q + \frac{1}{2}(\partial_\mu\sigma)^2 + \frac{1}{2}(\partial_\mu\vec{\pi})^2 - U(\sigma,\vec{\pi}) - \mathcal{U}(\ell,\ell^*)\ , \quad (2.36)$$

where $\mathcal{U}(\ell,\ell^*)$ is the potential for the gluon field expressed in terms of the traced Polyakov loop and its conjugate. As in the case for the chiral quark-meson model, meson fields have an $O(4)$ symmetry and the corresponding $SU(2)_L \times SU(2)_R$ representation given by $\phi = (\sigma,\vec{\pi})$ and $\sigma + i\vec{\tau}\cdot\vec{\pi}\gamma_5$ respectively. Thus, again one has $N_f^2 = 4$ mesonic degrees of freedom coupled to $N_f = 2$ flavors of constituent quarks q. The coupling between the effective gluon field and the quarks is implemented through a covariant derivative

$$D_\mu = \partial_\mu - iA_\mu, \quad (2.37)$$

where the spatial components of the gauge field are set to zero i.e. $A_\mu = \delta_{\mu 0}A_0$. The purely mesonic potential $U(\sigma,\vec{\pi})$ of the model is defined as

$$U(\sigma,\vec{\pi}) = \frac{\lambda}{4}\left(\sigma^2 + \vec{\pi}^2 - v^2\right)^2 - c\sigma \quad (2.38)$$

and the potential of the gluon field is given in the following form

$$\frac{\mathcal{U}(\ell,\ell^*)}{T^4} = -\frac{b_2(T)}{2}\ell^*\ell - \frac{b_3}{6}(\ell^3 + \ell^{*3}) + \frac{b_4}{4}(\ell^*\ell)^2\,, \quad (2.39)$$

with

$$b_2(T) \;=\; a_0 + a_1\left(\frac{T_0}{T}\right) + a_2\left(\frac{T_0}{T}\right)^2 + a_3\left(\frac{T_0}{T}\right)^3 \quad (2.40)$$

where $a_0 = 6.75$, $a_1 = -1.95$, $a_2 = 2.625$, $a_3 = -7.44$, $b_3 = 0.75$ and $b_4 = 7.5$. The coefficients are chosen in such a way as to reproduce the equation of state in pure gauge theory on the lattice. At the temperature $T_0 = 270$ MeV, which is the critical temperature obtained for pure gauge theory, the potential (2.39) yields a first order phase transition. However, the choice of the potential for the gluon field given by Eq. (2.39) is not the only one. Another possibility is to replace the higher order polynomial terms in ℓ and ℓ^* with a logarithmic term [24]. Thus, the potential $\mathcal{U}(\ell,\ell^*)$ can be also expressed in the following form [58]

$$\frac{\mathcal{U}(\ell,\ell^*)}{T^4} = -\frac{1}{2}a(T)\ell^*\ell + b(T)\log\left(1 - 6\ell^*\ell + 4(\ell^3 + \ell^{*3}) - 3(\ell^*\ell)^2\right)\,, \quad (2.41)$$

where

$$a(T) = a_0 + a_1\left(\frac{T_0}{T}\right) + a_2\left(\frac{T_0}{T}\right)^2, \qquad b(T) = b_3\left(\frac{T_0}{T}\right)^3. \quad (2.42)$$

The coefficients (a_0, a_1, a_2, b_3) have different numerical values then the coefficients in Eqs. (2.39) and (2.40).

The effective potential $\mathcal{U}(\ell, \ell^*)$ is constructed from lattice data and is required to satisfy the $Z(3)$ center symmetry like the pure gauge theory. Furthermore, in the pure gauge theory the mean value ℓ, ℓ^* are given by the minima of $\mathcal{U}(\ell, \ell^*)$. Thus, at low temperatures the effective Polyakov loop potential must have an absolute minimum at $\ell = 0$ in order to be consistent with lattice predictions. For temperatures above the critical one the minimum is shifted to some finite value of ℓ. Finally, at high temperatures i.e. in the limit $T \to \infty$ the value of the Polyakov loop is $\ell \to 1$.

We will finish this chapter with a few remarks. We have briefly discussed the strong interaction and some low-energy effective realization of it. We confined ourselves to the two-flavor model, knowing that QCD exhibits an approximate chiral symmetry in the up/down sector ($N_f = 2$) and, that QCD in this sector then belong to the same universality class as the $O(4)$ model. This particular feature we use in Chapter 4. Furthermore, we do not attempt to incorporate all effects of the confinement in the effective model. Rather, we combine a chirally symmetric model with the Polyakov loop potential constructed (with appropriately fitted parameters) so as to simulate the first order confinement/deconfinement phase transition. In Chapter 5 we present results which provide input for further theoretical/phenomenological studies in this direction.

Chapter 3

Renormalization group method

The Renormalization Group (RG) is a theoretical tool, which among many other available methods in physics, is considered to be one of the most important ideas in quantum field theory (QFT). Besides the RG there is a variety of other methods developed over the years one uses to tackle various problems encountered in QFT, such as perturbation theory or various numerical techniques. Although their usefulness in solving and understanding a large number of problems has been demonstrated, it often happens that the applicability of a particular method is restricted to a specific energy or length scale. Moreover, many problems cannot be investigated due the approximations used within these methods. Hence, there was a need for a method that, at least to some extent, overcomes all these problems. During the recent years the RG method has proven to be one of the most promising tools theorists have at hand. The applicability of RG covers a whole range of physics and physical phenomena that are usually plagued with divergences. Starting with its role as a novel method in QFT, the RG has developed into an uniquely effective technique widely used also in statistical physics, condensed matter theory and all other areas of physics where non-perturbative effects make systematic calculations difficult.

One of the most successful application of the RG has been to the theory of phase transitions and critical phenomena. Being in its nature highly non-perturbative, the critical phenomena turned out to be an ideal testing ground for the applicability of the RG method. In the vicinity of a second-order phase transition long range fluctuations are important and have to be accounted for in the calculations. Also, at the critical temperature T_c measurable physical observables diverge and a specific set of parmeters called *critical exponents* describe their behavior. Various experimental observations indicate that the critical exponents are universal and depend only on the symmetry and dimension of the physical system under investigation. In the light of these findings, one can understand the large amount of effort invested in

understanding the nature and origin of the singular behavior of thermodynamic functions at the critical point characterized by the critical exponents. For a long time there has been only one theoretical approach for describing phase transitions known as *mean field approximation*. Introduced by P. E. Weiss as a theory of magnetism, the mean field approximation where no fluctuations are taken into account, in many cases fails in giving an accurate and quantitatively correct description of phase transitions. Also the values for critical exponents calculated within this simple approximation often differ significantly from their known experimental values since mean field approximation neglects the influence of the fluctuations and other non-perturbative effects in the very vicinity of the phase transition. However, despite all drawbacks, the mean field approximation has been applied as a testing tool to investigate a new type of phase transition. The important theoretical breaktrough in understanding the physics behind critical phenomena (and other non-perturbative phenomena) came with Wilson's RG concept.

Wilson's idea is based on a simple and yet very shrewd observation that one can construct an *effective* theory for a specific set of degrees of freedom of some given physical system. This particular effective theory is constructed by integrating out degrees of freedom we are not interested in. Consequently we are left with a subset of the initial system where the original number of degrees of freedom has been reduced. The core of Wilson's idea is the procedure of *coarse-graining*. Within such an approach, Wilson conjectured that it should be possible to integrate out irrelevant degrees of freedom (short distance quantities or the "high energy modes") by an iterative procedure and in the limit of very small momenta (long distances) all relevant physical information should then be contained in the effective Hamiltonian.

On the other hand, in 1966 Kadanoff introduced a technique called *block spin transformation*. This approach is also often used to elucidate the RG idea. Again, one reduces the degrees of freedom of a model, now given as Ising spins located on a square lattice. The RG transformation is achieved through dividing the lattice into blocks with the same length. We assume that each block contains four spins located at every corner. The procedure of reduction of degrees of freedom is done assuming that four spins in one block can be treated as one single effective spin so that the original lattice can be replaced with a new one.

The whole idea concerning the RG transformation is based on one simple, but essential fact that physics is scale dependent. In other words, there is a minimum length a which one uses in describing a given set of physical phenomena. Different degrees of freedom as well as different dynamics reveal at each scale a. Thus, there is a whole set of physical theories used to investigate the properties and behavior of relevant degrees of freedom at a given scale. At scales $a \sim 1$ m, classical mechanics plays a crucial role in describing and explaining physical phenomena. By further lowering the scale a, other relevant degrees of freedom will emerge such as nucleons at scales $a \sim 10^{-13}$ cm or quarks at $a \sim (10^{-14} - 10^{-18})$ cm, for instance. Now it becomes clear why it is possible to apply this important and indispensable technique

of successively integrating out certain (irrelevant) degrees of freedom from a physical theory. Altough at first sight this procedure might look a bit unphysical or even illogical because of a possible lost of information, its core idea lies in the fact that theories at one scale decouple from theories valid at another scale. It might well be that at Planck length scales (length of approximately 10^{-35} m) the (super)string theory is relevant, but in order to describe the motion of a pendulum we do not need any knowledge about molecules, atoms, quarks or (super)strings.

One of the most significant advantages of the RG method is that it can describe physics across different momentum scales. In particular, within the RG framework one can capture the dynamics of the long-range fluctuations near the critical point. It should also be noted that in perturbation theory fluctuations of all wavelengths are treated on the same footing. Here, within the RG approach one can choose an appropriate approximation scheme and do all necessary summations within the chosen scheme.

From the mathematical point of view the RG can be thought of as a set of symmetry transformations that leave the physics invariant. Whenever there is some operation (in this case a binary one) that has a specific set of features one can speak of a group[1]. However, altough the RG is a continuous (or discrete) group of symmetry transformations it is not a group in a strict mathematical sense but only a *semigroup*. For treating the RG as a group in the algebraic sense, one important feature is missing and that is the inverse property. Generally, an RG transformation is not invertible (at least not without a serious ambiguity) and hence it is not a group.

The basic idea of the renormalization group and its important features are presented in this chapter following the arguments given in Refs. [15, 16]. One of the possible RG approaches, the Functional Renormalization Group (FRG), we introduce later in this chapter which we close with a derivation of the flow equation for the effective average action. For a more detailed discussion regarding the origin and applications of the RG method, we refer the interested reader to [15, 16, 17] and references therein.

[1]For a given binary operation $*$, a set $\mathcal{G}$ with elements $A, B, C \ldots \in \mathcal{G}$ represents a group if the following four properties are fulfilled

$$A, B \in \mathcal{G} \rightarrow A * B \in \mathcal{G} \qquad \text{closure},$$

$$A, B, C \in \mathcal{G} \rightarrow (A * B) * C = A * (B * C) \qquad \text{associativity},$$

$$\forall A \in \mathcal{G} \rightarrow \mathbb{I} * A = A * \mathbb{I} = A \qquad \text{identity},$$

$$\forall A \in \mathcal{G},\ \exists A^{-1} \in \mathcal{G} \rightarrow A * A^{-1} = A^{-1} * A = \mathbb{I} \qquad \text{inverse}.$$

3.1 Basic ideas of the renormalization group

Let us start with an infinitely dimensional space of Hamiltonians $\mathbb{H}$ or in other words a space of coupling constants $\vec{G}$. Here $\vec{G} = (G_1, G_2, \dots)$ stands for the strengths of all possible couplings compatible with the symmetries of a system. Furthermore, we pick some Hamiltonian of a given physical system $\mathcal{H}[s, \vec{G}] \in \mathbb{H}$. The set s that together with coupling constants $\vec{G}$ characterizes the Hamiltonian, represents some microscopic variables (vectors, tensors, etc. that can be thought of as quantum fields in a quantum field theory or spins located on discrete lattice sites in statistical physics). Each of these constants defines a point in the space $\mathbb{H}$. The renormalization group transformation can now be defined by introducing an operator $\mathbf{R}$ that acts on the Hamiltonian $\mathcal{H}[s, \vec{G}]$ in the following way

$$\mathbf{R}\mathcal{H}[s, \vec{G}] = \mathcal{H}'[s', \vec{G}']. \tag{3.1}$$

What is achieved by this transformation is that the initial Hamiltonian $\mathcal{H}[s, \vec{G}]$ is transformed or *renormalized* in order to obtain a new Hamiltonian $\mathcal{H}'[s', \vec{G}']$. Furthermore, the RG transformation operator $\mathbf{R}$ also reduces the number of degrees of freedom N to

$$N' = N/a^d \tag{3.2}$$

where d is the dimension of a system and a is some spatial rescaling factor.

Now, depending on the problem we want to handle, we might be interested only in the physics at long distances (compared to the rescaling factor a). We expect however that the characteristics of long wavelength fluctuations are independent of the microscopic details of a theory. Hence, the idea is to remove all irrelevant degrees of freedom from the theory.

Let us divide our original set of variables s into the following two subsets i.e.

$$s_< = sN', \tag{3.3a}$$
$$s_> = s(N - N'). \tag{3.3b}$$

Since we are not interested in the variables $s_>$, they will be removed from the problem by integrating them out. After doing so, what is left is an *effective Hamiltonian* of the original system $\mathcal{H}_{eff}[s_<, \vec{G}_<]$. This Hamiltonian contains only the information necessary to compute the long wavelength properties of the system.

Here we want to stress the fact that the RG transformation does not by any means change the partition function of the system. This is an essential feature that RG transformation has to satisfy in order to leave the "original" physics unchanged. Indeed, the partition function of the renormalized system can be written in the following form

$$\int_{N'} ds' e^{\mathcal{H}'[s', \vec{G}']} = \int_{N'} ds_< e^{\mathcal{H}_{eff}[s_<, \vec{G}_<]} = \int_{N'} ds_< \int_{N-N'} ds_> e^{\mathcal{H}[s_< + s_>, \vec{G}_< + \vec{G}_>]} = \int_{N} ds e^{\mathcal{H}[s, \vec{G}]}, \tag{3.4}$$

where from the last equation follows the "original " partition function of the system. The next step that has to be done is the rescaling of all spatial vectors i.e.

$$\mathbf{x}^{'} = \mathbf{x}/a \tag{3.5}$$

for coordinates, and

$$\mathbf{p}^{'} = \mathbf{p}\, a\,, \tag{3.6}$$

for momenta. Accordingly, the variables s also have to be rescaled by some rescaling factor [2] b in order to preserve their fluctuation magnitude.

Let us repeat what has been done up to now. We have basically rescaled the variables that the Hamiltonian $\mathcal{H}[s, \vec{G}]$ depends on, and obtained the renormalized Hamiltonian $\mathcal{H}_{eff}[s_<, \vec{G}_<] = \mathcal{H}'[s', \vec{G}']$ that retains all the original information of the system. This procedure can now be repeated using the renormalized Hamiltonian $\mathcal{H}'[s', \vec{G}']$ as the starting one i.e.

$$\mathbf{R}\mathcal{H}'[s', \vec{G}'] = \mathcal{H}''[s'', \vec{G}''], \quad \mathbf{R}\mathcal{H}''[s'', \vec{G}''] = \mathcal{H}'''[s''', \vec{G}'''], \ \ldots \tag{3.7}$$

An important question arises during this iteration procedure and that is the one regarding the end of the procedure. In other words, how many times can we spatially rescale variable s? The RG transformation of rescaling and relabeling stops at a *fixed point* that is defined as

$$\mathbf{R}\mathcal{H}^*[s^*, \vec{G}^*] = \mathcal{H}^*[s^*, \vec{G}^*]. \tag{3.8}$$

Here we have that a point under some RG transformation maps onto itself, thus the iteration procedure ends.

Here we should stress the importance and show a few interesting features of a fixed point. In the vicinity of a fixed point the RG equation defined by the transformation law Eq. (3.1), can be linearized. To do so, first we write the Hamiltonian $\mathcal{H}[s, \vec{G}]$ near a fixed point as

$$\mathcal{H}[s, \vec{G}] = \mathcal{H}^*[s^*, \vec{G}^*] + \delta\mathcal{H}[s, \vec{G}] \tag{3.9}$$

where $\delta\mathcal{H}[s, \vec{G}]$ is small. According to Eq. (3.1) and using the main characteristic of the RG transformation at the fixed point we have the following expression

$$\mathbf{R}\left(\mathcal{H}^*[s^*, \vec{G}^*] + \delta\mathcal{H}[s, \vec{G}]\right) = \mathcal{H}^*[s^*, \vec{G}^*] + \mathbf{R}_{\text{lin}}\delta\mathcal{H}[s, \vec{G}] = \mathcal{H}^*[s^*, \vec{G}^*] + \delta\mathcal{H}'[s', \vec{G}'], \tag{3.10}$$

where $\mathbf{R}_{\text{lin}}$ is a linear operator where higher order terms $\mathcal{O}((\delta\mathcal{H}[s, \vec{G}])^2)$ are neglected. The original RG transformation (or differential equation if we replace the operator $\mathbf{R}$ with a corresponding differential operator) has been reduced to a linear problem in the vicinity of a fixed point. This gives us the possibility to determine the eigenvalues and eigenvectors of the linear operator $\mathbf{R}_{\text{lin}}$. Thus, we may write

$$\mathbf{R}_{\text{lin}}\delta\mathcal{H}_k[s, \vec{G}] = \lambda_k(a)\delta\mathcal{H}_k[s, \vec{G}] \tag{3.11}$$

[2] Depending on the type of the variable s one has to use different rescaling factors.

and solve the eigenvalue problem to obtain the corresponding eigenvalues $\lambda_k(a)$ and eigenvectors (or "eigenoperators") $\delta\mathcal{H}_k$. Consequently, one can represent the Hamiltonian $\mathcal{H}[s,\vec{G}]$ using the following general expansion

$$\mathcal{H}[s,\vec{G}] = \mathcal{H}^*[s^*,\vec{G}^*] + \sum_k l_k \delta\mathcal{H}_k[s,\vec{G}], \tag{3.12}$$

where l_k are expansion coefficients. At this point we can introduce the notion of *relevance* of operators $\delta\mathcal{H}_k[s,\vec{G}]$. For $\lambda_k > 0$ the operator is *relevant* at the fixed point, for $\lambda_k < 0$ the operator is *irrelevant* and in the case where $\lambda_k = 0$ the operator is considered to be *marginal*. One can also raise a question regarding the importance of a fixed point. In order to obtain a fixed point solution of a given physical system we have to solve Eq. (3.8). This equation can be an algebraic or a differential equation. In the case that Eq. (3.8) has only a trivial solution the corresponding system has no interactions and this fixed point solution is known as the Gaussian fixed point. Needless to say, from a physical point of view, the most interesting solutions are the non trivial ones, the so called Wilson-Fisher fixed points. These non trivial fixed points represent then critical states of a given system. How the system in the critical state behaves, depends on the properties of the RG transformation. If some system, described by Hamiltonian $\mathcal{H}[s_1,\vec{G}_1] \in \mathbb{H}$, undergoes a second order phase transition at some critical temperature T_c, the correlation length ξ diverges. Under the RG transformation $\mathbf{R}$, Hamiltonian $\mathcal{H}[s_1,\vec{G}_1]$ maps onto $\mathcal{H}[s_2,\vec{G}_2]$, and again ξ diverges. Now, one can define the *critical surface* in the space $\mathbb{H}$ as a set of Hamiltonians $\mathcal{H}[s_i,\vec{G}_i]$, $i = 1,2,3\ldots$ for which $\xi \to \infty$. The critical surface is stable under RG transformations (3.1). Also, at the fixed point the physics is same at all scales.

Intimately related with the notion of a fixed point of the RG transformation is the concept of *universality*. In the space of Hamiltonians $\mathbb{H}$ we have, from a physical point of view a variety of systems (systems that differ significantly from each other by having different physical character) described by their corresponding Hamiltonians $\mathcal{H}[s,\vec{G}]$. Universality reflects the feature that, altough some physical systems show different properties or behavior, they belong to the same *universality class* if attracted by the same fixed point. This expedient feature is often used in the theory of critical phenomena. If two different physical systems belong to the same universality class, a full description of the critical behavior of, let us say, the first system can be obtained by studying the second system. In this case one usually says that these two systems have the same asymptotic long wavelength physics and thus the same universal behavior. As a consequence we can literally reduce the complexity of a problem.

3.2 Functional renormalization group

In this section we give a more detailed description of one particular RG method, namely the functional renormalization group (FRG). As the name indicates, this approach is based on the functional method used in computation of various generating functionals that contain all relevant information about some physical system. Thus, the FRG incorporates the basic idea of the RG transformation with the functional approach.

The FRG is an important tool for addressing nonperturbative problems within the quantum field theory. It is based on an infrared (IR) regularization with the momentum scale parameter k of the full propagator which turns the corresponding effective action into a scale dependent functional Γ_k [36, 37, 38, 39, 40, 41]. This method is just one of many other RG techniques presently available. Later in this section, we will outline the basics of FRG approach and derive its main part i.e. the flow equation for the effective average action that we later use as the starting point in our FRG based calculations.

3.2.1 Effective average action

Before we give the basic concepts of the FRG and derive the corresponding flow equation let us first introduce a few important objects that appear in quantum field theory and statistical physics and which allow us to introduce the notion of the effective average action.

The basic object in the context of quantum field theory is the generating functional of the n-point correlation functions. This functional is given by the following path integral representation in the presence of an external field or source $J(x)$ in the d-dimensional Euclidean space $\mathbb{R}^d$

$$Z[J] = \int D\chi e^{-S[\chi]+\int_x \chi(x)J(x)}, \tag{3.13}$$

where $\chi(x) : \mathbb{R}^d \to \mathbb{R}$ is a single-component real field variable. The classical action $S[\chi]$ that governs its dynamics is related to the corresponding Lagrangian[3] $\mathscr{L}$ of

[3]Here we will be somewhat lax, and refer to $\mathscr{L}$ as the Lagrangian and not the Lagrangian density. Usually, one introduces the action S as the time integral of the Lagrangian $\mathcal{L}$ by

$$S = \int dt\, \mathcal{L}\,,$$

where the Lagrangian $\mathcal{L}$ is given as the spatial integral of the Lagrangian density $\mathscr{L}$

$$\mathcal{L} = \int d^3x\, \mathscr{L}\,.$$

Consequently the integration over the space-time volume $V = dtd^3x$ of the system yields the

the system by

$$S[\chi] = \int_x \mathscr{L}, \qquad \int_x \equiv \int d^d x \tag{3.14}$$

and the usual Boltzmann factor is given by $\exp(-S[\chi])$. The functional integration that appears in the definition of the generating functional $Z[J]$ stands for the sum over all microscopic states. Consequently, the field $\chi(x)$ represents different physical observables such as spin, magnetization, mass field etc. The functional $Z[J]$ is also known as the partition function in statistical physics and without an external source $J(x)$ reads

$$Z = \mathrm{Tr} e^{-\hat{H}/T} = \sum_n e^{-E_n/T}\,, \tag{3.15}$$

where trace represents an integration over all microscopic degrees of freedom present in a system and E_n are eigenvalues of the Hamiltonian $\hat{H}$. The partition function Z can also be expressed in the following form

$$Z = \sum_i \int d\chi_i \, \langle \chi_i | e^{-\hat{H}/T} | \chi_i \rangle \,, \tag{3.16}$$

where the summation is to be performed over all states. By making an analytical continuation to imaginary time ($t \to -i\tau$) the partition function takes the form[4]

$$Z = \int \mathcal{D}\chi_i \, (\tau) e^{-S_E} \tag{3.17}$$

and S_E is the Euclidean action.

Now we turn back to the source dependent partition function $Z[J]$. Greens functions generated by taking functional derivatives of the functional $Z[J]$ with respect to the source J are *disconnected* Greens functions. Using this kind of Greens functions is not very suitable since they do not contribute to the S-matrix. Thus, one usually introduces a generating functional for the *connected* Greens functions as

$$W[J] = \ln Z[J]. \tag{3.18}$$

Now, by taking the functional derivatives of $W[J]$ with respect to the source $J(x)$ we obtain the average density correlation

$$\frac{\delta W[J]}{\delta J(x)} = \langle \chi(x) \rangle = \phi(x) \tag{3.19}$$

action S

$$S = \int_V \mathscr{L}\,.$$

[4]For details about the path integral formalism and imaginary time we refer the interested reader to Ref. [97].

or the density-density correlation

$$\frac{\delta^2 W[J]}{\delta J(x)\delta J(y)} = \langle\chi(x)\chi(y)\rangle - \langle\chi(x)\rangle\langle\chi(y)\rangle. \tag{3.20}$$

Finally, the effective action $\Gamma[\phi]$ is obtained by a Legendre transformation

$$\Gamma[\phi] = -W[J] + \int_x \phi(x)J(x)\,, \tag{3.21}$$

and represents the generating functional of the one-particle irreducible (1PI) correlation functions. For a given physical theory existing sources or external fields can now be obtained through the effective action $\Gamma[\phi]$ i.e.

$$\frac{\delta\Gamma[\phi]}{\delta\phi(x)} = J(x). \tag{3.22}$$

Furthermore, it is obvious from Eq. (3.22) that for vanishing external fields the equilibrium state of a theory is given by the minimum of $\Gamma[\phi]$. In other words the ground state of a theory is given by the minimum of the effective action. It should also be stressed that the second functional derivative of the effective action is equivalent to the inverse propagator. Another essential feature of $\Gamma[\phi]$ is that field equations derived from it include all quantum effects and thus are exact.

The effective average action Γ_k that depends on a scale k represents a simple generalization of the standard effective action $\Gamma[\phi]$ acting as the generating functional of the one-particle irreducible (1PI) Green functions. The main objective is to start at some high UV scale Λ where the physics is described by some classical action S and then to successively integrate out quantum fluctuations by lowering the scale k. In this way it is possible to calculate the generating functional for 1PI graphs. A particular feature Γ_k incorporates is that only fluctuations with momenta $q^2 \geq k^2$ are included whereas fluctuations with $q^2 \leq k^2$ are suppressed. This can be achieved following the same line of reasoning as by constructing the effective action $\Gamma[\phi]$ where we have introduced the generating functional of the n-point correlation functions $Z[J]$. Hence, we can define the k dependent generating functional $Z_k[J]$ as

$$Z_k[J] = \int_\Lambda D\chi e^{-S[\chi]+\int_x \chi(x)J(x)-\Delta S_k[\chi]}. \tag{3.23}$$

Here we have included a new term $\Delta S_k[\chi]$ that represents an infrared (IR) cutoff term and reads in the momentum space

$$\Delta S_k[\chi] = \frac{1}{2}\int \frac{d^d q}{(2\pi^d)}\chi^*(q)R_k(q)\chi(q) \tag{3.24}$$

where $\chi^*(q) = \chi(-q)$. There are several conditions that the cutoff function $R_k(q)$ has to fullfill. Generally, for the regulator is required the following

$$\lim_{q^2/k^2 \to 0} R_k(q^2) > 0. \tag{3.25}$$

This important requirement makes the effective propagator (at vanishing field) finite in the IR limit $q^2 \to 0$, and no IR divergences appear in the presence of massless modes. Consequently, the regulator R_k acts as an IR regulator. The second property

$$\lim_{k^2/q^2 \to 0} R_k(q^2) = 0 \tag{3.26}$$

ensures that R_k vanishes in the IR. In this way the regulator $R_k(q)$ is removed in the physical limit and we can obtain in the limit $k \to 0$ the 1PI generating functional ($\Gamma = \lim_{k\to 0} \Gamma_k$). Finally, by the third condition

$$\lim_{k \to \Lambda} R_k(q^2) \to \infty \tag{3.27}$$

the initial conditions at the UV scale Λ are recovered and the scale dependent effective action Γ_k approaches the microscopic action S in the UV limit.

The above mentioned features that the IR cutoff has to satisfy can be implemented by the e.g. following form

$$R_k(q) \sim \frac{q^2}{e^{q^2/k^2} - 1}. \tag{3.28}$$

Generally, it is not always an easy task to find an adequate cutoff function. If there are low mass fermions in a theory, the regulator must preserve chiral symmetry. For gauge theories the situation is even worse owing to gauge symmetry breaking by the regulator. In our work we do not encounter these problems[5]. In our calculations we shall use the so called optimized cutoff functions for reasons which will be explained in the forthcoming chapter. Their precise description will be given later in this section.

The next logical step in the derivation of the effective average action is to define the scale-dependent generating functional for the connected Greens functions by

$$W_k[J] = \ln Z_k[J]. \tag{3.29}$$

As in the case for the effective action $\Gamma[\phi]$ (cf. Eq. (3.19)) the expectation values of the fields χ in the presence of the cutoff term $\Delta S_k[\chi]$ are obtained by taking the functional derivatives of $W_k[J]$ with respect to the source $J(x)$. Finally, using a modified Legendre transformation of the form

$$\Gamma_k[\phi] = -W_k[J] + \int_x \phi(x)J(x) - \Delta S_k[\phi] \tag{3.30}$$

[5]The problem of gauge symmetry breaking in the presence of cutoff functions can be successfully circumvented via *modified* Ward-Takahashi identities that recover the original gauge invariance.

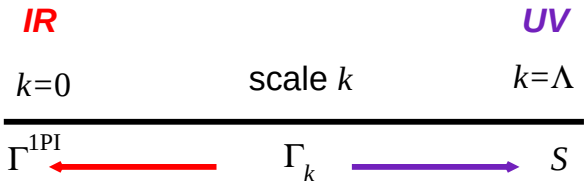

Figure 3.1: Illustration of interpolation of the effective average action Γ_k between the classical action S at some UV scale Λ and the full quantum action Γ in the limit $k \to 0$ in the IR.

we can define the effective average action Γ_k. The effective average action Γ_k governs the dynamics of a theory at a momentum scale k and interpolates between the bare action $\Gamma_{k=\Lambda} \equiv S$ and the full quantum effective action $\Gamma_{k=0} = \Gamma$. In Fig. 3.1 we represent graphically this interpolation of Γ_k between S and $\Gamma_{k=0}$. At $k = 0$ there is no IR cutoff present anymore. Thus all fluctuations are included and by definition the effective average action equals the standard action (the generating functional of 1PI Green functions). If there is some physical UV cutoff Λ in a theory the effective average action at the scale $k = \Lambda$ $\Gamma_{k=\Lambda}$ is associated with the microscopic (classical) action S.

3.2.2 Flow equation

Now we will derive the flow equation for the effective average action. This flow equation is essential and represents the crucial part in the FRG approach. Using this particular flow equation, we are able to follow the change of the scale dependent effective action Γ_k at scale k with a change of the RG scale.

For the sake of simplicity we will consider only a one component field ϕ (e.g. scalar theory). First, we take a derivative of Eq. (3.30) with respect to the scale k

$$\partial_k \Gamma_k[\phi] = -\partial_k W_k[J] - \int_x \frac{\delta W_k}{\delta J(x)} \partial_k J(x) + \int_x \phi(x) \partial_k J(x) - \partial_k \Delta S_k[\phi]. \tag{3.31}$$

According to Eq. (3.19) the second and third term cancel. Furthermore, it follows

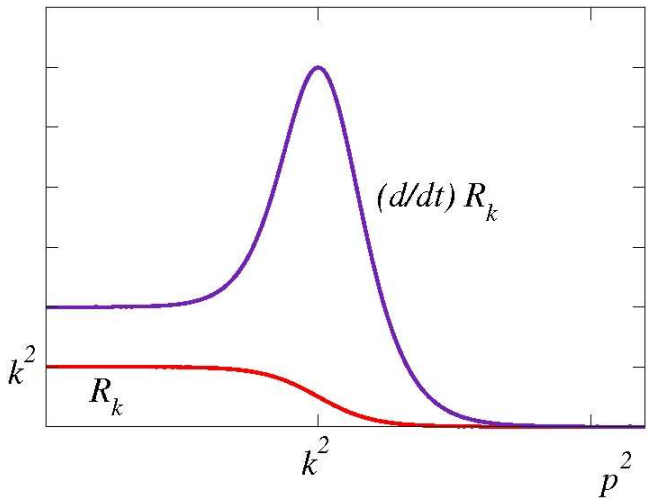

Figure 3.2: A typical cutoff function R_k and its derivative $\partial_t R_k$ in the FRG approach as a functions of momentum p^2. Both functions are shown for fixed k^2 [40].

from Eq. (3.24) that the derivative of the cutoff term $\Delta S_k[\phi]$ is of the form

$$\partial_k \Delta S_k[\phi] = \frac{1}{2} \int_{x,y} \phi(x) \partial_k R_k \phi(y). \tag{3.32}$$

In order to proceed with the derivation, we first have to find the scale derivative of the scale-dependent generating functional for the connected Greens functions $W_k[J]$ for a fixed source J. Thus, starting from Eq. (3.29) we have

$$\begin{aligned}
\partial_k W_k[J] &= \frac{1}{Z_k} \partial_k \int D\chi e^{-S[\chi] + \int_x \chi(x) J(x) - \Delta S_k[\chi]} \\
&= \frac{1}{Z_k} \int D\chi \left(-\partial_k \Delta S_k[\chi] \right) e^{-S[\chi] + \int_x \chi(x) J(x) - \Delta S_k[\chi]} \\
&= \frac{1}{Z_k} \int D\chi \left(-\frac{1}{2} \int_{x,y} \chi(x) \partial_k R_k \chi(y) \right) e^{-S[\chi] + \int_x \chi(x) J(x) - \Delta S_k[\chi]} \\
&= -\frac{1}{2} \int_{x,y} \partial_k R_k \underbrace{\frac{1}{Z_k} \int D\chi \, \chi(x)\chi(y) e^{-S[\chi] + \int_x \chi(x) J(x) - \Delta S_k[\chi]}}_{\langle \chi(x)\chi(y) \rangle}.
\end{aligned} \tag{3.33}$$

Now, we can use Eq. (3.19) and Eq. (3.20) to write the following decomposition

$$\langle \chi(x)\chi(y) \rangle = G(x,y) + \phi(x)\phi(y), \tag{3.34}$$

where we have introduced the notation

$$G(x,y) = \frac{\delta^2 W[J]}{\delta J(x)\delta J(y)} \tag{3.35}$$

for the connected two-point functions. Plugging this result into Eq. (3.31) we end up with the flow equation for the effective average action

$$\partial_k \Gamma_k[\phi] = \frac{1}{2}\int\limits_{x,y} G(x,y)\partial_k R_k. \tag{3.36}$$

Altough we have derived the flow equation for $\Gamma_k[\phi]$ we will go one step further and express this flow as a functional differential equation for the effective average action $\Gamma_k[\phi]$.

In order to do so let us first find the inverse of $G(x,y)$. The starting point is Eq. (3.30) and its variation with respect to the field $\phi(x)$. Thus, using the variation condition on the effective average action we have

$$\begin{aligned}
\frac{\delta\Gamma_k[\phi]}{\delta\phi(x)} &= -\frac{\delta W_k[J]}{\delta\phi(x)} + \int\limits_y \frac{\delta J(y)}{\delta\phi(x)}\phi(y) + \int\limits_y J(y)\delta(x-y) - \frac{\delta\Delta S_k[\phi]}{\delta\phi(x)} \\
&= -\int\limits_y \underbrace{\frac{\delta W_k[J]}{\delta J(y)}}_{\phi(y)}\frac{\delta J(y)}{\delta\phi(x)} + \int\limits_y \frac{\delta J(y)}{\delta\phi(x)}\phi(y) + J(x) - \frac{\delta\Delta S_k[\phi]}{\delta\phi(x)} \\
&= J(x) - \frac{\delta\Delta S_k[\phi]}{\delta\phi(x)} \\
&= J(x) - \phi(x)R_k.
\end{aligned} \tag{3.37}$$

The variation of the cutoff term is obtained using Eq. (3.24), but now given in coordinate space

$$\frac{\delta\Delta S_k[\phi]}{\delta\phi(x)} = \frac{\delta}{\delta\phi(x)}\left(\frac{1}{2}\int\limits_{y,z}\phi(y)R_k\phi(z)\right) = \phi(x)R_k \tag{3.38}$$

The second variation with respect to $\phi(y)$ gives

$$\frac{\delta^2\Gamma_k[\phi]}{\delta\phi(x)\delta\phi(y)} = \frac{\delta J(x)}{\delta\phi(y)} - R_k(x,y), \tag{3.39}$$

where we have introduced the short hand notation $R_k(x,y) = R_k\delta(x-y)$. The goal we aim for is to show the following identity

$$\frac{\delta J(x)}{\delta\phi(y)} = \left(\frac{\delta^2 W}{\delta J(x)\delta J(y)}\right)^{-1}. \tag{3.40}$$

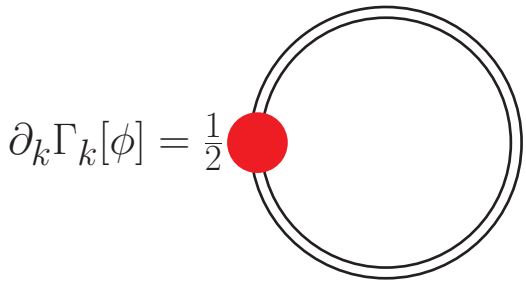

Figure 3.3: Graphical representation of the flow equation for the effective average action $\Gamma_k[\phi]$. The complete field dependent propagator is represented by the double line and the solid dot denotes the insertion of $\partial_k R_k$.

By taking a variation on Eq. (3.19) with respect to $\phi(y)$ we have

$$\frac{\delta}{\delta\phi(y)}\left(\frac{\delta W[J]}{\delta J(x)}\right) = \delta(x-y). \tag{3.41}$$

Thus, we can write the following set of identities

$$\begin{aligned}
\delta(x-y) &= \frac{\delta^2 W}{\delta J(x)\delta\phi(y)} = \int\limits_z \left(\frac{\delta^2 W}{\delta J(x)\delta J(z)}\frac{\delta J(z)}{\delta\phi(y)}\right)(z,y) \\
&= \int\limits_z \frac{\delta^2 W}{\delta J(x)\delta J(z)}\left(\frac{\delta^2\Gamma_k[\phi]}{\delta\phi(z)\delta\phi(y)} + R_k\right)(z,y) \\
&= \int\limits_z \frac{\delta^2 W}{\delta J(x)\delta J(z)}\left(\Gamma_k^{(2)}[\phi] + R_k\right)(z,y).
\end{aligned} \tag{3.42}$$

From the last step follows Eq. (3.40). Finally, we can write the flow equation for the effective average action $\Gamma_k[\phi]$ as

$$\partial_k\Gamma_k[\phi] = \frac{1}{2}\int\limits_{x,y} G(x,y)\partial_k R_k = \frac{1}{2}\int\limits_x \left[\left(\Gamma_k^{(2)}[\phi] + R_k\right)^{-1}\partial_k R_k\right]. \tag{3.43}$$

Since no approximations have been introduced during the derivation of flow equation for the effective average action $\Gamma_k[\phi]$, this flow is in the literature also referred to as the *exact* RG flow equation. However, as one starts with the tedious procedure of solving the exact flow equation, various approximation schemes and truncations have to be used and the exactness is lost.

The flow equation can be written in momentum space and extended to include fermions as well. The full form of the flow equation is usually written in the following

more compact matrix form

$$\partial_k \hat{\Gamma}_k[\Phi, \bar{\psi}, \psi] = \frac{1}{2}\mathrm{STr}\left[\left(\hat{\Gamma}_k^{(2)}[\Phi, \bar{\psi}, \psi] + \hat{R}_k\right)^{-1} \partial_k \hat{R}_k\right] \tag{3.44}$$

where the matrix $\hat{\Gamma}_k^{(2)}[\Phi, \bar{\psi}, \psi]$ has the following block substructure in boson-antifermion-fermion space

$$\hat{\Gamma}_k^{(2)}[\Phi, \bar{\psi}, \psi] = \begin{pmatrix} \Gamma^{(2)}_{k,\Phi\Phi} & \Gamma^{(2)}_{k,\Phi\bar{\psi}} & \Gamma^{(2)}_{k,\Phi\psi} \\ \Gamma^{(2)}_{k,\bar{\psi}\Phi} & \Gamma^{(2)}_{k,\bar{\psi}\bar{\psi}} & \Gamma^{(2)}_{k,\bar{\psi}\psi} \\ \Gamma^{(2)}_{k,\psi\Phi} & \Gamma^{(2)}_{k,\psi\bar{\psi}} & \Gamma^{(2)}_{k,\psi\psi} \end{pmatrix}, \tag{3.45}$$

and the elements of matrix (3.45) are second order functional derivatives of Γ_k with respect to corresponding fields. The supertrace STr in the Eq. (3.44) denotes a momentum integration and a summation over all internal indices like e.g. flavor, color, and/or Dirac indices and Φ and $\bar{\psi}$, ψ denote bosonic and (anti)fermionic fields, respectively. The cutoff function has also an appropriate matrix structure

$$\hat{R}_k = \begin{pmatrix} R_{kB} & 0 & 0 \\ 0 & 0 & R_{kF} \\ 0 & -R_{kF} & 0 \end{pmatrix}, \tag{3.46}$$

where R_{kB} denotes bosonic and R_{kF} fermionic regulator. It should be noted that the IR cutoff does not mix bosons and fermions.

The flow equation for the effective average action is a functional differential equation because of the appearance of the exact propagator $(\Gamma_k^{(2)}[\phi] + R_k)^{-1}$. Also, the bare action S enters the flow only in the form of an initial condition. A specific physical system investigated within the FRG approach is completely defined via Eq. (3.44) and the initial condition $\Gamma_\Lambda = S$. Together with a given form of the cutoff function R_k one has a closed system with no infinities in the flow equation and all microscopic physics is encoded in the microscopic effective action Γ_Λ. The reason why infinities are absent in the flow equation is because the term $\partial_k R_k$ is present. Indeed, only momenta $q^2 \leq k^2$ contribute to the flow at scale k i.e. the high momentum modes $q^2 \geq k^2$ are effectively integrated out. As a consequence we are left with a completely finite flow, both in the UV and in the IR regime.

The flow equation has also a simple one loop structure as shown in Fig. 3.3. Contrary to the perturbation theory where n-loop diagrams require n dimensional integrals, here one has to deal with only one integral.

In the end, it is interesting to note a close resemblance of the flow equation (3.44) to a one-loop equation. Indeed, for the lowest non-trivial order of the loop expansion one obtains

$$\Gamma_k[\phi] = S[\phi] + \frac{1}{2}\mathrm{Tr}\log\left(S^{(2)}[\phi] + R_k\right). \tag{3.47}$$

Now, if we take a k-derivative of Eq. (3.47) we will get a one-loop flow equation that looks very much like Eq. (3.44). If we now replace the second functional derivative of the classical action $S^{(2)}[\phi]$ with $\Gamma_k^{(2)}$ one obtains a non-perturbative flow equation[6].

3.2.3 Optimized regulator functions

We have already mentioned the particular features that cutoff R_k has to satisfy in order to serve as an IR regulator. Here, we represent a special kind of regulator functions, the so called *optimized* cutoff functions The main objective for constructing such cutoff functions is to achieve good convergence and stability properties of the flow equation. Here, we follow the line of reasoning given in [47].

It has been argued that FRG flow is well-defined if the following condition holds

$$\min_{q^2\geq 0}\left(\Gamma_k^{(2)}[\phi]\Big|_{\phi=\phi_0}+R_k(q^2)\right)=Ck^2>0. \tag{3.48}$$

Otherwise, the flow equation given in Eq. (3.44) would be ill defined at points where the full inverse propagator develops zero modes. One has to introduce an optimization criterion that consists in maximizing the gap C over the space of all possible regulator functions. This procedure should then yield a set of regulators that preserve the maximum of the gap C. Hence, the corresponding flow equation should have good convergence properties.

To put everything together, let us summarize the main features a regulator must have in order to be considered as an optimized regulator. First, it must solve the optimization criterion. Further, the choice for the regulator must be based on the stability criterion for approximate flows and finally it should lead to simple explicit expression for the flow equation. Here we will not go into details and present an explicit derivation of the optimized regulator functions. Instead, we give their general form

$$R_{B,k}^{\mathrm{opt}}(q^2)=(k^2-q^2)\theta(k^2-q^2), \tag{3.49}$$

for bosons and

$$R_{F,k}^{\mathrm{opt}}(q)=\not{q}\left(\sqrt{\frac{k^2}{q^2}}-1\right)\theta(k^2-q^2) \tag{3.50}$$

for fermions. The reader interested in more details concerning the derivation and features of these regulators is referred to Ref. [47]. The regulator functions (3.49) and (3.50) incorporate several advantages compared with other regulators used within the FRG approach. Dimensional reduction and fermion decoupling are correctly described. Also, the flow equation for the scale dependent potential at finite

[6]The replacement $S^{(2)}[\phi]\rightarrow\Gamma_k^{(2)}[\phi]$ is also known as the "full renormalization group improvement".

temperature and chemical potential that is derived using the set of optimized regulators, can be factorized into a thermal and vacuum part. Consequently, the thermal and vacuum part contribute additively to the flow. Numerical stability of the solutions of the flow equation is also achieved by using the regulators (3.49) and (3.50).

In the forthcoming chapter we will use the above mentioned regulators, slightly modify them and adapt them to suit our needs in the case for finite temperatures and chemical potential and in the presence of a gluonic background.

Chapter 4

Critical phenomena and $O(4)$ scaling

The understanding of the phase structure and the critical properties of the strongly interacting medium is one of the central problems that is addressed in the context of QCD. Lattice Gauge Theory (LGT) calculations show that at finite temperature there is a clear separation between the confined-hadronic and deconfined, quark-gluon plasma phase. Following universality arguments, it is expected, that two-flavor QCD exhibits the second order chiral phase transition and belongs to the same universality class as the $O(4)$ spin system in three dimensions [52, 53, 54, 55, 56, 57]. Consequently, the long-range properties of the chiral phase transition can be studied independently of the specific dynamics within various effective models. The chiral quark-meson model is often used as an effective realization of the low-energy sector of the QCD belonging to the $O(4)$ universality class [66]. The concept of universality allows us to study the chiral quark-meson model (or any other suitable effective model that belongs to the same $O(4)$ class) instead of QCD itself in order to extract information concerning the critical behavior. Thus, by exploring the thermodynamics near the phase transition within this model, one can unravel the leading singularities of thermodynamic quantities in two-flavor QCD at the second order chiral phase transition. Clearly, any description of the QCD chiral phase transition within the quark-meson model has some limitations. First, one cannot address to the deconfinement phenomena in QCD and second, one cannot obtain quantitative information on the thermodynamics outside the chiral critical region or on non-universal quantities like the critical temperature T_c. However, by exploring the thermodynamics of this model, we can study the problem of the universal properties related with the dynamical chiral symmetry breaking at finite temperature and/or density. In general, the phase transition and critical phenomena are connected with a singular behavior of various susceptibilities which are related to fluctuations of physical quantities. In a system with a second order phase transition there are long

range critical correlations that appear due to the presence of massless modes. This results in divergent fluctuations.

The mean field theory, often used to describe the chiral phase transition [58, 59, 42], usually fails to give a correct description of the critical phenomena since it neglects the influence of the fluctuations and non-perturbative effects near the phase transition. However, the methods based on the renormalization group (RG) can account for both these important effects (see eg. [17]). The advantage of the RG method is that it can describe physics across different momentum scales. In particular, within the RG framework one can capture the dynamics of the long-range fluctuations near the critical point. The Wilsonian RG techniques such as the functional renormalization group (FRG) are particularly useful in describing phase transitions [39].

The phase transition in the chiral quark-meson model has already been studied using different RG approaches [60, 61, 62, 63, 64, 65, 66, 67] both in the vacuum as well as in the medium at finite temperature and chemical potential. Also, various critical exponents at the critical point have also been calculated. One of the important results of the RG theory is the prediction, that near the phase transition, the models belonging to the same universality class should have the same critical exponents and the scaling functions.

In this chapter we study the universal properties of the chiral phase transition within the FRG method applied to the chiral quark-meson model. Furthermore, we also examine the scaling functions for different physical quantities and the equation of state. We obtain the critical exponents for the order parameter and its transverse and longitudinal susceptibilities as well as the correlation lengths and calculate the *effective critical exponents* in the presence of a chiral symmetry breaking field. Finally, we show a direct way for determining the critical exponents, and explore the scaling behavior of different ratios of the susceptibilities and the order parameter. We close this chapter by showing that within the FRG method and upon application of the suitable truncation of the FRG flow equation, the chiral quark-meson model exhibits the universal behavior that is quantitatively consistent with that obtained recently in the LGT calculations for the $O(4)$ spin system in three dimensions.

4.1 FRG method at finite temperature and chemical potential

We start with the chiral quark-meson model in order to explore the scaling properties of the chiral phase transition and the corresponding critical equation of state. This particular effective model is relevant for studying strongly interacting hot and dense matter with two degenerate light-quark flavors, since it is expected to belong to the same universality class as QCD at the chiral phase transition.

We use the FRG method to explore the critical properties near the chiral phase transition. The advantage we have of using this RG scheme is that we can obtain a quantitatively correct description of critical phenomena, since the influence of fluctuations and non-perturbative effects are taken into account within this method. We are also able to find an effective potential at finite temperature and density.

We start with the flow equation (3.44) written in the form where bosonic and fermionic contributions to the flow are separated. Here we do not have fermion sources (constant fermionic background) so that Eq. (3.44) reduces to

$$\partial_k \Gamma_k[\Phi,\psi] = \frac{1}{2}\mathrm{Tr}\left[\left(\Gamma_k^{(2)}[\Phi,\psi]+R_{kB}\right)^{-1}\partial_k R_{kB}\right] - \mathrm{Tr}\left[\left(\Gamma_k^{(2)}[\Phi,\psi]+R_{kF}\right)^{-1}\partial_k R_{kF}\right], \tag{4.1}$$

where $\Gamma_k^{(2)}$ denotes the second functional derivative of $\Gamma_k[\Phi,\psi]$ with respect to the field variables and corresponds to the inverse exact propagator at the scale k. The regulators R_{kB} and R_{kF} denote bosonic and fermionic cutoff functions respectively. Finally, the trace in Eq. (4.1) denotes a momentum integration and a summation over all internal indices like e.g. flavor, color, and/or Dirac indices.

The effect of fluctuations, which is of crucial importance if we want to obtain a correct picture of chiral phase transition, is gradually included in Γ_k by solving the FRG flow equation (4.1). This procedure corresponds to solving an infinite tower of coupled functional differential equations. Needless to say, such a demand poses an unavailing task. Thus, in practice one has to find a suitable truncation of this system of equations and a corresponding approximation to the effective average action. Here, we employ the following truncation for the effective action given in Euclidean space-time

$$\Gamma_k = \int d^4x \left[\frac{1}{2}Z_{\phi,k}\left(\partial_\mu\phi\right)^2 + Z_{\psi,k}\bar{\psi}\partial\!\!\!/\psi + g\bar{\psi}\left(\sigma + i\vec{\tau}\cdot\vec{\pi}\gamma_5\right)\psi + U_k(\rho)\right], \tag{4.2}$$

where the field ρ is introduced as

$$\rho = \frac{1}{2}\phi^2 = \frac{1}{2}\left(\sigma^2+\vec{\pi}^2\right), \qquad \phi = (\sigma,\vec{\pi}). \tag{4.3}$$

and the fermionic field ψ carries two flavors corresponding to the up and down quarks.

In the following we assume that each spectral function is dominated by a pole, corresponding to a quasiparticle. Furthermore, we neglect the wavefunction renormalization for both the bosonic and fermionic fields ($Z_{\phi,k} = Z_{\psi,k} = 1$), i.e. the anomalous dimension is set to zero. Thus, changes of quasiparticle properties in the medium are accounted for, but the fragmentation of single-particle strength is ignored. Finally, we neglect the scale dependence of the Yukawa coupling g in Eq. (4.2). Consequently, the only scale dependence we are left with is that of the

potential $U_k(\rho)$. This is expected to be a good approximation, since the anomalous dimension η is small in $O(4)$.

This approximation to the average effective action Γ_k in (4.2) corresponds to the local potential approximation (LPA) of the effective action, which is obtained as the leading order term in a systematic expansion in powers of the derivatives of the fields. For uniform field configurations, the effective average action Γ_k evaluated in LPA is proportional to the effective potential $U_k(\rho)$ since

$$\Gamma_k^{\mathrm{LPA}} = \int d^4x\, U_k(\rho), \tag{4.4}$$

and represents the lowest order in a derivative expansion of Γ_k. The advantage of using the LPA is that it leads to a very good convergence of the flow equation.

Our next step is to include the temperature T and the chemical potential μ. In order to do so, we treat bosons and fermions in thermal equilibrium in the standard imaginary time Matsubara formalism. In thermal equilibrium the (fermion) boson fields satisfy (anti-) periodic boundary conditions in the Euclidean time direction with periodicity $1/T$. The momentum integration in Eq. (4.1) is replaced by the Matsubara sum as follows:

$$\int \frac{d^dq}{(2\pi)^d} \to T\sum_{n\in\mathbb{Z}} \int \frac{d^{d-1}q}{(2\pi)^{d-1}} \tag{4.5}$$

where the zeroth component of the momentum integration is replaced by a sum over the discrete Matsubara frequencies

$$q_0(n) = 2n\pi T, \qquad q_0(n) = (2n+1)\pi T\,, \quad n \in \mathbb{Z} \tag{4.6}$$

for bosons and fermions respectively.

In this context, the phenomenon of *dimensional reduction* is revealed. This means that for finite temperatures a four-dimensional theory can be interpreted as a three-dimensional one. According to the replacement (4.6) there are $n \in \mathbb{Z}$ bosonic and fermionic degrees of freedom. Only the zero bosonic mode does not have a temperature-dependent effective mass term, which implies that at high temperatures all massive Matsubara modes decouple from the dynamics of the theory. Thus, what is left is a three dimensional theory with bosonic zero mode as the only relevant degree of freedom in this regime.

The finite quark chemical potential μ is introduced by the following replacement of the time derivative

$$\partial_0 \to \partial_0 + i\mu \tag{4.7}$$

in the fermionic part of the effective action (4.2).

Up to now, we have defined a truncation of the system of flow equations and included temperature and chemical potential. In addition, one also needs to specify

the regulator functions R_k. As we have already mentioned in the previous chapter, we will use the optimized cutoff functions throughout this work. However, we employ a slightly modified form of the optimized regulator, where the Euclidean 4-momentum squared q^2 is replaced by the 3-momentum squared $\mathbf{q}^2$. Thus, as a bosonic regulator function we use the following choice

$$R_{B,k}^{\text{opt}}(\mathbf{q}^2) = (k^2 - \mathbf{q}^2)\theta(k^2 - \mathbf{q}^2). \tag{4.8}$$

The fermionic cutoff function should be consistent with chiral symmetries of the system under investigation. One possibility to preserve this consistency is to require the same Lorentz structure for the fermionic regulator R_{kF} as for the kinetic term for free fermions. At finite chemical potential μ we use [48]

$$R_{F,k}^{\text{opt}}(q) = \left(\not{q} + i\mu\gamma^0\right)\left(\sqrt{\frac{(q_0 + i\mu)^2 + k^2}{(q_0 + i\mu)^2 + \mathbf{q}^2}} - 1\right)\theta(k^2 - \mathbf{q}^2). \tag{4.9}$$

Clearly, the modified regulator functions are invariant only under spatial rotations of the momentum $\mathbf{q}$ in a particular frame, but not under Euclidean rotations involving the imaginary time direction. However, this is not a crucial issue in calculations at finite temperature and chemical potential, where the heath bath anyway defines a preferred frame. Furthermore, the Euclidean invariant form leads to various difficulties, as pointed out in [68]. A great advantage of the regulators (4.8) and (4.9) is that in the quasiparticle approximation, the Matsubara sums for the one loop diagrams are identical to those appearing in a free theory.

Let us now derive the flow equation for the effective average action at finite T and μ with the above generalization. First, we note that one can separate the contributions from bosonic and fermionic fluctuations, respectively

$$\partial_k U_k(\rho) = \partial_k U_{k,B}(\rho) + \partial_k U_{k,F}(\rho). \tag{4.10}$$

We start the derivation by considering only the bosonic part of the flow in the vacuum and include temperature later.

Within the LPA, the bosonic part of the flow is given by the following expression in momentum space

$$\partial_k U_{k,B}(\rho) = \frac{1}{2}\text{Tr}\left[\left(\frac{\partial^2 U_k(\rho)}{\partial\phi_i\partial\phi_j} + (q^2 + R_{kB})\delta_{ij}\right)^{-1}\partial_k R_{kB}\right]. \tag{4.11}$$

Further, according to Eq. (4.3) the derivatives of the effective potential are

$$\frac{\partial U_k(\rho)}{\partial\phi_i} = \frac{\partial U_k(\rho)}{\partial\rho}\frac{\partial}{\partial\phi_i}\left(\frac{1}{2}\phi_n\phi_n\right) = \frac{\partial U_k(\rho)}{\partial\rho}\phi_n\delta_{in} \tag{4.12}$$

and

$$\begin{aligned}\frac{\partial^2 U_k(\rho)}{\partial\phi_i\partial\phi_j} &= \frac{\partial}{\partial\phi_j}\left(\frac{\partial U_k(\rho)}{\partial\rho}\phi_n\delta_{in}\right) = \left(\frac{\partial}{\partial\phi_j}\frac{\partial U_k(\rho)}{\partial\rho}\right)\phi_n\delta_{in} + \frac{\partial U_k(\rho)}{\partial\rho}\delta_{jn}\delta_{in} \\ &= \frac{\partial^2 U_k(\rho)}{\partial\rho^2}\phi_m\delta_{jm}\phi_n\delta_{in} + \frac{\partial U_k(\rho)}{\partial\rho}\delta_{jn}\delta_{in} \\ &= \frac{\partial^2 U_k(\rho)}{\partial\rho^2}\phi_i\phi_j + \frac{\partial U_k(\rho)}{\partial\rho}\delta_{ij}. \end{aligned} \tag{4.13}$$

For the uniform field configuration ϕ we can choose in the broken symmetry phase

$$\phi = \begin{pmatrix} \sigma \\ 0 \\ 0 \\ 0 \end{pmatrix}, \tag{4.14}$$

which gives

$$\begin{aligned}&\frac{\partial^2 U_k(\rho)}{\partial\phi_i\partial\phi_j} + (q^2 + R_{kB})\delta_{ij} = \\ &= \begin{pmatrix} U_k^{'} + 2\rho U_k^{''} + q^2 + R_{kB} & 0 & 0 & 0 \\ 0 & U_k^{'} + q^2 + R_{kB} & 0 & 0 \\ 0 & 0 & U_k^{'} + q^2 + R_{kB} & 0 \\ 0 & 0 & 0 & U_k^{'} + q^2 + R_{kB} \end{pmatrix}. \end{aligned} \tag{4.15}$$

Next, we have to invert the matrix (4.15) and compute the remaining trace over $O(4)$ indices. Finally, the bosonic part of the flow in the vacuum is then given by

$$\begin{aligned}\partial_k U_{k,B}(\rho) &= \frac{1}{2}\int\frac{d^4q}{(2\pi)^4}\left[\left(\frac{1}{U_k^{'} + 2\rho U_k^{''} + q^2 + R_{kB}} + \frac{3}{U_k^{'} + q^2 + R_{kB}}\right)\partial_k R_{kB}\right] \\ &= \frac{1}{2}\int\frac{d^4q}{(2\pi)^4}\tilde{\partial}_k\left[\log(M_\sigma^2 + q^2 + R_{kB}) + 3\log(M_\pi^2 + q^2 + R_{kB})\right], \end{aligned} \tag{4.16}$$

where we have defined a new operator

$$\tilde{\partial}_k \equiv \partial_k R_{kB}\frac{\partial}{\partial R_{kB}}, \tag{4.17}$$

that will help to bring the right hand side of the flow equation (4.16) into a form more suitable for performing the summation over the Matsubara modes. The effective masses of the sigma and pion field in Eq. (4.16) are

$$M_\sigma^2 = U_k^{'} + 2\rho U_k^{''}, \qquad M_\pi^2 = U_k^{'} \tag{4.18}$$

where the primes denote derivatives with respect to the field ρ. Evaluated at the vacuum expectation value the masses reduce to the physical masses at the scale $k = 0$.

Now, in the bosonic part of the vacuum flow (4.16) we can include a temperature T via Eq. (4.5) ($q_0 = q_0(n) = 2n\pi T$) and make use of the optimized bosonic regulator (4.8). Being now in a heath bath, we can switch our notation, and use, instead of the k-dependent effective potential $U_k(\rho)$ a scale dependent grand canonical potential $\Omega_k(T, \mu; \rho)$. In the LPA, the effective average action Γ_k is proportional to the effective potential (cf. Eq. (4.4)) and generally, the effective action Γ can be expressed in terms of the effective potential (i.e. the grand canonical potential) as

$$\Omega = \frac{T}{V}\,\Gamma\,. \tag{4.19}$$

Thus, for the bosonic contribution we have the following

$$\begin{aligned}\partial_k \Omega_{k,B}(T,\mu;\rho) &= \frac{1}{2}\int \frac{d^3\mathbf{q}}{(2\pi)^3} T \sum_{n=-\infty}^{+\infty} \frac{\partial}{\partial k}\left[\log(q_0^2+\mathbf{q}^2+M_\sigma^2+k^2-\mathbf{q}^2)\right.\\ &+ \left. 3\log(q_0^2+\mathbf{q}^2+M_\pi^2+k^2-\mathbf{q}^2)\right]. \end{aligned}\tag{4.20}$$

Due to the form of the optimized cutoff function, the momentum integration is trivial to perform, thus we are left only with the following sum over the Matsubara modes

$$\partial_k \Omega_{k,B}(T,\mu;\rho) = \frac{k^4}{6\pi^2} T \sum_{n=-\infty}^{+\infty}\left(\frac{1}{q_0^2+E_\sigma^2}+\frac{3}{q_0^2+E_\pi^2}\right) \tag{4.21}$$

where

$$E_\sigma = \sqrt{k^2+M_\sigma^2}, \qquad E_\pi = \sqrt{k^2+M_\pi^2} \tag{4.22}$$

denote the sigma and pion energies, respectively. Finally, using the standard results, we can perform the Matsubara summation as follows

$$\sum_{n=-\infty}^{+\infty}\left(\frac{1}{q_0^2+\omega^2}\right) = \frac{1}{2T\omega}\coth\left(\frac{\omega}{2T}\right). \tag{4.23}$$

Let us now turn to the fermionic part of the flow that can be written in the following form

$$\partial_k U_{k,F}(\rho) = -\mathrm{Tr}\left[\left(\Gamma_k^2 + R_{kF}\right)^{-1}\partial_k R_{kF}\right], \tag{4.24}$$

where the functional derivatives of Γ_k with respect to the fields $\bar\psi$ and ψ have to be taken in the fermion-antifermion space and read

$$\Gamma_k^2[\bar\psi,\psi] = \not{q} + i\mu\gamma_0 + g(\sigma + i\vec\tau\cdot\vec\pi\gamma_5). \tag{4.25}$$

The trace in the fermion-antifermion space represents now both, momentum integration and summation over flavor, color, and Dirac indices. Defining the fermionic analogue of the operator (4.17), summing over internal indices and using the identity $\mathrm{Tr}\log = \log\det$ we have[1]

$$\partial_k U_{k,F}(\rho) = -\nu_q \int \frac{d^4q}{(2\pi)^4}\frac{\partial}{\partial k}\log\det\Big[\not{q} + i\mu\gamma_0 + g(\sigma + i\vec{\tau}\cdot\vec{\pi}\bar{\gamma}) + R_{kF}\Big]. \tag{4.26}$$

With $\nu_q = 2N_cN_f = 12$ we have denoted the number of internal quark degrees of freedom. After calculating the determinant in (4.26) one obtains

$$\partial_k U_{k,F}(\rho) = -\nu_q \int \frac{d^4q}{(2\pi)^4}\frac{\partial}{\partial k}\log\Big((q_0 + i\mu)^2 + k^2 + M_q^2\Big), \tag{4.27}$$

where M_q is the effective quark mass

$$M_q^2 = 2\rho g^2. \tag{4.28}$$

Inclusion of temperature in (4.27) and calculation of the momentum integral (this is again trivial, due to the optimized fermionic cutoff function (4.9)) leads to the following expression for the fermionic contribution to the flow of k-dependent grand canonical potential

$$\partial_k\Omega_{k,F}(T,\mu;\rho) = -2\nu_q\frac{k^4}{6\pi^2}T\sum_{n=-\infty}^{n=+\infty}\frac{1}{(q_0 + i\mu)^2 + E_q^2}\,, \tag{4.29}$$

where we now have $q_0 = q_0(n) = (2n+1)\pi T$ and the quark energy given by

$$E_q = \sqrt{k^2 + 2\rho g^2}. \tag{4.30}$$

The sum appearing in Eq. (4.29) has to be slightly rearranged in order to perform Matsubara summation. A simple algebraic manipulation yields

$$\sum_n \frac{1}{(q_0 + i\mu)^2 + E_q^2} = \frac{1}{2E_q}\sum_n\left(\frac{E_q - \mu}{q_0^2 + (E_q - \mu)^2} + \frac{E_q + \mu}{q_0^2 + (E_q + \mu)^2}\right). \tag{4.31}$$

Finally, using again standard techniques, the Matsubara summation can be performed with the following result

$$\sum_{n=-\infty}^{+\infty}\left(\frac{1}{q_0^2 + \omega^2}\right) = \frac{1}{2T\omega}\tanh\left(\frac{\omega}{2T}\right). \tag{4.32}$$

[1]Here we deal with a determinant of $2 \times N_c \times N_f = 12$ dimensional matrix in Dirac, color and flavor space.

Now we can put all the pieces together and write down the flow equation for the scale dependent grand canonical potential $\Omega_k(T,\mu)$ within the FRG approach for the chiral quark-meson model

$$\begin{aligned}\partial_k\Omega_k(T,\mu;\rho) &= \frac{k^4}{12\pi^2}\left[\frac{3}{E_\pi}\coth\left(\frac{E_\pi}{2T}\right)+\frac{1}{E_\sigma}\coth\left(\frac{E_\sigma}{2T}\right)\right.\\ &\left.-\nu_q\frac{1}{E_q}\left(\tanh\left(\frac{E_q-\mu}{2T}\right)+\tanh\left(\frac{E_q+\mu}{2T}\right)\right)\right]. \quad (4.33)\end{aligned}$$

By rewriting Eq. (4.33) by means of occupation numbers, we obtain a more transparent form of the flow equation [48]

$$\begin{aligned}\partial_k\Omega_k(T,\mu;\rho) &= \frac{k^4}{12\pi^2}\left[\frac{3}{E_\pi}\Big(1+2n_B(E_\pi)\Big)+\frac{1}{E_\sigma}\Big(1+2n_B(E_\sigma)\Big)\right.\\ &\left.-\frac{2\nu_q}{E_q}\Big(1-n_F(E_q)-\bar{n}_F(E_q)\Big)\right]. \quad (4.34)\end{aligned}$$

Here $n_B(E_{\pi,\sigma})$ and $n_F(E_q), \bar{n}_F(E_q)$ represent the well known bosonic and fermionic distribution functions respectively,

$$n_B(E_{\pi,\sigma}) = \frac{1}{e^{E_{\pi,\sigma}/T}-1} \quad (4.35)$$

$$n_F(E_q) = \frac{1}{e^{(E_q-\mu)/T}+1}, \quad \bar{n}_F(E_q) = \frac{1}{e^{(E_q+\mu)/T}+1}. \quad (4.36)$$

In the flow equation (4.34) the vacuum and thermal contributions are clearly separated.

A this point we want to stress the fact that the flow equations (4.33) and (4.34) are identical to the ones obtained within the proper time renormalization group (PTRG) scheme [66, 46]. In fact, it was shown by Litim [47] that, in vacuum, the PTRG scheme, with a properly chosen cutoff function, is equivalent to the optimized FRG flow in the LPA.

The flow equation for $\Omega_k(T,\mu;\rho)$ is solved numerically. One can either discretize the potential on a grid or expand it in powers of the fields (σ,ρ) where ρ is given by Eq. (4.3). This means that we have simply made a change of variables $(\sigma,\pi)\to(\sigma,\rho)$. Here, we apply the second method and expand the potential $\Omega_k(T,\mu)$, except for the symmetry breaking term, in a Taylor series in a local coupling around the minimum $\sigma_0=\sqrt{2\rho_0}$,

$$\Omega_k(T,\mu) = \sum_m \frac{a_{m,k}(T,\mu)}{m!}(\rho_k-\rho_0)^m - c\sigma_k. \quad (4.37)$$

For an explicit broken symmetry ($c \neq 0$) the condition

$$\left.\frac{d\Omega_k(T,\mu)}{d\sigma}\right|_{\min} = 0 \tag{4.38}$$

determines the position of the physical minimum at the scale k. Using Eq. (4.38) we find

$$c = a_1\sigma_0 \tag{4.39}$$

which relates the coupling a_1 and the expectation value of the scalar field σ_0. In order to obtain a finite set of differential equations, we truncate the Taylor expansion in Eq. (4.37) at $m = 3$. We use the following identity

$$\frac{d\Omega_k^{'}}{dk} = \frac{\partial\Omega_k^{'}}{\partial\rho}\frac{d\rho}{dk} + \frac{\partial\Omega_k^{'}}{\partial k} \tag{4.40}$$

and the corresponding relations for $\Omega^{''}$ and $\Omega^{'''}$. In Eq. (4.40) the terms $\partial\Omega_k^{'}$ etc. are evaluated using the expansion (4.37) truncated at $m = 3$. However, it should be noted that $\partial\Omega_k/\partial\rho$ vanishes, due to the gap equation (4.38), so that $d\Omega_k/d\rho = \partial\Omega_k/\partial\rho$.

Finally, we obtain the following set of coupled differential equations

$$\frac{da_0}{dk} = \frac{c}{\sqrt{2\rho_k}}\frac{d\rho}{dk} + \partial_k\Omega_k, \tag{4.41a}$$

$$\frac{d\rho}{dk} = -\frac{1}{(c/(2\rho_k)^{3/2} + a_2)}\,\partial_k\Omega_k^{'}, \tag{4.41b}$$

$$\frac{da_2}{dk} = a_3\frac{d\rho}{dk} + \partial_k\Omega_k^{''}, \tag{4.41c}$$

$$\frac{da_3}{dk} = \partial_k\Omega_k^{'''}\,. \tag{4.41d}$$

In the following we consider only the case of vanishing chemical potential, thus we put $\mu = 0$, while the external field is kept finite in our calculations. The chiral limit is then obtained by setting $c \to 0$.

The flow equations are solved numerically starting at a cutoff scale $\Lambda = 1.2$ GeV. The initial parameters are chosen to reproduce in the vacuum the physical pion mass $m_\pi = 138$ MeV, the pion decay constant $f_\pi = 93$ MeV, the sigma mass $m_\sigma = 600$ MeV and the constituent quark mass $m_q = 300$ MeV. The strength of the external field c_0 and the Yukawa coupling ($g = 3.2$) are fixed by the pion mass and the constituent quark mass. The pion and the sigma masses at a given momentum scale k, are given by

$$m_{\pi,k}^2 = \frac{c}{\sqrt{2\rho_k}}, \quad m_{\sigma,k}^2 = \frac{c}{\sqrt{2\rho_k}} + 2\rho_k a_{2,k} \tag{4.42}$$

whereas the constituent quark mass is obtained from

$$m_{q,k}^2 = 2g^2\rho_k. \tag{4.43}$$

The numerical solution of the flow equations yields a non–perturbative thermodynamic potential at finite temperatures. This can then be used to explore the critical properties of thermodynamic observables in the vicinity of the chiral phase transition.

4.2 Critical behavior and the $O(4)$ scaling

In the chiral limit the chiral quark-meson model exhibits a second order phase transition. The critical behavior of this model (and QCD according to universality arguments) is expected to be governed by the fixed point of the $O(4)$ Heisenberg model in three dimensions. Universality class arguments lead to predictions for the functional form of various thermodynamic quantities in the vicinity of the critical temperature T_c. These all emerge from the scaling form of the singular part of the Gibbs free energy density

$$\mathcal{F}_s(t,h) = b^{-d}\mathcal{F}_s(b^{y_t}t, b^{y_h}h). \tag{4.44}$$

The scaling relation (4.44) is a direct consequence of a general RG argument regarding the scaling law of the Gibbs free energy

$$\mathcal{F}(t,h) = \mathcal{F}_r(t,h) + \mathcal{F}_s(u_1,u_2), \tag{4.45}$$

where the regular part of the Gibbs free energy density $\mathcal{F}_r(t,h)$ is an analytic function of t and h also at the critical point, and u_1, u_2 represent some scaling fields that can be associated for instance, with the temperature and external field (magnetic field, cf. Eq. (4.44)). There are two relevant parameters in $\mathcal{F}_s(t,h)$ which control the critical behavior of thermodynamic quantities: the reduced temperature t and the external field h

$$t = \frac{T-T_c}{T_c}\,, \qquad h = \frac{c}{c_0}\,. \tag{4.46}$$

The scaling relation Eq. (4.44) determines the properties of $\mathcal{F}_s$ under a scale transformation of all lengths by a factor b. All physical information concerning the phase transition can be encoded in the equation of state which relates the order parameter, external field and reduced temperature in the vicinity of the critical point. The way in which different thermodynamic quantities behave as the critical point is approached is entirely controlled by the values of the thermal, y_t and the magnetic, y_h critical exponents defined by the following relation

$$y_t = \frac{1}{\nu}, \quad y_h = \frac{1}{\nu_c} = \frac{\beta\delta}{\nu}. \tag{4.47}$$

The critical exponents are used to describe the behavior of various physical observables in the vicinity of a critical temperature T_c. In this region physical observables show a power law behavior characterized by the corresponding critical exponent. There are many critical exponents $(\alpha, \beta, \delta, \gamma, \nu, \eta)$ and some of them we calculate later in the following subsections. Here we mention also the so called hyperscaling relations that the critical exponents satisfy

$$\delta - 1 = \frac{\gamma}{\beta}, \tag{4.48a}$$
$$\gamma = \nu(2 - \eta), \tag{4.48b}$$
$$d\nu = \beta(1 + \delta), \tag{4.48c}$$
$$\alpha = 2 - d\nu. \tag{4.48d}$$

The scaling relations Eqs.(4.48b) and (4.48d) are known as Fisher's and Josephson's law respectively. We should note here the fact that Eq. (4.48d) is not valid for $d > 4$.

4.2.1 Order parameter

A phase transition involving spontaneous symmetry breaking, is signaled by the vanishing of an order parameter, when approached from the broken symmetry phase. In the quark meson model, a possible order parameter related with chiral symmetry breaking is obtained by differentiating the free energy with respect to the external field h. Thus, it follows from Eqs. (2.22) and (4.3) that the order parameter can be identified with the thermodynamic average of the sigma field

$$\langle \sigma \rangle = \sqrt{2\rho_0}. \tag{4.49}$$

In the FRG approach, the $\langle \sigma \rangle$ is directly obtained from the flow equation (4.41b). Indeed, for a given temperature T by solving the set of coupled flow equations we get $\langle \sigma \rangle$ by substituting for ρ_0 the value of ρ_k obtained at the end of the flow ($k \to 0$). In this way the order parameter contains the relevant contributions from fluctuations.

In Fig. 4.1 we show the resulting order parameter dependence on the reduced temperature t and for different values of the external field h. In the chiral limit i.e. for $h = 0$, the order parameter $\langle \sigma \rangle$ smoothly decreases with increasing T and finally vanishes exactly at the critical temperature where $t = 0$. This is a typical behavior that is expected in a system with the second order phase transition. For the finite h, the chiral symmetry of the Lagrangian is explicitly broken. The external field destroys the second order phase transition which turns into a crossover. Consequently, for small h, $\langle \sigma \rangle$ still shows a very abrupt change in a narrow temperature interval, at the so called pseudo-critical temperature. However, in this case the order parameter remains non-zero, even at very high temperatures, as seen in Fig. 4.1. Consequently, for $h \neq 0$ there is no true phase transition.

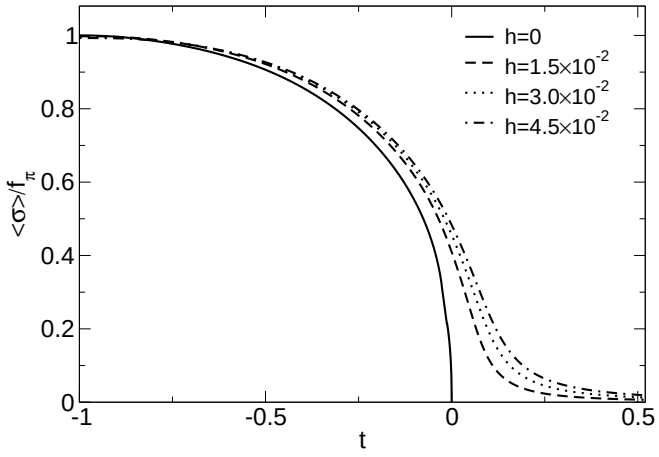

Figure 4.1: The order parameter normalized with the pion decay constant f_π in vacuum as a function of the reduced temperature t for different values of the field h.

In the vicinity of the critical point the scaling of the order parameter $\langle\sigma\rangle$ can be obtained from the universal form of the free energy. Indeed, choosing the scale factor b in the Eq. (4.44) such that $b^{y_h}h = 1$ or $b^{y_t}|t| = 1$ one gets

$$\mathcal{F}_s = h^{d\nu_c}\mathcal{F}_s(th^{-1/\beta\delta}, 1) \quad \text{for} \quad b^{y_h}h = 1 \tag{4.50a}$$

$$\mathcal{F}_s = |t|^{d\nu}\mathcal{F}_s(1, h|t|^{-\beta\delta}) \quad \text{for} \quad b^{y_t}|t| = 1\,. \tag{4.50b}$$

Consequently, from the definition of the order parameter

$$\langle\tilde{\sigma}\rangle = -\frac{\partial\mathcal{F}_s}{\partial h}\,, \tag{4.51}$$

where $\langle\tilde{\sigma}\rangle = \langle\sigma\rangle/f_\pi$ is the reduced order parameter one finds the corresponding equation of state for the magnetization

$$\langle\tilde{\sigma}\rangle = h^{1/\delta}F_h(z) \tag{4.52}$$

and

$$\langle\tilde{\sigma}\rangle = |t|^\beta\mathcal{F}_s'(1, h|t|^{-\beta\delta}), \tag{4.53}$$

with $z \equiv th^{-1/\beta\delta}$ and with the universal function $F_h(z)$ obtained from Eq. (4.50a) by differentiation with respect to the h following Eq. (4.51).

The Eqs. (4.52) and (4.53) result in the well known scaling behavior of the magnetization

$$\langle\tilde{\sigma}\rangle = \begin{cases} B(-t)^\beta, & h = 0,\ t < 0 \\ B_c h^{1/\delta}, & t = 0,\ h > 0 \end{cases}\,, \tag{4.54}$$

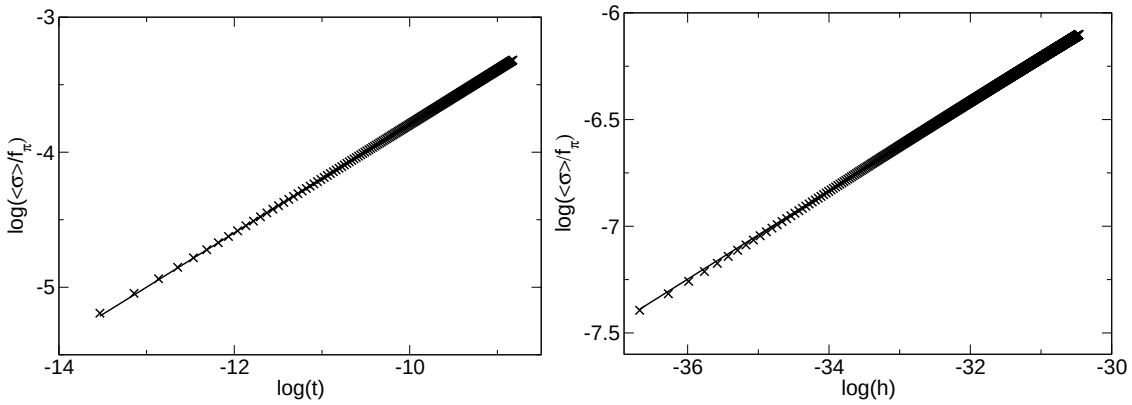

Figure 4.2: The critical exponent β (left panel) and δ (right panel). See text for details.

where B and B_c are the amplitudes of the magnetization at the critical point ($t = 0$) and at the so called coexistence line ($t < 0$, $h = 0$) [78]. The scaling behavior of the order parameter in the chiral limit, when approaching the critical temperature $t = 0$ from below, is controlled by the critical exponent β. Thus, β can be obtained as the slope of the logarithm of $\langle\tilde{\sigma}\rangle$ if plotted as a function of $\log(t)$. On the other hand, the critical exponent δ controls the scaling behavior of $\langle\tilde{\sigma}\rangle$ at the critical point $t = 0$ as $h \to 0$.

Fig. 4.2 shows the scaling properties of $\langle\tilde{\sigma}\rangle$ close to the critical point ($t \to 0$) for vanishing external field as well as the scaling with h at the (pseudo)critical point ($t = 0$).

In both cases the order parameter calculated in the quark-meson model within the FRG method shows a scaling behavior that is expected from the Eq. (4.44). This demonstrates that, in the parameter range considered, the free energy of the quark-meson model is dominated by the singular part (cf. Eq. (4.44)). Applying a linear logarithmic fit to the results from Fig. 4.2 we have obtained the following values for the critical exponents

$$\beta \simeq 0.402 \qquad \text{and} \qquad \delta \simeq 4.818. \tag{4.55}$$

In the mean field approximation one also finds scaling of the order parameter $\langle\sigma\rangle$ close to the critical point, but with different critical exponents, $\beta = 0.5$ and $\delta = 3$. Thus, the singularity at the chiral phase transition is modified substantially by fluctuations.

The values (4.55) of β and δ obtained from the fit to the functional dependencies of $\langle\tilde{\sigma}\rangle$ shown in the Fig. 4.2 are consistent with that expected in the $O(4)$ universality class. Indeed, in a Monte Carlo simulation of the three-dimensional $O(4)$ spin model, Kanaya and Kaya [76] find $\beta = 0.3836(46)$ and $\delta = 4.851(22)$. The agreement with

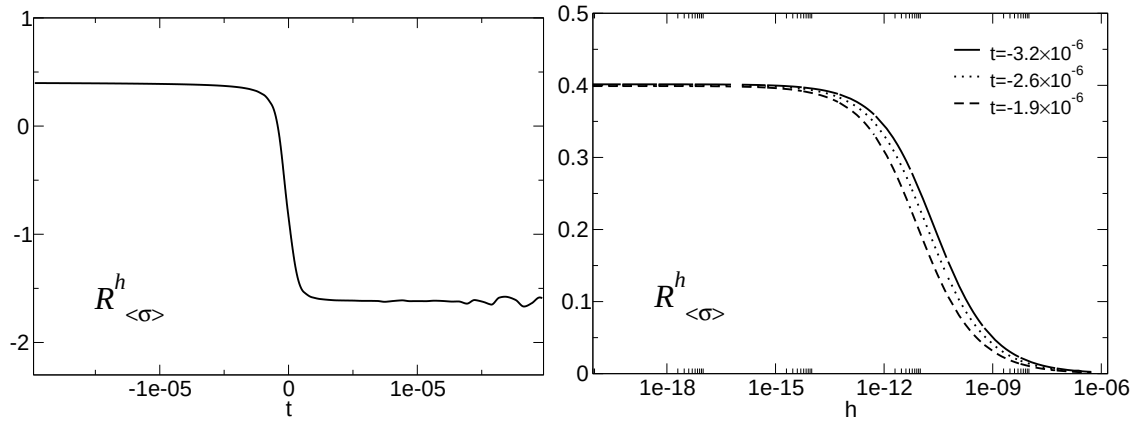

Figure 4.3: The left-hand figure: the ratio $R^h_{\langle\sigma\rangle}$ as a function of t calculated at fixed $h = 5.65 \times 10^{-13}$. The right-hand figure: the ratio as a function of h for three different values of the reduced temperature t.

this precision calculation is satisfactory, given our simple Ansatz. Consequently, we conclude that the critical properties of the chiral order parameter in the quark-meson model are indeed governed by the $O(4)$ universality class. Our results, obtained in the relatively simple LPA, illustrate the efficiency of the FRG approach to correctly account for a non-perturbative, long distance physics near a phase transition.

In the formulation of the flow equation for the quark-meson model we have neglected the wavefunction renormalization for both bosonic and fermionic fields. The coincidence of our critical exponents for chiral order parameter with $O(4)$ lattice results as well as with the previous studies [61] which account for anomalous dimension in the FRG flow, indicates that this effect is not of particular relevance when quantifying the singular properties of the order parameter at the chiral phase transition.

So far we have discussed the scaling of the order parameter $\langle\sigma\rangle$ with t for $h = 0$ in the chirally broken phase and with h at $t = 0$. In the chiral limit, the order parameter vanishes identically in the symmetric phase, i.e. for $t > 0$. Thus, the order parameter does not exhibit a singularity when the critical point is approached from above. However, since for $h \neq 0$ the order parameter is always non-zero, it is interesting to explore its behavior for small but finite values of h, when the critical point is approached from the broken ($t < 0$) as well as from the symmetric ($t > 0$) phase. The scaling behavior is in this case characterized by a so-called effective critical exponent [69, 70].

For a given h, this exponent is defined by

$$R^h_{\langle\sigma\rangle} \equiv \frac{d\log\langle\tilde{\sigma}\rangle}{d\log t} = \frac{t}{\langle\tilde{\sigma}\rangle}\frac{\partial\langle\tilde{\sigma}\rangle}{\partial t}. \tag{4.56}$$

From Eqs. (4.54) and (4.56) it is clear that for $h = 0$ and $t < 0$, $R^{h=0}_{\langle\sigma\rangle}$ coincides with the critical exponent β. For $h \neq 0$, Eq. (4.56) can be used to extract the leading singularity of the order parameter in the symmetric region close to the critical point.

In the left panel of Fig. 4.3 we show the resulting dependence of the effective critical exponent (4.56) on the reduced temperature for a fixed, very small, value of the field h. The exponent $R^h_{\langle\sigma\rangle}$ exhibits the expected scaling behavior. In the broken ($t < 0$) as well as in the symmetric ($t > 0$) phase, it is essentially independent of t. However, the effective critical exponents are different in the broken and symmetric phases.

In the broken phase ($t < 0$) the exponent $R^h_{\langle\sigma\rangle}$ is consistent with the value of the critical exponent β, extracted from the scaling properties (4.54) of the order parameter. This observation is confirmed by the right panel of Fig. 4.3, where we show the dependence of the effective critical exponent upon h in the broken phase for three different values of t. Clearly, in the limit $h \to 0$ and for a small t, the $R^h_{\langle\sigma\rangle}$ converges to the critical exponent β obtained from the logarithmic fit to the temperature dependence of $\langle\tilde{\sigma}\rangle$, shown in Fig. 4.2.

Also in the symmetric phase ($t > 0$), the exponent $R^h_{\langle\sigma\rangle}$ shows a power law behavior, however with a different value of the exponent. In the transition region, $R^h_{\langle\sigma\rangle}$ behaves like a smoothened step function, interpolating between the asymptotic regions. The sharpness of the step depends on the value of h. The effective critical exponent changes from $R^h_{\langle\sigma\rangle} \simeq 0.4$ in the broken phase to $R^h_{\langle\sigma\rangle} \simeq -1.5$ in the symmetric phase near $t = 0$. This change in the critical behavior of the order parameter can be understood using the universal scaling behavior of the singular part of the free energy. To see this, we first write the equation of state (4.52) and (4.53) in the Widom-Griffiths form

$$y = f(x), \tag{4.57}$$

where

$$y \equiv \frac{h}{\langle\tilde{\sigma}\rangle^{\delta}} \quad , \quad x \equiv \frac{t}{\langle\tilde{\sigma}\rangle^{1/\beta}}. \tag{4.58}$$

The scaling relations (4.54) are, modulo constant factors, obtained if $f(0) = 1$ and $f(-1) = 0$. The constant factors are recovered by a simple rescaling of t and h. A comparison of the Widom-Griffits form of the equation of state (4.57) with that given in Eq. (4.52), shows that the following relations hold:

$$F_h(z) = f(x)^{-1/\delta} \quad , \quad z = xy^{-1/\beta\delta}. \tag{4.59}$$

Consequently, the Eq. (4.52) can be written as

$$\langle\tilde{\sigma}\rangle = B_c h^{1/\delta} f(x)^{-1/\delta}, \tag{4.60}$$

where we have reinstated the constant factor B_c.

This equation of state can be used to explore the scaling properties of $\langle\tilde{\sigma}\rangle$ when approaching the critical point from the symmetric phase. For $t > 0$ and for $h \to 0$, the chiral order parameter (normalized to its value in vacuum) is very small. Consequently, the argument x of the function $f(x)$ in equation (4.60) is very large and the scaling behavior of $\langle\tilde{\sigma}\rangle$ for $t > 0$ and for small but finite h is determined by the asymptotic form of the scaling function $f(x)$ for $x \to \infty$. In this limit, $f(x)$ is given by Griffiths' analyticity condition [79],

$$f(x) = \sum_{n=1}^{\infty} f_n x^{\gamma - 2(n-1)\beta}. \tag{4.61}$$

Approximating the scaling function $f(x)$ by the leading term, $f(x) \simeq x^{\gamma}$ and following the Eq. (4.60), one finds that for $t > 0$ and $h \to 0$ the equation of state scales as

$$\begin{aligned} \langle\tilde{\sigma}\rangle &= B_c h^{1/\delta} f(x)^{-1/\delta} \sim h^{1/\delta} x^{-\gamma/\delta} \\ &= h^{1/\delta} \left(t\langle\tilde{\sigma}\rangle^{-1/\beta}\right)^{-\gamma/\delta} \\ &= h^{1/\delta} t^{-\gamma/\delta} \langle\tilde{\sigma}\rangle^{\gamma/\beta\delta}. \end{aligned} \tag{4.62}$$

From the last line in (4.62) one has

$$\langle\tilde{\sigma}\rangle^{1-\gamma/\beta\delta} = h^{1/\delta} t^{-\gamma/\delta} \;\longrightarrow\; \langle\tilde{\sigma}\rangle = t^{-\gamma} h, \tag{4.63}$$

where we have used the hyperscaling relation Eq. (4.48a). Thus, for $t > 0$ and $h \neq 0$, the order parameter diverges for $t \to 0$, while for $h = 0$ it vanishes identically, indicating that this equation remains correct also in the chiral limit.

From the scaling behavior of $\langle\tilde{\sigma}\rangle$ shown in the left panel of Fig. 4.3, we find $\gamma \simeq 1.6$. This is consistent with the lattice result for the $O(4)$ spin system obtained in Ref. [76], $\gamma \simeq 1.5$. Thus, the FRG method applied to the quark meson model yields a scaling behavior of the order parameter, which is consistent with that found for the $O(4)$ universality class. This is the case at the critical point, on the coexistence line and when approaching the critical point from the high temperature phase for a finite value of the external magnetic field.

4.2.2 Chiral susceptibility

The critical properties of a thermodynamic system can be explored by studying the fluctuations of various observables. In particular, the fluctuations of the order parameter are a sensitive probe of the order of the phase transition and the position of a possible critical end point. In statistical physics, fluctuations are reflected in the corresponding susceptibilities χ. In the case of the chiral order parameter, the corresponding susceptibility is defined as the response to a change of the external

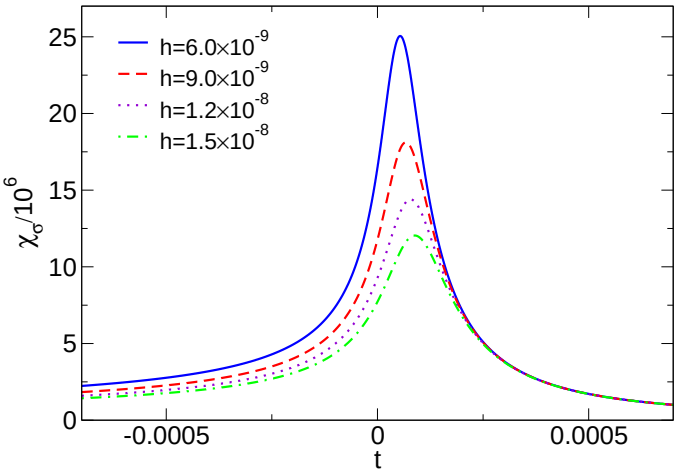

Figure 4.4: Normalized susceptibility χ_σ as a function of the reduced temperature t for different values of the field h.

field h; the susceptibility χ is obtained by taking the second derivative of the effective potential with respect to h. The susceptibility in other channels is computed analogously. It follows that the susceptibilities are inversely proportional to the corresponding mass squared. Consequently, the divergence of a susceptibility, e.g. at the critical end point, signals a zero-mass mode of some effective field.

In the chiral quark-meson model, we are not only dealing with a massless sigma field but also with a pseudo-Goldstone mode, controlled by the pion mass. The sigma and the pion represent the longitudinal and transverse modes of the $O(4)$ field ϕ, respectively. Consequently, one distinguishes between the longitudinal and transverse order parameter susceptibilities.

The longitudinal susceptibility is introduced as the usual derivative of the magnetization with respect to the external field

$$\chi_l = \chi_\sigma = \frac{\partial \langle \tilde{\sigma} \rangle}{\partial h}, \tag{4.64}$$

whereas the transverse susceptibility, which is directly related to the fluctuation of the Goldstone modes, is obtained from

$$\chi_t = \chi_\pi = \frac{\langle \tilde{\sigma} \rangle}{h}. \tag{4.65}$$

The latter expression is a direct consequence of the $O(4)$ invariance of the free energy for $h = 0$ and follows from the corresponding Ward identity [74].

The critical behavior of the longitudinal and transverse chiral susceptibility can be obtained from the scaling form of the singular part of the free energy or directly

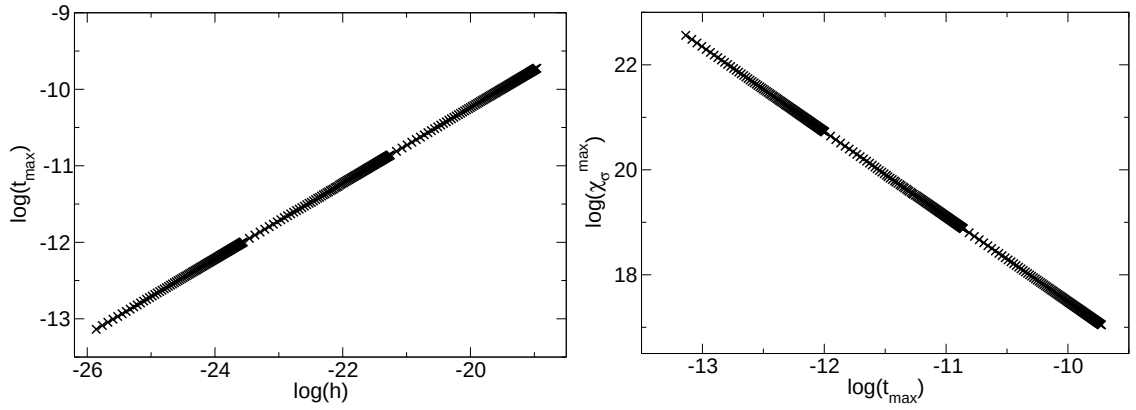

Figure 4.5: Scaling of the pseudo-critical temperature corresponding to the maximum of the χ_σ (left panel) and the scaling of the maxima of χ_σ (right panel).

from the magnetic equation of state (4.60). In Fig. 4.4 we show the longitudinal susceptibility normalized to its value in vacuum (χ_σ/χ_0) as a function of the reduced temperature for several values of the symmetry breaking field h. At finite h, this susceptibility shows a peak structure with a maximum at the pseudo-critical temperature $t_{\max}(h)$. With decreasing h, there is a shift of $t_{\max}$ and an increase of the fluctuations at the pseudo-critical point. In the chiral limit χ_σ diverges at the transition temperature, because the mass of the sigma field vanishes.

Using the results shown in the Fig. 4.4, one can define a pseudo-critical line in the (t, h)-plane that characterizes the dependence of the transition temperature $t_{\max}$ on the symmetry breaking field h. Renormalization group arguments imply that the pseudo-critical temperature and the maximum of the longitudinal susceptibility should exhibit universal scaling according to [75]:

$$t_{\max}(h) \simeq T_p h^{1/(\gamma+\beta)}, \quad \chi_\sigma(t_{\max}, h) \simeq C_p t_{\max}^{-\gamma}, \tag{4.66}$$

with $O(4)$ critical exponents.

In Fig. 4.5 we confront the scaling behavior of the susceptibility with Eq. (4.66). The critical exponents are extracted by performing a linear logarithmic fit to the pseudo-critical temperature and the maximum value of the susceptibility. We find,

$$1/(\gamma+\beta) = 0.494 \qquad \text{and} \qquad \gamma = 1.618\,,$$

which implies $\beta = 0.406$, in good agreement with the results obtained above using Eqs. (4.54) and (4.63). Thus, the scaling of χ_σ with the symmetry breaking field h is also consistent with $O(4)$ universality.

In the symmetric phase the longitudinal and the transversal susceptibility should coincide ($\chi_\sigma = \chi_\pi$). In addition, the strength of the singularities of both these

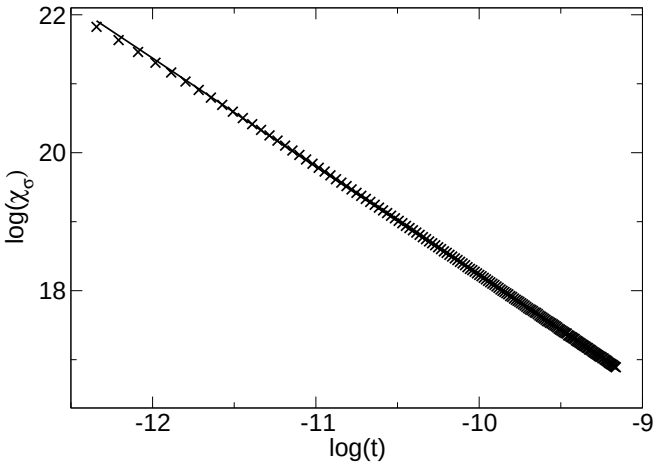

Figure 4.6: The logarithm of the susceptibility for $h \to 0$ for different values of $\log(t)$ in the symmetric phase. The solid line is a linear fit.

susceptibilities at the critical point $t = 0$ should be controlled by the same critical exponents. To find the right scaling behavior of susceptibilities when approaching the critical point from the symmetric phase we use the Widom-Griffits form of the equation of state (4.60) together with the large-x expansion of the scaling function $f(x)$. From Eqs. (4.63), (4.64) and (4.65) it is clear that in the symmetric phase $(t > 0)$ and $h \to 0$

$$\chi_\sigma = \chi_\pi \simeq t^{-\gamma}. \tag{4.67}$$

Thus, when approaching the critical point from the symmetric phase the scaling behavior of the longitudinal and transverse susceptibility should be controlled by the critical exponent γ. Fig. 4.6 shows the scaling behavior of the susceptibility for $t > 0$ and in the limit of $h \to 0$. From the slope of the line we obtain

$$\gamma = 1.575.$$

This value of the critical exponent γ differs only slightly from that obtained when analyzing the scaling of the maxima of the χ_σ following the Eq. (4.66). One of the reasons for this small difference can be traced back to the problem with an exact determination of the critical temperature.

In the broken phase, along the coexistence line, the longitudinal and transverse susceptibilities show different critical behavior. In the chiral limit, the order parameter is finite in the broken phase as long as $t < 0$. Thus, knowing that the transverse susceptibility χ_π is directly related to the order parameter through Eq. (4.65), one expects that it diverges as

$$\chi_\pi \sim h^{-1} \qquad \text{for} \qquad T < T_c \tag{4.68}$$

due to the appearance of the Goldstone bosons. A less obvious result is the expected divergence of the longitudinal susceptibility on the coexistence line where the leading order term has a divergence of the form [57]

$$\chi_\sigma \sim h^{-1/2} \qquad \text{for} \qquad T < T_c. \tag{4.69}$$

The scaling properties of the longitudinal and the transverse susceptibilities can be directly obtained from the Widom-Griffiths form of the equation of state. Let us start with the longitudinal susceptibility χ_σ that has the following scaling

$$\chi_\sigma = B_c h^{1/\delta-1} \frac{\beta f(x)^{1-1/\delta}}{\beta\delta f(x) - x f'(x)}\,. \tag{4.70}$$

Starting from Eqs. (4.60) and (4.64) we have

$$\begin{aligned} \chi_\sigma &= \frac{\partial\langle\tilde{\sigma}\rangle}{\partial h} = \frac{\partial}{\partial h}\left(B_c h^{1/\delta} f(x)^{-1/\delta}\right) \\ &= \frac{1}{\delta} B_c h^{1/\delta-1} f(x)^{-1/\delta} - \frac{1}{\delta} B_c h^{1/\delta} f(x)^{-1/\delta-1} f'(x) \frac{\partial x}{\partial h}. \end{aligned} \tag{4.71}$$

In order to proceed, we have to find the derivative $\partial x/\partial h$. Indeed, using Eq (4.58) one gets

$$\frac{\partial x}{\partial h} = \frac{\partial}{\partial h}\left(\frac{t}{\langle\tilde{\sigma}\rangle^{1/\beta}}\right) = -\frac{t}{\beta}\frac{1}{\langle\tilde{\sigma}\rangle^{1/\beta+1}}\frac{\partial\langle\tilde{\sigma}\rangle}{\partial h} = -\frac{x}{\beta}\frac{1}{\langle\tilde{\sigma}\rangle}\chi_\sigma. \tag{4.72}$$

Now, plugging this result back into Eq. (4.71) yields the following expression

$$\begin{aligned} \chi_\sigma &= \frac{1}{\delta} B_c h^{1/\delta-1} f(x)^{-1/\delta} + B_c h^{1/\delta} \frac{x}{\beta\delta}\frac{1}{\langle\tilde{\sigma}\rangle} f(x)^{-1/\delta-1} f'(x)\chi_\sigma \\ &= \frac{1}{\delta} B_c h^{1/\delta-1} f(x)^{-1/\delta} + \frac{x}{\beta\delta} f(x)^{-1} f'(x)\chi_\sigma \end{aligned} \tag{4.73}$$

where we have used Eq. (4.60) in the last step. By solving the above equation for χ_σ, we finally obtain Eq. (4.70). For the scaling of the transverse susceptibility χ_π one gets

$$\chi_\pi = B_c h^{1/\delta-1} f(x)^{-1/\delta}, \tag{4.74}$$

which is trivial to obtain using Eqs. (4.60) and (4.65).

Now, we will scrutinize the behavior of susceptibilities in the broken phase. It has been already mentioned that both, χ_σ and χ_π diverge as $h^{-1/2}$ and h^{-1} respectively for all $T < T_c$. Indeed, from the scaling behavior of $\langle\sigma\rangle$ in the broken phase i.e. at the coexistence line (4.54) and using Eq. (4.65) follows

$$\chi_\pi \sim h^{-1}(-t)^\beta. \tag{4.75}$$

This scaling behavior could also be obtained from Eq. (4.74). The scaling of χ_σ is less trivial to obtain, but still feasible and fortunately, not tedious. However, some

approximation of the scaling function $f(x)$ has to be used. In the vicinity to the coexistence line where $x \to -1$ the scaling function was shown to behave as [78]

$$f(x) \approx (1+x)^2, \tag{4.76}$$

with

$$1 + x = a_1 y^{1/2} + a_2 y + \dots \tag{4.77}$$

for the system in three dimensions. Having these results at hand, Eq. (4.70) can be rewritten as

$$\chi_\sigma \simeq h^{1/\delta-1} \frac{(1+x)^{2-2/\delta}}{\beta\delta(1+x)^2 - 2x(1+x)} = h^{1/\delta-1} \frac{(1+x)^{1-2/\delta}}{\beta\delta(1+x) - 2x} \simeq h^{1/\delta-1}(1+x)^{1-2/\delta}. \tag{4.78}$$

In the last step we have used the fact that the denominator is approximately constant for $x = -1$. Now, the next approximation we use is Eq. (4.77) that together with Eq. (4.58) yields

$$\chi_\sigma \simeq h^{1/\delta-1} y^{1/2-1/\delta} = h^{1/\delta-1} \left(h\langle\tilde{\sigma}\rangle^{-\delta}\right)^{1/2-1/\delta} = h^{-1/2}\langle\tilde{\sigma}\rangle^{-\delta/2+1}. \tag{4.79}$$

Again, we make use of our knowledge of how $\langle\tilde{\sigma}\rangle$ scales for $T < T_c$ given by Eq. (4.54) and finally obtain

$$\chi_\sigma \sim h^{-1/2}(-t)^{\beta-(\beta\delta)/2}. \tag{4.80}$$

Consequently, Eqs. (4.80) and (4.75) clearly show, how the longitudinal and transverse susceptibilities diverge in the broken phase and near the coexistence line. Fig. 4.7 shows the behavior of the longitudinal and transverse susceptibilities as a function of t and h near the coexistence line as obtained in the quark meson model within the FRG method. Both susceptibilities show the scaling behavior as expected from the Eqs. (4.80) and (4.75). From the linear fit to the results in the Fig. 4.7–left we get the values 0.499 and 1.000 for the critical exponents of the χ_σ and χ_π susceptibilities respectively. These results are in excellent agreement with that expected from the Eqs. (4.80) and (4.75). The corresponding fit to χ_σ and χ_π in Fig. 4.7-right gives,

$$(\beta - \beta\delta/2) = -0.617 \qquad \text{and} \qquad \beta = 0.395,$$

the values that are also consistent with our previous findings for the critical exponents β and δ calculated from the scaling of the order parameter.

In order to show the scaling behavior of the longitudinal and transverse susceptibility in a broad parameter range which covers the broken and symmetric phase we introduce the ratio

$$R^h_{\chi_{\pi,\sigma}} = \frac{t}{\chi_{\pi,\sigma}} \frac{\partial\chi_{\pi,\sigma}}{\partial t} \tag{4.81}$$

for the transverse χ_π and the longitudinal χ_σ susceptibilities. The quantity $R^h_{\chi_{\pi,\sigma}}$, similarly to (4.56) defines an effective critical exponent. In the Fig. 4.8 we summarized the t and h dependence of the $R^h_{\chi_\pi}$ and $R^h_{\chi_\sigma}$ in the vicinity of the critical point.

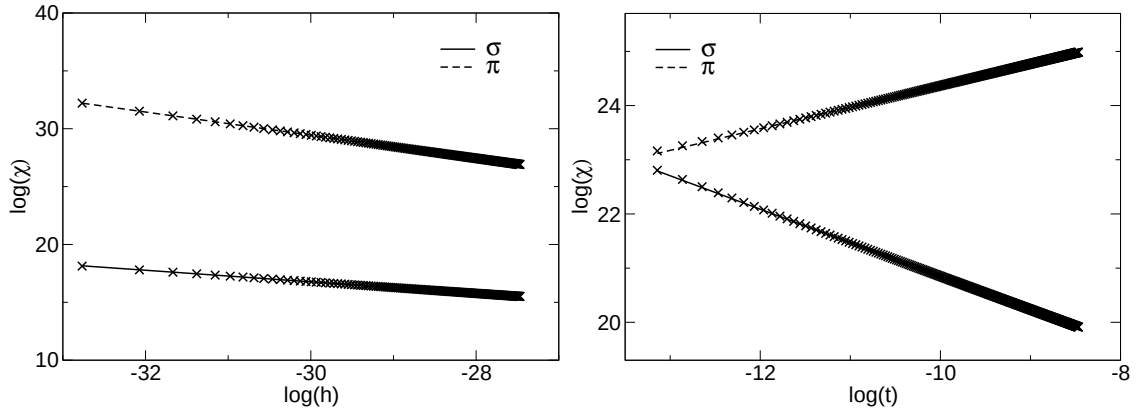

Figure 4.7: Critical exponents for the χ_σ and χ_π in the broken phase ($t < 0$) close to the critical point. See text for details.

In the left-hand figure we illustrate how the critical exponents of the susceptibilities are changing from the broken to symmetric phase for a fixed h. In the right-hand figure we show the h–dependence of $R^h_{\chi_{\pi,\sigma}}$ in the symmetric phase for a few values of t.

In the symmetric phase χ_π and χ_σ coincide, thus their critical behavior is determined by the same exponent ($\gamma \sim 1.58$) as obtained from the Fig. 4.8-left. This scaling of $R^h_{\chi_{\pi,\sigma}}$ is also shown in the Fig. 4.8-right for fixed $t > 0$ as a function of h.

In the broken phase (see Fig. 4.8–left) there is a clear splitting in the numerical values of the critical exponents,

$$R^h_{\chi_\pi} \sim \beta$$

and

$$R^h_{\chi_\sigma} \sim \beta(1 - \delta/2)$$

indicating a different sensitivity of the longitudinal and the transverse susceptibilities to the chiral symmetry breaking.

The coincidence of the transverse and longitudinal susceptibilities and their similar scaling properties at the transition point, can be used to directly obtain the critical exponent δ [71, 72, 73]. Indeed, considering the ratio of χ_π and χ_σ such that

$$\Delta(t, h) = \frac{\chi_\pi^{-1}}{\chi_\sigma^{-1}} = \frac{h\chi_\sigma}{\langle\tilde{\sigma}\rangle} \tag{4.82}$$

and applying the scaling behavior of the chiral susceptibilities one finds that

$$\lim_{h\to 0} \Delta(t, h) = \begin{cases} 1, & t > 0 \\ 1/\delta, & t = 0 \\ 0, & t < 0 \end{cases} \tag{4.83}$$

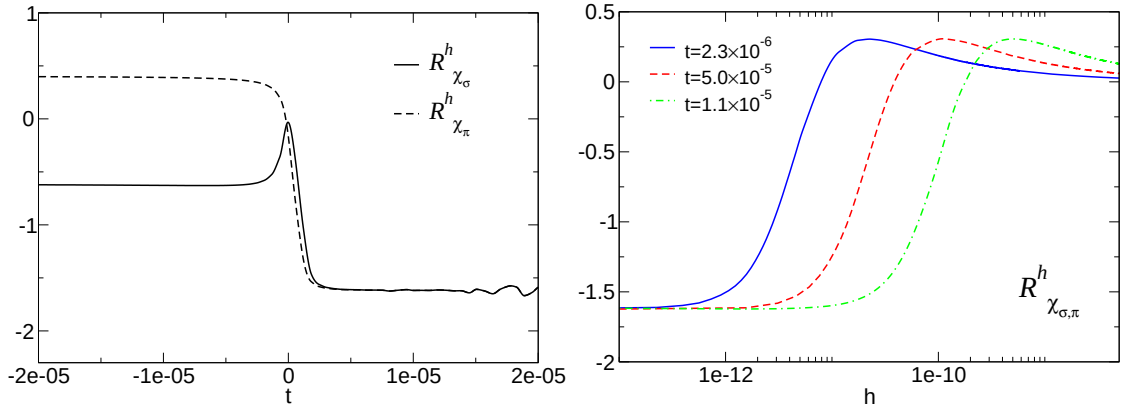

Figure 4.8: The $R^h_{\chi_{\sigma,\pi}}$ ratio as a function of h at different temperatures in the symmetric phase ($t > 0$) (right panel) and $R^h_{\chi_{\sigma,\pi}}$ as a function of t for small h (left panel).

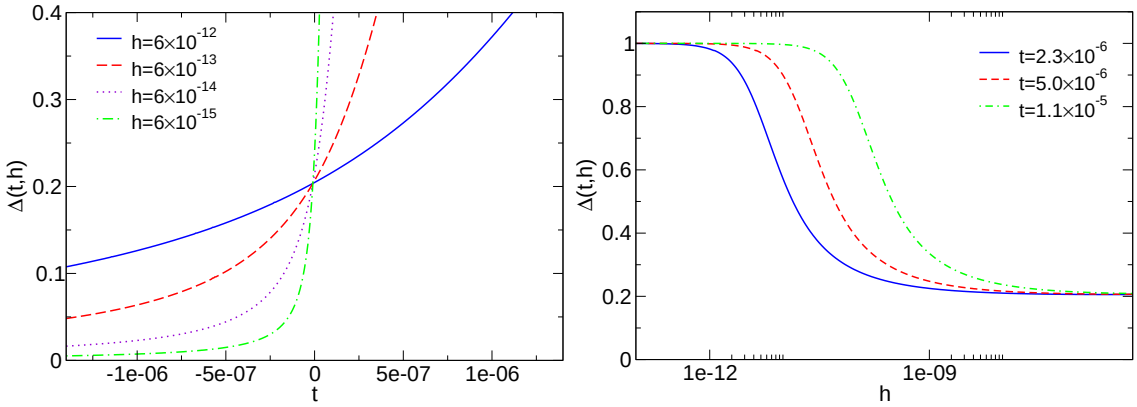

Figure 4.9: The ratio $\Delta(t, h)$ from the Eq. (4.82) as a function of the reduced temperature t and the external field h. The crossing point, in the left-hand figure is given by the coordinate $(0, 1/\delta)$.

Consequently, $\Delta(t,h)$ can be used to directly extract the value of the critical exponent δ without any logarithmic fits. In addition, this ratio can also be used to find a position of the critical point where all $\Delta(t,h)$ are plotted as a function of t for different values of h crosses.

In the Fig. 4.9-left we show the resulting behavior of $\Delta(t,h)$ as a function of t for different values of h. As expected all lines for different h cross at $t=0$ giving

$$\delta \approx 4.91.$$

This value slightly deviates from that obtained previously using a logarithmic fit but agrees better with the LGT expectations [71].

Fig. 4.9-right shows the scaling of $\Delta(t,h)$ as a function of h for fixed $t>0$. In the chiral limit, that is for $h=0$ the longitudinal and transverse susceptibility coincide, thus $\Delta(t,h)=1$ as seen in this figure. On the other hand for $h\to\infty$, $\Delta(t,h)\to 1/\delta$. The last behavior is a direct consequence of the equation of state (4.53) and the definition (4.82). Indeed, from these equations one finds that

$$\Delta(t,h) = \frac{h\chi_\sigma}{t^\beta \mathcal{F}_s'(1,ht^{-\beta\delta})} \simeq F(h/t^{\beta\delta})\,,$$

with $F(x)$ being some scaling function. Consequently, the limits $t\to 0$ at finite h or $h\to\infty$ at finite t should result in the same value of $\Delta(t,h)$.

4.2.3 Correlation length

The phase transition can be identified not only by considering the critical behavior of the order parameter or its susceptibilities, but also the correlation length ξ which governs the exponential decay of the correlation function. The correlation length is quantified by the relevant mass scale in a system. In the chiral model considered here, there are two relevant mass scales, the transverse mass connected to the pion and the longitudinal mass related to the sigma field. Consequently, one introduces the transverse ξ_π and the longitudinal ξ_σ correlation lengths. In the critical region the ξ_t and ξ_l can also be connected with the corresponding susceptibilities [77]

$$\chi_l \sim \xi_l^2 \quad , \quad \chi_t \sim \xi_t^2. \tag{4.84}$$

Consequently, in the chiral quark-meson model, the correlation lengths are connected with the pion and the sigma masses

$$\xi_\sigma \sim \frac{1}{m_\sigma}, \quad \xi_\pi \sim \frac{1}{m_\pi}. \tag{4.85}$$

Fig. 4.10 shows the correlation lengths, ξ_σ and ξ_π calculated at the critical point $t=0$ as a function of the external field h. Both, ξ_σ and ξ_π diverge as $h\to 0$. This

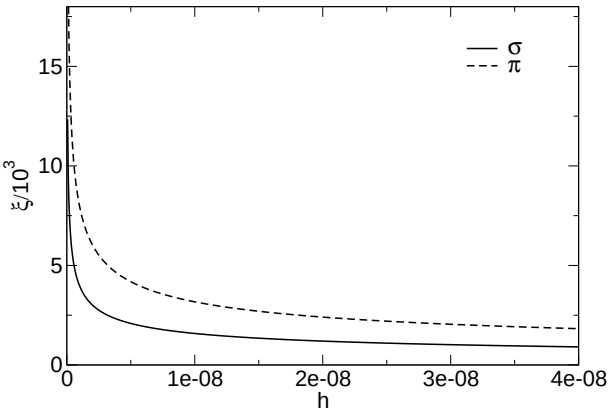

Figure 4.10: Correlation lengths ξ_σ and ξ_π at the critical point $t = 0$ as a function of the external field h.

behavior is clear since a divergence of the longitudinal and the transverse correlation length is expected to signal the second order phase transition and the Goldstone mechanism respectively. The scaling of the correlation length in the critical region can be obtained from the scaling function (4.44) and the relation (4.84).

On the critical line ($t = 0, h \to 0$) the transverse and longitudinal correlation lengths have the same behavior controlled by the exponent ν_c [57]

$$\xi_{\sigma,\pi} \sim h^{-\nu_c}, \tag{4.86}$$

In the symmetric phase ($t > 0$) the correlation lengths ξ_σ and ξ_π coincide and

$$\xi_{\sigma,\pi} \sim t^{-\nu}. \tag{4.87}$$

Thus, their critical behavior is controlled by the critical exponent ν.

In Fig. 4.11 we show the scaling behavior of the correlation lengths at the critical line in the symmetric phase. From the slopes of the fitted lines one gets the values of the critical exponents

$$\nu_c = 0.396 \qquad \text{and} \qquad \nu = 0.787.$$

In the broken phase ($t < 0$) and near the coexistence line the critical behavior of the transverse and longitudinal susceptibility should be different. The critical exponents for ξ_σ and ξ_π in the broken phase can be directly obtained from the corresponding susceptibilities following definition (4.84). Thus, as in the Fig. 4.8 ξ_σ and ξ_π exhibit two different effective critical exponents in the broken phase ($t < 0$) and a common exponent in the symmetric phase

We compare our results with the recent lattice findings and the mean field theory for the $O(4)$ model. The mean field values clearly deviate from those obtained

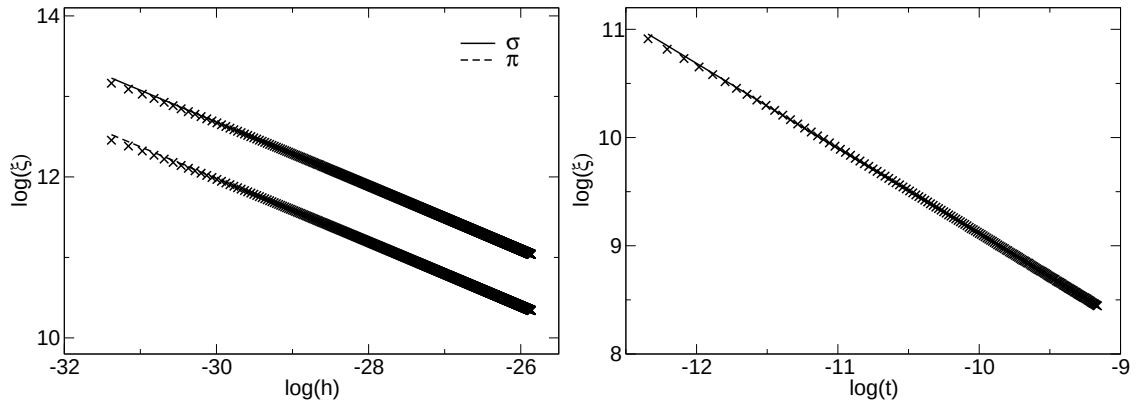

Figure 4.11: The critical exponent ν_c for correlation lengths ξ_σ and ξ_π on the critical line $t = 0$ (left panel) and the critical exponent ν in the symmetric phase $t > 0$ (right panel). The solid lines represent linear fits.

within the FRG approach, showing the importance of quantum fluctuations near the critical point. Our results for different critical exponents are found to be in a quite good agreement with the Monte Carlo lattice results [76] in spite of the fact, that we have neglected the anomalous dimension terms in the flow equation. The scale η, of the anomalous dimension defined as

$$\eta \equiv -\frac{\partial}{\partial t} \log Z, \tag{4.88}$$

where Z is the wavefunction renormalization can be extracted through the hyper-scaling relation

$$\delta = \frac{d + 2 - \eta}{d - 2 + \eta}, \tag{4.89}$$

which together with our value for δ results in

$$\eta \approx 0.031.$$

This result appears in the range obtained within LGT calculations where ($\eta = 0.0254$ [76]). The small value of η explains why the anomalous dimension leads to a rather small corrections for different exponents and the scaling properties of the physical observables within the FRG approach. We have summarized our results for different critical exponents in Table 4.1.

4.3 Conclusions

In this chapter we have discussed the critical properties of the quark-meson effective model related with the chiral phase transition at finite temperature. We have focused

	β	δ	γ	ν	ν_c	α
$O(4)$ lattice[a]	0.3836	4.851	1.477	0.7479	0.4019[b]	-0.244
Mean Field	0.5	3	1	0.5	1/3	0
FRG (our work)	0.397(2)	4.818	1.603(9)	0.801(47)	0.396	-0.361[b]

Table 4.1: The critical exponents for the $O(4)$ model from the FRG studies, the LGT and the mean-field calculations. The quoted errors in our results are due to different methods that were used to find the critical exponents (see text); [a]data taken from [76]; [b]from the hyperscaling relations.

on the universal scaling behavior of different physical quantities. In order to correctly account for the quantum fluctuations and non-perturbative effects we have applied the functional renormalization group method. Deriving the flow equation for the scale dependent thermodynamic potential at finite temperature and density in the presence of an external field we have used the polynomial truncation method to solve this equation numerically. We have shown, that with our particular choice of the optimized regulator functions this method provides numerically stable results. We have neglected the bosonic and fermionic wave function renormalization and the running of the Yukawa coupling. However, we have argued, that such effects lead only to the sub-leading corrections to a scaling near the phase transition.

Within the scope of our investigations, we have calculated different thermodynamical quantities that are sensitive to the chiral phase transition. In particular, we have analyzed the scaling behavior of the chiral order parameter, its longitudinal and transverse susceptibilities as well as the correlation lengths in the chiral limit and in the presence of an external field. The results show that the chiral order parameter and its susceptibilities scale near the chiral phase transition following the universal scaling behavior of the singular part of the free energy. Here we have extracted the corresponding critical exponents at the critical point and at the coexistence line and have also analyzed the scaling of the pseudocritical temperature and the maxima of the longitudinal susceptibility at the finite external field.

As the most interesting case we have analyzed the leading scaling behavior of the longitudinal and transverse susceptibilities and their different ratios when approaching the critical point from the symmetric and the broken phase with finite external field. Our results show that this scaling is consistent with the Widom-Griffiths magnetic equation of state in the systematic ϵ-expansion of the scaling function. The critical exponents obtained in this work are in a very good agreement with the recent LGT results obtained for the $O(4)$ spin system. This confirms the expectations that the chiral phase transition of the 2-flavor effective chiral Lagrangian belongs to the $O(4)$ universality class. This also supports the validity of the FRG approach and the truncation methods of the flow equation used in our calculations to cor-

rectly account for the quantum fluctuations and the non-perturbative long distance dynamics near the chiral phase transition.

Chapter 5

Thermodynamics of hot and dense matter

During recent years the importance of studying the phase structure of strongly interacting matter has been widely recognized. The phase diagram of a thermodynamic system may be mapped out by studying fluctuations and their response to changes of the thermodynamic parameters. Understanding the critical properties of the QCD medium and its phase diagram is a central problem in strong interaction physics, which is being addressed in both theoretical and experimental studies. The phase diagram of QCD, a theory that is considered to govern the strong interaction, can be accessed experimentally in heavy-ion collision experiments at the BNL Relativistic Heavy-Ion Collider (RHIC), the CERN Super Proton Synchrotron (SPS) and the Large Hadron Collider (LHC). It is expected that under extreme conditions such as high temperature and/or density the vacuum of strongly interacting matter changes, rendering novel phases. One usually speaks of a chirally symmetric or deconfined phase or a color superconducting phase. These phase transitions are also very important in the physics of the early universe and for understanding the composition and properties of compact stars. A proper understanding of the phase diagram of strongly interacting matter will be an important step towards the clarification of the dynamics of QCD. The most important and at the same time highly intriguing phenomena of QCD in the nonperturbative regime are chiral symmetry breaking and confinement. The interplay of the two is still an open issue and the subject of immense interest. Usually one speaks of two different QCD phase transitions that take place if either the temperature or the density crosses some critical point. Each transition is well defined in some limit of QCD. In the limit of infinite quark masses the deconfinement phase transition occurs. On the other hand, for vanishing quark masses, the chiral (symmetry-restoring) phase transition takes place instead. For

physical quark masses, neither of the two transitions is, due to the explicit symmetry breaking, strictly speaking a phase transition. Nevertheless, the corresponding crossover transition can be identified by studying the relevant susceptibilities. The underlying reason for the coincidence of the two transitions, observed in lattice QCD calculations, is presently subject of intense investigations.

In order to give satisfying answers to a variety of questions regarding the origin and nature of QCD phase transitions quite a few theoretical and phenomenological models and approaches have been developed and during the years further extended and improved. Lattice Gauge Theory (LGT), in particular, has provided substantial insight into the physics of the transition between the low temperature hadronic and high temperature quark-gluon plasma phase [80, 83, 84, 85, 86, 87, 88, 89, 90, 91, 45, 81, 82]. Effective models also provide a useful qualitative description of the chiral phase transition [43, 24, 92, 93, 94, 95, 44, 33]. Also, the physics of color deconfinement and its relation to chiral symmetry breaking has been recently studied in terms of effective chiral models [20, 21, 22, 23, 24, 25, 26, 27, 42, 28, 29, 30, 31, 32, 33]. Here, the expectation that the critical behavior of such models is governed by the same universality class as QCD [52] is of central importance. Furthermore, recent experimental data from heavy-ion collisions at RHIC and SPS provide new insight into the properties and behavior of a deconfined medium created in dynamical systems [96].

In this chapter, we investigate some thermodynamic aspects of hot and dense matter in both, the mean field and FRG approach. As an effective model of QCD we use the quark-meson Lagrangian coupled to the Polyakov loop [33]. Here, we focus on the phase structure and several thermodynamic observables sensitive to the phase transition. These observables include the fluctuations of the net quark number density and the ratio of its fourth to second order cumulant moments (kurtosis). We use universality arguments, relating QCD with chiral effective models, to explore the properties of the kurtosis and the inverse compressibility in hot and dense matter. We also study the dependence of these observables on the pion mass near the chiral transition. Furthermore, we compare our results with the chiral quark-meson model without Polyakov loops to emphasize the importance of the gluon degrees of freedom. Within the FRG approach, the phase structure and thermodynamics of the PQM model is the main point of our investigation. Here however, a full RG treatment of all fields is very complex and beyond the scope of this thesis. Instead, in this exploratory investigation we treat the Polyakov loop on a mean field level, while for the quarks and meson fields we employ the full RG machinery. We see a qualitative difference when comparing with the full RG treatment of chiral quark-meson model without Polyakov loops. Also, the phase diagram of the PQM model in mean field approximation changes once fluctuations are included. In the end we try to link the effective model with QCD, using ideas presented in Ref. [46], in order to circumvent the cutoff problem inevitably present in the RG approach.

5.1 Chiral models in mean field approximation

In this section we consider the PQM model in the mean field approximation. We begin with the grand canonical partition function

$$\mathcal{Z} = \mathrm{Tr}\exp\left[-(\mathcal{H}-\mu N)/T\right] = \int\prod_a \mathcal{D}\varphi_a \exp\left[\int d^4x\big(\mathscr{L}_{\mathsf{pqm}} + \mu\bar{q}\gamma^0 q\big)\right], \tag{5.1}$$

where a runs over all fields φ present in the PQM model and the Lagrangian of the PQM model $\mathscr{L}_{\mathsf{pqm}}$ has been introduced in Chapter 2. The mean field approximation consists in replacing the meson fields by their expectation values. All vacuum and thermal fluctuations are then neglected while the (anti)quarks are retained as quantum fields. Thus, we have the following representation of the partition function $\mathcal{Z}$ of the PQM model in mean field approximation (up to an overall normalization factor)

$$\mathcal{Z} = \exp\left[-\frac{V}{T}\left(U(\sigma,\vec{\pi}) + \mathcal{U}(\ell,\ell^*)\right)\right]\int\mathcal{D}\bar{q}\mathcal{D}q\exp\left[\int_0^{1/T} d\tau\int d^3x\big(\mathscr{L}_{\mathsf{quark}} + \mu\bar{q}\gamma^0 q\big)\right], \tag{5.2}$$

where

$$\mathscr{L}_{\mathsf{quark}} = \bar{q}\left(i\not{\partial} - g(\sigma + i\gamma_5\vec{\tau}\vec{\pi})\right)q. \tag{5.3}$$

The action given in the exponent of Eq. (5.1) is quadratic in quark fields, hence the functional integral is of the Gaussian type. The integration over fermions (quarks) is then easily performed by using standard techniques [97, 98]. Here we use the following formula for a n-dimensional Gaussian type integral over the fermionic fields η, given the symmetric matrix $\hat{A}$ [97, 98]:

$$\int\prod_{i=1}^n d\eta_i^* d\eta_i \exp\left[-\sum_{i,j}\eta_i^* A_{ij}\eta_j\right] = \det A. \tag{5.4}$$

This integration results in the following expression for the partition function

$$\mathcal{Z} = \exp\left[-\frac{V}{T}\left(U(\sigma,\vec{\pi}) + \mathcal{U}(\ell,\ell^*)\right)\right]\det D_f, \tag{5.5}$$

where $\det D_f$ represents the fermionic determinant and

$$D_f = \left(\not{p} - g(\sigma + i\vec{\tau}\cdot\vec{\pi}\gamma_5) + \gamma^0(\mu + A_0)\right)/T. \tag{5.6}$$

In a spatially uniform system the grand canonical potential per unit volume $\Omega(T,\mu)$ is a function of temperature T and chemical potential μ and is determined as the logarithm of the partition function $\mathcal{Z}$ in the following way

$$\Omega(T,\mu) = -\frac{T}{V}\log\mathcal{Z}. \tag{5.7}$$

All relevant thermodynamic quantities can then be obtained from the grand canonical potential

$$\Omega(T,\mu) \;=\; \mathcal{U}(\ell,\ell^*) + U(\sigma) + \Omega_{\bar{q}q}(\ell,\ell^*,\sigma). \tag{5.8}$$

This potential is obtained from the mean field Lagrangian by introducing averaged meson fields and after integrating out fermions. The quark/antiquark contribution reads as follows

$$\Omega_{\bar{q}q} = -2N_f T\int\frac{d^3p}{(2\pi)^3}\mathrm{Tr}_c\left\{\ln(1+Le^{-(E_p-\mu)/T}) + \ln(1+L^\dagger e^{-(E_p+\mu)/T})\right\}, \tag{5.9}$$

where the divergent part in Eq. (5.9) which is due to the negative energy states of the Dirac sea, is neglected [1]. More precisely, the divergence can be absorbed in renormalized vacuum quantities. The term that is neglected is a finite logarithmic correction to the thermodynamic potential $\Omega(T,\mu)$. The quasi-particle energy present in Eq. (5.9) is given by

$$E_p = \sqrt{\vec{p}^{\,2}+m_q^2} \tag{5.10}$$

where $m_q = g\sigma$ is the constituent quark mass and μ the quark chemical potential.

What is left to be done is to evaluate the remaining trace in color space. To do so, we start with the Polyakov gauge given by Eq. (2.35). Now, using Eq. (2.32) and having in mind that we work with three colors ($N_c = 3$) it is straightforward to obtain the following expressions

$$\ell \;=\; \frac{1}{3}\left(e^{i\varphi} + e^{i\varphi'} + e^{-i(\varphi+\varphi')}\right), \tag{5.11a}$$

$$\ell^* \;=\; \frac{1}{3}\left(e^{-i\varphi} + e^{-i\varphi'} + e^{i(\varphi+\varphi')}\right). \tag{5.11b}$$

With this at hand and, using the relation $\mathrm{Tr}\ln = \ln\det$, we can proceed with the

[1] This is different in Nambu-Jona-Lasinio (NJL) model, which is another effective chiral model used for exploring qualitative features of the chiral symmetry in QCD. Here, the part coming from the Dirac sea cannot be neglected. This contribution is regularized by introducing a momentum cutoff. The remaining finite quark/antiquark contribution is in the NJL model responsible for the dynamical breaking of chiral symmetry.

calculation of the color trace and finally obtain

$$\begin{aligned}
\mathrm{Tr}_c \ln\left(1+Le^{-(E_p-\mu)/T}\right) &= \ln\det\left(1+Le^{-(E_p-\mu)/T}\right) \\
&= \ln\det\left[\begin{pmatrix}1&0&0\\0&1&0\\0&0&1\end{pmatrix} + e^{-(E_p-\mu)/T}\begin{pmatrix}e^{i\varphi}&0&0\\0&e^{i\varphi'}&0\\0&0&e^{-i(\varphi+\varphi')}\end{pmatrix}\right] \\
&= \ln\left[(1+e^{-(E_p-\mu)/T}e^{i\varphi})(1+e^{-(E_p-\mu)/T}e^{i\varphi'})(1+e^{-(E_p-\mu)/T}e^{-i(\varphi+\varphi')})\right] \\
&= \ln\Bigg[1+e^{-2(E_p-\mu)/T}\underbrace{(e^{-i\varphi}+e^{-i\varphi'}+e^{i(\varphi+\varphi')})}_{3\ell^*} \\
&\qquad + e^{-(E_p-\mu)/T}\underbrace{(e^{i\varphi}+e^{i\varphi'}+e^{-i(\varphi+\varphi')})}_{3\ell}+e^{-3(E_p-\mu)/T}\Bigg] \\
&= \ln\left[1+3(\ell+\ell^* e^{-(E_p-\mu)/T})e^{-(E_p-\mu)/T}+e^{-3(E_p-\mu)/T}\right]. \qquad (5.12)
\end{aligned}$$

The second trace in Eq. (5.9) is obtained using the same procedure

$$\mathrm{Tr}_c \ln\left(1+L^\dagger e^{-(E_p+\mu)/T}\right) = \ln\left[1+3(\ell^*+\ell e^{-(E_p+\mu)/T})e^{-(E_p+\mu)/T}+e^{-3(E_p+\mu)/T}\right]. \qquad (5.13)$$

After this algebraic exercise, we obtain the quark/antiquark contribution to the grand canonical potential in the form

$$\begin{aligned}
\Omega_{\bar{q}q} &= -2N_f T\int\frac{d^3p}{(2\pi)^3}\left\{\ln\left[1+3(\ell+\ell^* e^{-(E_p-\mu)/T})e^{-(E_p-\mu)/T}+e^{-3(E_p-\mu)/T}\right]\right. \\
&\qquad \left. +\ln\left[1+3(\ell^*+\ell e^{-(E_p+\mu)/T})e^{-(E_p+\mu)/T}+e^{-3(E_p+\mu)/T}\right]\right\}. \qquad (5.14)
\end{aligned}$$

The form of the potential (5.14) incorporates an interesting feature of the PQM model. First, under the charge conjugation transformation, $\mu \to -\mu$, the roles of quarks and antiquarks are exchanged. Furthermore, also the roles of the Polyakov loop and its conjugate are exchanged under this transformation.

It is interesting to examine the low and high temperature behavior of the PQM model. Again, we start with Eq. (5.14) and deduce from it the expected behavior at low temperatures. Indeed, in the limit of $\ell, \ell^* \to 0$ (which is what one anticipates in the low temperature limit) there is a suppression of one- and two-quark states, so that effectively only three-quark states are left. This is easy to see from Eq. (5.14) when $\ell, \ell^* \to 0$. On the other hand, for high temperatures the Polyakov loops approach unity, i.e. $\ell, \ell^* \to 1$ so that (5.12) (and (5.13) accordingly) yields

$$\begin{aligned}
&\ln\left[1+3(1+e^{-(E_p-\mu)/T})e^{-(E_p-\mu)/T}+e^{-3(E_p-\mu)/T}\right] \\
&\qquad = \ln\left[\left(1+e^{-(E_p-\mu)/T}\right)^3\right] = 3\ln\left[1+e^{-(E_p-\mu)/T}\right]. \qquad (5.15)
\end{aligned}$$

In this way one recovers from Eq. (5.14) the standard quark and antiquark contributions to the grand canonical potential for the two flavor chiral quark-meson model

$$\Omega_{\bar{q}q} = -6N_f T \int \frac{d^3p}{(2\pi)^3} \left(\ln[1 + e^{-(E_p-\mu)/T}] + \ln[1 + e^{-(E_p+\mu)/T}] \right) , \tag{5.16}$$

with three colors ($N_c = 3$).

In order to start with the investigation of the PQM model, we have to set the starting point, i.e. formulate the gap equations. The phase structure of the model and all relevant thermodynamics can be deduced from the solution of the equations of motion (gap equations for the relevant fields present in the model). These are obtained by extremizing the thermodynamic potential with respect to the three uniform mean fields σ, ℓ and ℓ^*

$$\frac{\partial\Omega}{\partial\sigma} = \frac{\partial\Omega}{\partial\ell} = \frac{\partial\Omega}{\partial\ell^*}\bigg|_{\sigma=\langle\sigma\rangle,\ell=\langle\ell\rangle,\ell^*=\langle\ell^*\rangle} = 0\,. \tag{5.17}$$

The solutions of the three coupled equations determine the behavior of the chiral order parameter $\langle\sigma\rangle$ and the Polyakov loop expectation values $\langle\ell\rangle$ and $\langle\ell^*\rangle$ as functions of T and μ. In other words, by using the mean field approach we approximate the three independent fields σ, ℓ and ℓ^* by their thermal averages, which are determined by the stationary points of the thermodynamic potential.

In the calculations that follow, we fix the model parameters in vacuum by requiring that the experimental values of the pion decay constant $f_\pi = 93$ MeV, the pion mass $m_\pi = 138$ MeV, the sigma mass $m_\sigma = 600$ MeV as well as the constituent quark mass $m_q = 300$ MeV are reproduced. The Yukawa coupling g is fixed by choosing a value for the constituent quark mass in vacuum $g = m_q/f_\pi$. For a given pion mass m_π the explicit symmetry breaking parameter is given by $c = f_\pi m_\pi^2$. The quartic coupling λ is determined by the sigma mass m_σ via the relation $\lambda = (m_\sigma^2 - m_\pi^2)/(2f_\pi^2)$. Finally, the parameter v^2 is found by minimizing the potential in radial direction and is given by $v^2 = \langle\sigma\rangle^2 - c/(\lambda\langle\sigma\rangle)$. Thus, the remaining parameters in the PQM model c, v, λ and g are set to $c = 1.77 \times 10^6$ MeV^3, $v = 87.6$ MeV, $\lambda = 19.7$ and $g = 3.2$.

We neglect the possible μ-dependence of the parameter T_0 [33], and choose $T_0 = 208$ MeV in all calculations, at $\mu = 0$ as well as at nonvanishing μ. We also note that our value for T_0 differs from that of Refs. [42, 27]. For a detailed discussion concerning the μ-dependence of the temperature T_0 in the Polyakov loop potential we refer the interested reader to Ref. [33].

We will also do calculations in the chiral quark-meson model (i.e. without Polyakov loops). We stress the fact, that the parameters of this model are tuned in such a way as to obtain the same physical values in the vacuum as in the PQM model. In this way we obtain a consistent picture for both models and a comparison makes sense.

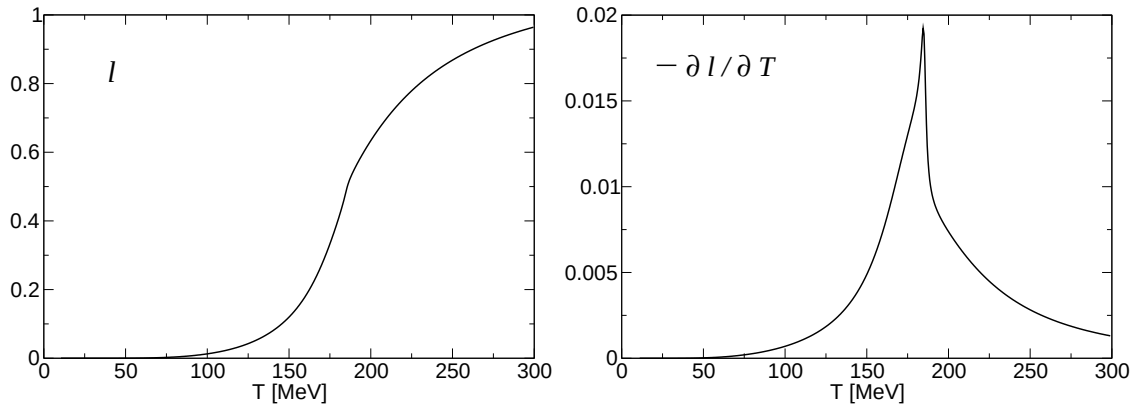

Figure 5.1: Polyakov loop variable ℓ for $\mu = 0$ in the mean field approximation (left panel) and its derivative $\partial\ell/\partial T$ (right panel).

5.1.1 Thermodynamics and phase structure

In order to analyze the thermodynamics and the phase structure of the PQM model let us start with the mean field analysis of the Polyakov loop expectation value. The basic properties of confinement have already been discussed in Chapter 2 and we have seen that the Polyakov loop serves as an order parameter of the $Z(3)$ symmetry. For vanishing chemical potential, the Polyakov loop and its conjugate are equal i.e. $\ell = \ell^*$. In Fig. 5.1-left we show the temperature dependence of ℓ at $\mu = 0$ for a physical pion mass. It is well known that the temperature derivative of an order parameter is peaked near the transition temperature. In fact, this peak can be used to define pseudocritical temperature in the presence of an explicit symmetry breaking term[2]. In order to find the pseudocritical temperature associated with the Polyakov loop we thus investigate the temperature dependence of the temperature derivative $\partial\ell/\partial T$. From the position of the peak one can read off the corresponding value for the pseudocritical temperature as shown in Fig. 5.1-right. With the parameter set given above, we thus find $T_{dec} \simeq 184$ MeV for the deconfinement temperature.

Our next aim is to study the in-medium meson and quark masses. The meson masses are obtained by taking the second derivatives of the grand canonical potential $\Omega(T,\mu)$ with respect to the corresponding fields. These derivatives have to be evaluated at the minimum of the potential $\Omega(T,\mu)$ defined by Eq. (5.17). Here, we calculate the sigma and pion mass for the PQM model. According to the considerations given above, the in-medium meson masses are given by

$$m_\sigma^2(T,\mu) = \left.\frac{\partial^2\Omega(T,\mu)}{\partial\sigma^2}\right|_{\rm min}, \qquad m_{\pi_i}^2(T,\mu) = \left.\frac{\partial^2\Omega(T,\mu)}{\partial\pi_i\partial\pi_i}\right|_{\rm min} \tag{5.18}$$

[2]Another possible definition is obtained by having the peak of the corresponding susceptibility. In the limit of weak explicit symmetry breaking one expects the various definitions to agree.

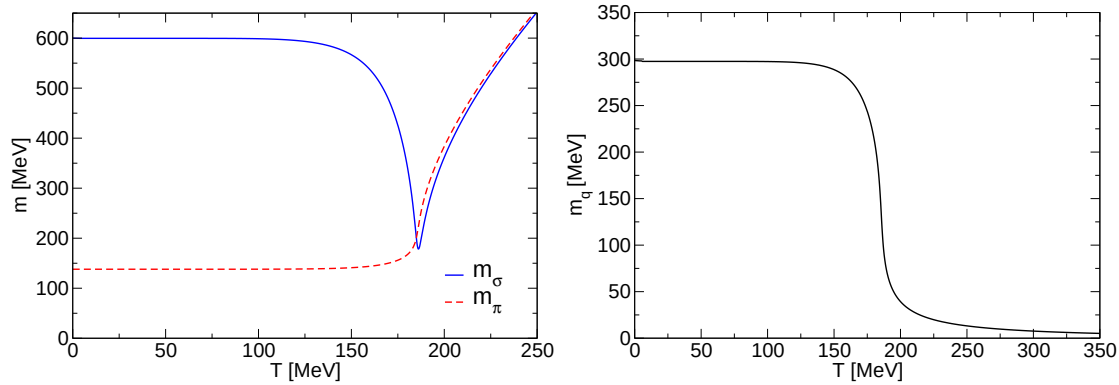

Figure 5.2: The pion and sigma masses (left panel) and constituent quark mass (right panel) as function of the temperature at $\mu = 0$ for the PQM model in mean field approximation.

while the constituent quark mass in the medium is given by $m_q = g\sigma$.

In Fig. 5.2-left we show the temperature dependence of the sigma and pion masses for $\mu = 0$. At high temperatures the masses are approximately degenerate for $T \geq 190$ MeV and increase roughly linearly with temperature T. For a relative broad range of temperatures the pion mass is almost constant, but at high temperatures m_π increases, together with the sigma mass, signalling chiral symmetry restoration. On the other hand, the sigma mass exhibits a dip at approximately $T \simeq 184$ MeV (i.e. the chiral susceptibility χ_σ has a maximum at this temperature). We remind the reader that we found $T_{dec} \simeq 184$ MeV for the deconfinement transition temperature. These results are in accordance with recent findings about the coincidence of deconfinement and chiral transition for vanishing chemical potential in the PQM model [33]. For finite values of μ this coincidence is in general not present anymore.

The behavior of the quark mass m_q at $\mu = 0$ as a function of the temperature T is shown in Fig. 5.2-right. The constituent quark mass is almost constant, $m_q \simeq 300$ MeV, up to T_{crit} (here, T_{crit} stands for both, the chiral and deconfinement transition temperature) and then it shows an abrupt change in a narrow temperature interval and rapidly decreases. In contrast to the chiral limit (i.e. without an explicit symmetry breaking term i.e. $m_\pi = 0$), m_q never reaches zero value in the case of a physical pion mass.

In the following we focus on the quark sector of the thermodynamic potential. Following the procedure in LGT studies [80], we use the Taylor expansion of the presure in μ/T to compute various observables. In LGT the extrapolation to finite values of the chemical potential μ is impeded by the so called *sign problem*[3]. One

[3]The introduction of a finite chemical potential in LGT leads to the sign problem. The complete

possible way to circumvent this problem is to use the aforementioned Taylor expansion in powers of μ/T around $\mu = 0$. In particular the thermodynamic pressure is expressed as

$$\frac{P\left(T,\mu\right)}{T^4} = \sum_{n=0}^{\infty} \frac{1}{n!} c_n(T) \left(\frac{\mu}{T}\right)^n \tag{5.19}$$

with the expansion coefficients

$$c_n(T) = \left.\frac{\partial^n (p\left(T,\mu\right)/T^4)}{\partial(\mu/T)^n}\right|_{\mu=0} . \tag{5.20}$$

It should be stressed that only even powers appear in Eq. (5.19) due to the charge conjugation symmetry of a system at $\mu = 0$.

The Taylor coefficients are generalized susceptibilities corresponding to moments of the net quark number [80, 45, 81, 82]. In particular, the first two non-vanishing derivatives, c_2 and c_4 are the second and fourth order cumulants which are related to fluctuations of net quark number, $\delta N_q = N_q - \langle N_q \rangle$, as follows:

$$\begin{aligned} c_2 &= \frac{\chi_q}{T^2} = \frac{1}{T^3 V}\left(< (\delta N_q)^2 >\right) = \frac{1}{T^3 V}\left(< N_q^2 > - < N_q >^2\right) \\ c_4 &= \frac{1}{T^3 V}\left(< (\delta N_q)^4 > -3 < (\delta N_q)^2 >^2\right) \quad , \end{aligned} \tag{5.21}$$

with

$$\chi_q = \frac{\partial n_q(T,\mu)}{\partial \mu} = -\frac{\partial^2 \Omega(T,\mu)}{\partial \mu^2} \tag{5.22}$$

being the quark number susceptibility. The quark number density $n_q(T,\mu)$ is defined as

$$n_q(T,\mu) = -\frac{\partial \Omega(T,\mu)}{\partial \mu} \tag{5.23}$$

and is related to the net baryon density n_B by $n_q = 3n_B$.

We will start with our investigation of the behavior of coefficients c_2 and c_4 in the mean field approximation and without Polyakov loops. This means that we start with the chiral quark-meson model in our study. We use the expansion given by Eq. (5.19) and calculate c_2 and c_4 at vanishing chemical potential. Our results are shown in Fig. 5.3. The most prominent feature is the expected absence of suppression of quark degrees of freedom at low temperatures. This behavior is best seen in Fig. 5.3-left. The second notable feature is that both, c_2 as well as c_4 vary sharply

form of the partition function on the lattice is given by [1]

$$\mathcal{Z} = \int [dU] \mathrm{Det} F[U] \exp(-S_g(U)) ,$$

where the gauge fields are represented by the group element U, the measure is the Haar measure

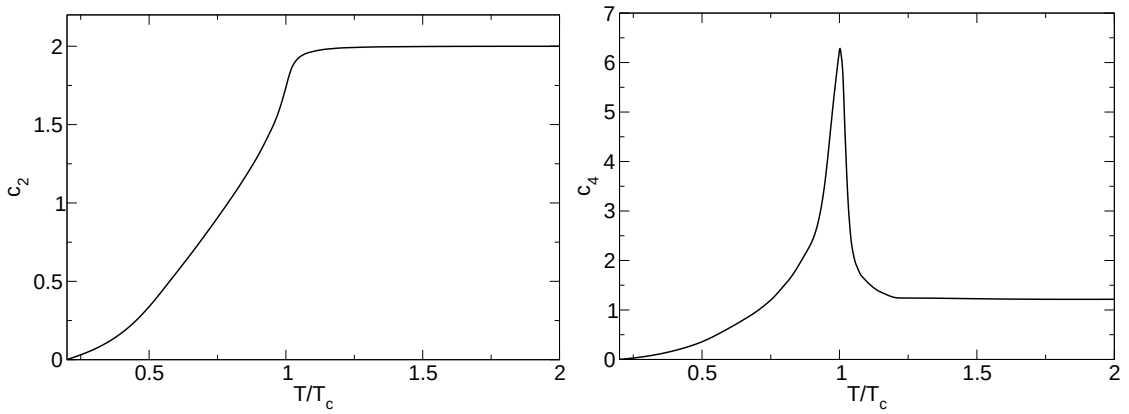

Figure 5.3: Coefficient c_2 (left panel) and coefficient c_4 (right panel) in the mean field approximation for the chiral quark-meson model.

in the vicinity of the critical temperature. The coefficient c_4 shows a peak at the (pseudo)critical temperature T_c as seen in Fig. 5.3-right. In the high temperature limit both coefficient show a very nice convergence towards their corresponding Stefan-Boltzmann limit. In the Stefan-Boltzmann limit, the coefficients c_2 and c_4 have only contributions from fermions and in the high temperature region the quark-antiquark contribution to the thermodynamic pressure converges to that of an ideal gas of quarks given by the following expression[4]

$$\frac{P_{q\bar{q}}(T,\mu)}{T^4} = N_f N_c \left[\frac{1}{12\pi^2}\left(\frac{\mu}{T}\right)^4 + \frac{1}{6}\left(\frac{\mu}{T}\right)^2 + \frac{7\pi^2}{180}\right]. \tag{5.24}$$

By comparing Eq. (5.24) with the expression for the Taylor expanded pressure (5.19), the Stefan-Boltzmann limits for c_2 and c_4 can easily be determined

$$c_2 = 2!\,\frac{N_c N_f}{6} = 2, \qquad T \to \infty, \tag{5.25a}$$

$$c_4 = 24!\,\frac{N_c N_f}{12\pi^2} = \frac{12}{\pi^2}, \qquad T \to \infty. \tag{5.25b}$$

The Stefan-Boltzmann values exactly match the values c_2 and c_4 approach in Fig. 5.3.

Next, we would like to investigate how a gluonic background (here introduced via Polyakov loop and its conjugate coupled to the quarks) affects the behavior of coefficients c_2 and c_4. We use the same expansion of pressure as in the previous case

dU and $\mathrm{Det}F[U]$ is the fermionic determinant. At finite μ and for $N_c = 3$, the fermionic determinant is complex and since the partition function is real, there is a cancellation among various gauge configurations.

[4]The reader interested in derivation of Eq. (5.24) can consult Appendix B where we discuss the low- and high-temperature limits of the fermion contribution to the pressure in more detail.

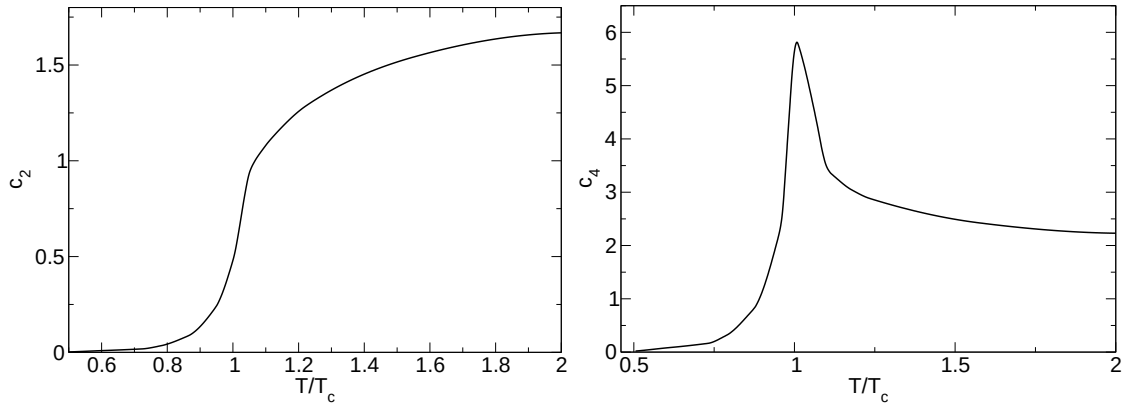

Figure 5.4: Coefficient c_2 (left panel) and coefficient c_4 (right panel) in the mean field approximation for the PQM model.

given by Eq. (5.19) and calculate the coefficients c_2 and c_4 for PQM model in the mean field approximation. The results obtained are shown in Fig. 5.4. The expected suppression of quark degrees of freedom at low temperatures, due to the presence of Polyakov loops is clearly seen in the behavior of c_2 in Fig. 5.4-left. Further, what can also be seen in Fig. 5.4-left is that coefficient c_2 shows the well known continuous increase towards the high temperature ideal gas value. However, here we note that c_2 reaches about 85% of its Stefan-Boltzmann value at $T \simeq 2\,T_c$, yet this is still consistent with lattice data. In the critical region close to the critical temperature T_c the coefficient c_2 again varies quite rapidly. A rapid variation in the vicinity of the critical temperature is characteristic for the fourth order coefficient c_4 as well. In Fig. 5.4-right we observe a pronounced peak at the critical temperature T_c. The high temperature behavior of c_4 is quite different in the PQM model than in the case when Polyakov loops are absent. Here, the coefficient c_4 shows a very slow convergence to its ideal gas value. In fact, the value obtained for c_4 at very high temperatures is almost twice the corresponding ideal gas value. The different high-temperature behavior of the chiral quark-meson model with and without Polyakov loops is clearly a consequence of the coupling of the quarks to the Polyakov loop rather than an effect of the mean field dynamics, as conjectured in Ref. [44].

Our next point of study, in connection with coefficients c_2 and c_4, is their ratio. Studies of QCD on the lattice at finite temperature and density show that the ratio of the quartic to quadratic fluctuations of the net quark number $R_{4,2}$ is a valuable probe of deconfinement and chiral dynamics [45, 90, 91, 81, 82]. We focus on the ratio

$$R_{4,2} = \frac{\langle (\delta N)^4 \rangle}{\langle (\delta N)^2 \rangle} - 3\langle (\delta N)^2 \rangle = \frac{c_4}{c_2}, \tag{5.26}$$

which we refer to as the kurtosis of the quark number fluctuations. Generally, the

kurtosis is introduced in probability theory as a measure of peakedness of a distribution. Strictly speaking, in statistics the kurtosis is given by the fourth moment divided by the second moment squared

$$r_{4,2} = \frac{\langle (\delta N)^4 \rangle}{\langle (\delta N)^2 \rangle^2} \,. \tag{5.27}$$

One can also define the kurtosis excess $\tilde{R}_{4,2}$ as

$$\tilde{R}_{4,2} = r_{4,2} - 3 \,. \tag{5.28}$$

Depending on the sign of the kurtosis, one defines a distribution which peakedness is described by the kurtosis $\tilde{R}_{4,2}$ as

$$\text{distribution} = \begin{cases} \text{leptokurtic} \,, & \tilde{R}_{4,2} > 0 \\ \text{mesokurtic} \,, & \tilde{R}_{4,2} = 0 \\ \text{platykurtic} \,, & \tilde{R}_{4,2} < 0 \end{cases} \tag{5.29}$$

Our definition of the ratio $R_{4,2}$ given in Eq. (5.26) corresponds to the kurtosis excess but with an atypical normalization. The reason for choosing this definition is that it is sensitive to the baryon number of the effective fermion degrees of freedom.

Before considering $R_{4,2}$ near the chiral phase transition, we first focus on its behavior well above and below the transition region. For high temperatures, i.e. $T \gg T_0$, the ratio $m_q/T \ll 1$ and the Polyakov loop $l \to 1$. Hence, the quark-antiquark contribution to the thermodynamic pressure converges to that of an ideal gas of massless quarks given by (5.24). From Eqs. (5.25a) and (5.25b), it trivially follows

$$R_{4,2}|_{T \gg T_0} = \frac{6}{\pi^2}, \tag{5.30}$$

where $R_{4,2}$ is evaluated at $\mu = 0$. One of the main features of a chiral Lagrangian coupled to the Polyakov loop is "statistical confinement" which implies, that at small T, the effective degrees of freedom are three quark states [43, 24]. This is explicitly seen in Eq. (5.14), where for small $T \ll T_0$ the Polyakov loop $l \simeq 0$, implying suppression of the one- and two-quark states in the partition sum. Consequently, in the Boltzmann approximation[5] the fermion contribution to the pressure is

$$\frac{P_{q\bar{q}}(T,\mu)}{T^4} \simeq \frac{2N_f}{27\pi^2} \left(\frac{3m_q}{T}\right)^2 K_2\left(\frac{3m_q}{T}\right) \cosh\frac{3\mu}{T}. \tag{5.31}$$

Thus, at low temperatures the quark/antiquark contribution to the thermodynamic pressure is that of a non-interacting gas composed of particles and antiparticles

[5] The Boltzmann approximation is valid for $\mu \approx 0$ if $3m_q/T \gg 1$. This condition is clearly satisfied for $T < T_0 \simeq 200$ MeV since $m_q \simeq 300$ MeV.

with mass $M = 3m_q$ and baryon number $B = 1$ and $B = -1$, respectively. The effective degeneracy of these particles is $2N_f/27$. The suppression by a factor $1/27$, compared to a gas of free nucleons, is due to the rescaling of the momenta implied by the transformation

$$3\sqrt{p^2 + m^2} \to \sqrt{k^2 + (3m)^2}\,.$$

For more details on the derivation of Eq. (5.31) we refer again to Appendix B. An important feature of the pressure (5.31) is the factorization of the M/T and μ/T dependence,

$$\frac{P_{q\bar{q}}(T,\mu)}{T^4} = f\left(\frac{M}{T}\right)\cosh\frac{3\mu}{T}\,. \tag{5.32}$$

A similar factorization occurs in the hadron resonance gas model HRG, although with a more complicated function $f(M/T)$. In the HRG, the corresponding function involves a sum over all baryon states [45, 99, 100, 101]. We note, that the Polyakov-loop models fail to reproduce the pressure of a resonance gas, even when the HRG is restricted to a gas of nucleons and Δ resonances (more generally the lowest three-quark multiplets) and their masses are approximated by $M_N \sim M_\Delta \sim 3m_q$. The origin of this failure is twofold: on the one hand the suppression factor mentioned above and, on the other hand, an incorrect dependence on N_f. The latter is due to the fact that only states where all three quarks have the same flavor are counted in (5.31).

Since the HRG seems to provide a satisfactory description of the QCD equation of state at low temperatures [45, 99, 100, 101], the effective model considered here can, strictly speaking, be valid only near the phase transition, where the dynamics is controlled by chiral symmetry. However, the model may still be useful outside the critical region, for computing observables that are not sensitive to details of the mass spectrum. The kurtosis (5.26) fulfils this criterion at least at low temperatures. Indeed, from Eqs. (5.26) and (5.32) it follows that the function $f(M/T)$, which depends on the mass spectrum, cancels in the ratios, leading to

$$R_{4,2}|_{T\ll T_0} = 9. \tag{5.33}$$

The kurtosis (5.26) depends on the net quark content of the baryon number carrying effective degrees of freedom. For instance, at low temperatures, $R_{4,2} = (3B)^2$. Consequently, in the low-temperature confining phase, $B = 1$ and $R_{4,2} = 9$, as found also in the hadron resonance gas model [80, 45]. On the other hand, in the pure quark-meson model, i.e. neglecting the effects of the Polyakov loop, the relevant fermionic degrees of freedom are single quarks, at all temperatures. Therefore, the corresponding value of the kurtosis in the low temperature limit is $R_{4,2} = 1$. Clearly, in an effective chiral model with quark degrees of freedom, the Polyakov loop is essential for obtaining the correct low temperature behavior of the kurtosis. Here we should stress again that Polyakov loop models can reproduce the correct value of

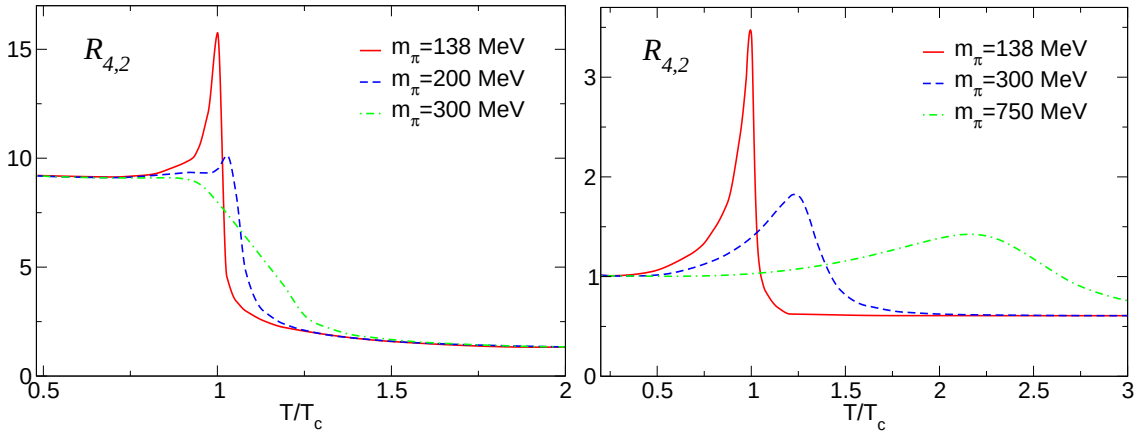

Figure 5.5: The kurtosis $R_{4,2}$ for various values of the pion mass in the PQM (left panel) and in the chiral quark-meson model (right panel). The temperature is normalized to the pseudocritical temperature T_c for a physical value of the pion mass.

$R_{4,2}$, although they do not yield a realistic description of the pressure at low temperatures, because the dependence on details of the baryon spectrum cancels in the ratio c_4/c_2.

Let us now discuss the temperature dependence of $R_{4,2}$. By inspection of Eqs. (5.30) and (5.33) we conclude that the kurtosis, for fixed μ/T, is temperature independent far above and below the transition. However, the high- and low-temperature values differ considerably, implying that $R_{4,2}$ must vary near the phase transition. The major contribution to the change of the kurtosis $R_{4,2}$ between the low and high temperature limits is due to the change of the relevant baryon number carrying degrees of freedom, from three-quark states to single quarks. Thus, indeed the kurtosis is, as noted in [45], an excellent probe of deconfinement. It is clear from this discussion that, well above and below the transition, $R_{4,2}$ is independent of m_π. However, as illustrated in Fig. 5.5 this is not the case in the phase transition region.

In Fig. 5.5 we also show, that for $T < T_c$ the kurtosis in both the PQM and QM models converges fairly rapidly to its low-temperature limit, independently of the value of m_π. The temperature (in)dependence of $R_{4,2}$ in both models is consistent with LGT findings in 2- and 2+1-flavor QCD [80, 45]. However, as discussed above, only the PQM model correctly reproduces the low T limit, $R_{4,2}|_{T\ll T_c} = 9$.

At high temperatures, the kurtosis in the QM model reaches the asymptotic value already at $T \simeq 1.5T_c$, independently on the value of the pion mass, in full agreement with LGT results [80, 45]. However, this is not the case for the PQM model, where even at $T > 2T_c$, $R_{4,2}$ is still by factor 2 above the ideal gas value. Clearly, the kurtosis $R_{4,2}$ represents the ratio of the coefficients c_4 and c_2 (cf. Eq. (5.26)), thus

we expect the deviation from the Stefan-Boltzmann limit as already seen for c_4. Thus, the coupling of the Polyakov loops to the quarks induces the deviation of $R_{4,2}$ of the ideal gas value. The ideal gas value of $R_{4,2}$ is in the PQM model reached at high T if both $m_q/T \ll 1$ and $l \simeq 1$. The first requirement is indeed satisfied already at $T > (1.2-1.5)T_c$, but the second one is not valid even at $T > 2T_c$. This is a direct consequence of the parametrization of the Polyakov loop effective potential in the PQM Lagrangian (2.36). The parameters of the effective potential were fixed by fitting $SU(3)$ lattice results, where l approaches its asymptotic value very slowly. This discussion points to a clear limitation of the applicability of the PQM model to the interpretation of LGT results at high temperatures where e.g., the interactions of quarks with space-like Wilson loops, not included in the PQM model, could be relevant.

Near the chiral transition, the kurtosis is strongly dependent on the pion mass. For a physical pion mass, $R_{4,2}$ exhibits a peak in both models. With increasing m_π the peak height gradually decreases and its position is shifted to larger temperatures, reflecting an increase in the (pseudo)critical temperature T_c. The dependence of the kurtosis on the pion mass is stronger in the QM than in the PQM model. A comparison with LGT results [80, 45] show that the PQM model yields a much better overall description of the LGT data. For large m_π there is a smooth change of the kurtosis between its limiting high- and low-temperature values, in agreement with 2-flavor QCD on the lattice [80, 45]. On the other hand, for physical m_π, $R_{4,2}$ increases at T_c beyond the low-temperature value $R_{4,2} \simeq 9$. Both these results, together with the low temperature limit, are consistent with the LGT results in 2 and 2+1 flavor [90, 91] QCD, obtained for $m_\pi \simeq 770$ MeV and $m_\pi \simeq 220$ MeV, respectively. The only problem of the PQM model in this context is the high-temperature behavior of $R_{4,2}$, discussed above, while the QM model yields an incorrect low-temperature limit and a too strong dependence on the pion mass near the phase transition. Consequently, we restrict our discussion below to the PQM model.

As a consequence of $O(4)$ scaling, one expects a strong variation of the kurtosis with m_π near the chiral phase transition [45]. At $\mu = 0$, the singular part of the net quark number fluctuations and the fourth order cumulant scale as

$$\chi_q \simeq t^{1-\alpha} \tag{5.34a}$$

$$c_4 \simeq t^{-\alpha}, \tag{5.34b}$$

where $t = |T - T_c|/T_c$ and α is the critical exponent of the specific heat. In the $O(4)$ universality class, α is small and negative, $\alpha \simeq -0.26$. Consequently, the regular part dominates in the susceptibility χ_q, whereas the singular part of c_4 corresponds to a cusp. In the presence of a term that explicitly breaks the $O(4)$ symmetry, the cusp is smoothened and can, for small pion masses, be seen in $R_{4,2}$ as a peak at T_c. For larger m_π, c_4 is dominated by the regular part, resulting in monotonic change of $R_{4,2}$ in the transition region. These expectations, which are borne out in the PQM model, are consistent with LGT results.

In the following we discuss a thermodynamic observable that can be used in the process of locating the critical point in a phase diagram. It has been conjectured that the compressibility represents such an observable. The compressibility of a system can be thought of as a response to a pressure change. The observable we are interested in, is the dimensionless ratio of the inverse isothermal compressibility given by

$$\kappa^{-1} = -V \left(\frac{\partial p}{\partial V} \right)_T = \frac{n_q^2}{\chi_q}, \tag{5.35}$$

and Gibb's free energy density defined as

$$G = \mu n_q. \tag{5.36}$$

Thus, taking the ratio of Eqs. (5.35) and (5.36) we consider the following observable

$$R_\kappa = \frac{\kappa^{-1}}{\mu n_q} = \frac{n_q}{\mu \chi_q}. \tag{5.37}$$

Before we investigate the behavior of R_κ, we shall discuss, as we have already done for the kurtosis, its low and high temperature limits. We use again Eq. (5.24) and the definitions of χ_q and n_q given by Eqs. (5.22) and (5.21) and obtain

$$R_\kappa|_{T \gg T_0} = \frac{(\mu/T)^2 + \pi^2}{3(\mu/T)^2 + \pi^2}. \tag{5.38}$$

In contrast to the discussion of $R_{4,2}$ (that has been evaluated at $\mu = 0$), for R_κ we here retain the μ dependence in anticipation of the application below.

We have already discussed the unreliability of the PQM model for describing the pressure of a resonance gas at low temperatures. However, we have seen that for the kurtosis as well as for other observables, insensitive to the mass spectrum useful results can still be obtained. Thus, we also employ R_κ outside the critical region, at low temperatures.

In this case, from the fermionic contribution to the pressure at low temperatures (5.31) and Eqs. (5.22) and (5.21) we find

$$R_\kappa|_{T \ll T_0} = \frac{T}{3\mu} \tanh \frac{3\mu}{T}. \tag{5.39}$$

For reference we also give the dimensionless inverse compressibility in the approximation, where n_q and χ_q are computed to next-to-leading order in μ/T

$$R_\kappa|_{T \ll T_0} = \frac{2 + 3(\mu/T)^2}{2 + 9(\mu/T)^2}. \tag{5.40}$$

From Eq. (5.38) we conclude that R_κ is temperature independent (here we assume a fixed value of μ/T) above the phase transition. Since there are significant

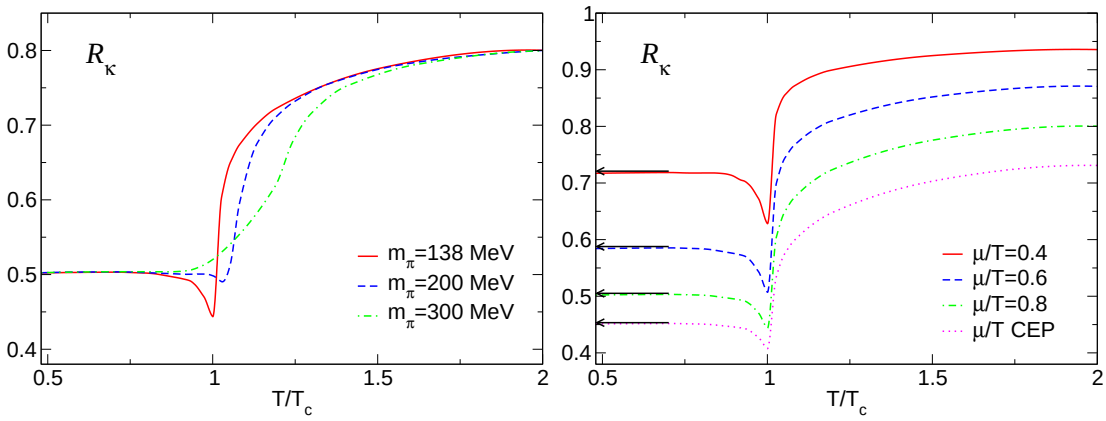

Figure 5.6: The inverse dimensionless compressibility R_κ computed in the PQM model at fixed $\mu/T = 0.8$ for various values of m_π (left panel) and at fixed $m_\pi = 138$ MeV for different μ/T (right panel). The curve labelled CEP corresponds to the value of μ/T at the critical end point. The arrows in the right panel indicate the low-temperature values of R_κ at a given μ/T. The temperature is normalized as in the Fig. 5.5.

differences in the value of R_κ at low and high temperatures, R_κ must vary in the vicinity of the phase transition.

Apart from being temperature independent outside the critical region, R_κ also does not depend on the pion mass m_π far above and far below the phase transition region. As we have already discussed, due to $O(4)$ scaling, the kurtosis shows a strong variation with m_π near the chiral phase transition. We have shown the scaling of χ_q and c_4 at $\mu = 0$ (cf. Eqs. (5.34a) and (5.34b)). However, at finite chemical potential, the singularity is stronger. This means that c_4 diverges at the $O(4)$ line whereas the quark number susceptibility χ_q develops a cusp. Furthermore, χ_q diverges at the critical end point (CEP), in accordance with $Z(2)$ universality. Consequently, the inverse compressibility, which depends on the susceptibility χ_q (cf. Eq. (5.37)), is an interesting observable that can be used to verify the existence of the CEP, to identify its position, provided it exists and to establish the universality class of the chiral transition.

Let us now also discuss how R_κ depends on the pion mass, as we have done for the kurtosis $R_{4,2}$. Near the chiral transition, R_κ shows a rather strong dependence on the pion mass. For large m_π, R_κ is smoothly increasing between the low- and high-temperature values. On the other hand, for the physical value of the pion mass ($m_\pi = 138$ MeV), a dip develops in the vicinity of T_c. As shown in the right panel of Fig. 5.6, the value of R_κ at the dip drops with increasing μ/T. This is consistent with recent lattice results [90, 91] obtained in 2+1 flavor QCD for $m_\pi = 220$ MeV.

For the parameters used in our calculations, the CEP appears in the PQM model

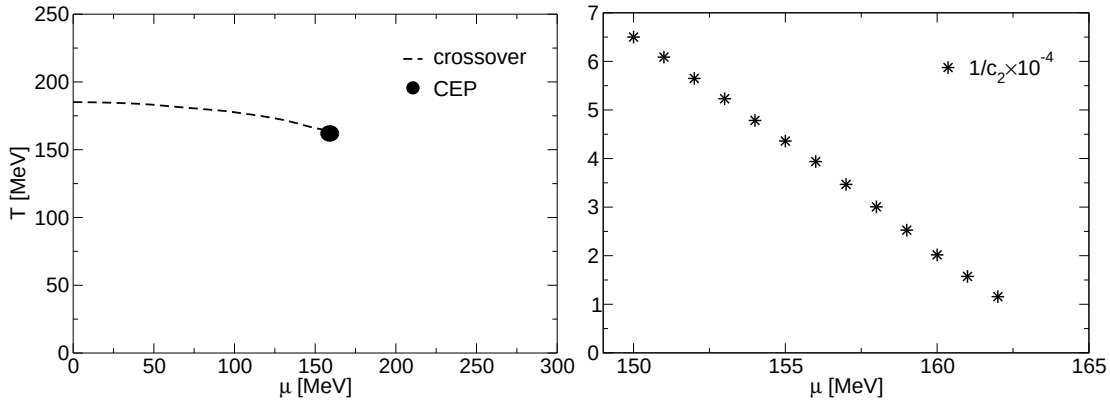

Figure 5.7: The phase diagram of the PQM model in mean field approximation with the CEP located at $(T_c, \mu_c) = (163, 164)$ MeV (left panel) and inverse of the coefficient c_2 along the crossover line in the vicinity of CEP (right panel).

at $\mu/T \simeq 1$. Consequently, at this value of μ/T, R_κ should vanish at the critical temperature. It is clear from the right panel of Fig. 5.6 that R_κ reflects the $O(4)$ critical dynamics. However, the approximate R_κ, obtained by a Taylor expansion of the numerator and the denominator, is not adequate to identify the position of the CEP by a zero of R_κ. Although the value of R_κ at T_c drops with increasing μ/T, as the CEP is approached, it remains different from zero. This is clearly a consequence of the Taylor expansion, since the zero of R_κ is due to the singularity of the quark number susceptibility, which is not reproduced by a polynomial of finite order.

In the left panel of Fig. 5.6 we show the temperature dependence of the dimensionless inverse compressibility R_κ (5.37) computed in the PQM model for fixed $\mu/T = 0.8$ and for various values of m_π. We follow the procedure in the LGT calculations of [80, 45], and compute n_q and χ_q keeping only the first two non-vanishing coefficients, c_2 and c_4. The low T values of R_κ are consistent with the low-temperature limit (5.40), indicated by the arrows in the right panel. For large temperatures, $T \gg T_c$, R_κ is independent of m_π and slowly converges to the ideal gas value (5.30). Similarly as in the case of $R_{4,2}$, R_κ deviates substantially from the Stefan-Boltzmann result, due to the gentle approach of the Polyakov loop to unity.

In the end of the mean field analysis, we shall explore the phase diagram of the PQM model and locate the critical endpoint. One of the most interesting studies concerning QCD thermodynamics is the phase structure and the corresponding phase diagram. Several effective theories predict the existence of the CEP in the QCD phase diagram. The CEP marks the end of the first order phase transition line and for temperatures above the CEP a smooth crossover takes place. Even for physical pion masses the phase transition at the CEP is a second order one. Thus,

a divergence of the quark number susceptibility χ_q signals the location of the CEP. Since the chiral susceptibility χ_σ is proportional to the inverse of the sigma mass squared

$$\chi_\sigma \sim \frac{1}{m_\sigma^2},$$

a zero of the sigma mass m_σ along the chiral boundary can be used to determine the position of the CEP. The values of T and μ were $m_\sigma = 0$ correspond to the position of CEP. Equivalently, one can consider the net quark number fluctuations c_2 which, according to the $Z(2)$ universality, diverge at the CEP. This is easy to see from Eq. (5.21) where $c_2 \sim \chi_q$. We will follow a similar line of reasoning and use Eq. (5.19) where the coefficient c_2 is defined. It is clear that the Taylor coefficient c_2 can be interpreted as the quark number susceptibility (divided by the temperature squared) at $\mu = 0$. The idea is to use the expansion (5.19) also at finite values of chemical potential μ and not only at $\mu = 0$. In this way we can calculate the susceptibility c_2 along the crossover line. As we approach the CEP we expect to see a rapid increase in c_2 and finally a divergence at the CEP.

Our results for the behavior of c_2 along the crossover line in the vicinity of the CEP are shown in Fig. 5.7-right. Here we plot the inverse of the coefficient c_2 along the crossover line and observe a decrease towards zero as the CEP is approached. The CEP is located at $(T_c, \mu_c) = (163, 164)$ MeV which is in perfect agreement with the value obtained in [33]. The corresponding phase diagram of the PQM model in the mean field approximation with the CEP is shown in Fig. 5.7-left. The crossover line itself is determined by finding the maximum of the chiral susceptibility (i.e. the inverse of sigma mass squared). Under mean field dynamics the PQM model exhibits a smooth crossover on the temperature axis as shown in Fig. 5.7-left, where to the right of the CEP, the transition is first order (not shown in the figure).

5.2 Chiral models in FRG approach

In this section we treat the PQM model within the FRG approach, in order to go beyond the mean field approximation and to include vacuum and thermal fluctuations. However, we stress the fact that altough we use the FRG formalism, the Polyakov loop variables will be treated on a mean field level. In the flow of quarks and mesons we include a coupling of the quarks with a background gluonic field. Altough we treat Polyakov loops only on a mean field level, we expect to see the influence of gluonic background on the flow. In this way we can extend various renormalization group treatments of the chiral quark meson model by including gluonic degrees of freedom in the flow equation. This approximation is a first step towards full RG treatment of the PQM model.

In the analysis of the vacuum and thermal fluctuations and the thermodynamics

in the PQM model, we start with the following truncated action

$$\Gamma_k = \int d^4x \left\{ \frac{1}{2} \left(\partial_\mu \phi\right)^2 + \bar{\psi} \partial\!\!\!/ \psi + g \bar{\psi} \left(\sigma + i \vec{\tau} \cdot \vec{\pi} \gamma_5\right) \psi + U_k(\rho) \,, \right\}, \tag{5.41}$$

and introduce the finite quark chemical potential μ and the gauge potential A_0 through the following substitution of the time derivative

$$\partial_0 \to \partial_0 + i(\mu + iA_0). \tag{5.42}$$

In Eq. (5.41) we do not show the explicit contribution of the Polyakov loop potential (2.39). Here, we will apply, as in the Chapter 4, the optimized cutoff functions. For bosons, the cutoff function that depends only on spatial components reads

$$R_{B,k}^{\rm opt}(\mathbf{q}^2) = (k^2 - \mathbf{q}^2)\theta(k^2 - \mathbf{q}^2). \tag{5.43}$$

whereas for fermions we use [49]

$$R_{F,k}^{\rm opt}(\mathbf{q}) = (\not{q} + i\gamma^0 \alpha_0) \left(\sqrt{\frac{(q_0 + i\alpha_0)^2 + k^2}{(q_0 + i\alpha_0)^2 + \mathbf{q}^2}} - 1 \right) \theta(k^2 - \mathbf{q}^2). \tag{5.44}$$

where $\alpha_0 = \mu + iA_0$ is modified due to coupling of the fermions to the background gluons. Using Eq. (5.41) with the cutoff functions given above we obtain the following flow equation for the scale dependent grand canonical potential $\Omega_k(T,\mu)$ for finite temperature and chemical potential in a gluonic background [49]

$$\begin{aligned} \partial_k \Omega_k(T,\mu) \;\; = \;\; & \frac{k^4}{12\pi^2} \left[\frac{3}{E_\pi} \Big(1 + 2n_B(E_\pi) \Big) + \frac{1}{E_\sigma} \Big(1 + 2n_B(E_\sigma) \Big) \right. \\ & \left. - \frac{2\nu_q}{E_q} \Big(1 - N(\ell, \ell^*; T, \mu) - \bar{N}(\ell, \ell^*; T, \mu) \Big) \right] . \end{aligned} \tag{5.45}$$

The functions $N(\ell, \ell^*; T, \mu)$ and $\bar{N}(\ell, \ell^*; T, \mu)$ in the fermionic part of the flow represent the modified distribution functions given by

$$N(\ell, \ell^*; T, \mu) = \frac{1 + 2\ell^* \exp(\beta(E_q - \mu)) + \ell \exp(2\beta(E_q - \mu))}{1 + 3\ell \exp(2\beta(E_q - \mu)) + 3\ell^* \exp(\beta(E_q - \mu)) + \exp(3\beta(E_q - \mu))} \tag{5.46}$$

and

$$\bar{N}(\ell, \ell^*; T, \mu) = \frac{1 + 2\ell \exp(\beta(E_q + \mu)) + \ell^* \exp(2\beta(E_q + \mu))}{1 + 3\ell \exp(\beta(E_q + \mu)) + 3\ell^* \exp(2\beta(E_q + \mu)) + \exp(3\beta(E_q + \mu))}. \tag{5.47}$$

The symmetry under charge conjugation introduced above is easily seen in the form of $N(\ell, \ell^*; T, \mu)$ and $\bar{N}(\ell, \ell^*; T, \mu)$. For $\mu \to -\mu$ the Polyakov loop and its conjugate are interchanged,

$$N(\ell^*, \ell; T, -\mu) = \bar{N}(\ell, \ell^*; T, \mu). \tag{5.48}$$

Furthermore, in the high temperature limit where $\ell, \ell^* \to 1$ the usual Fermi-Dirac distribution functions are recovered

$$\begin{aligned} N(\ell, \ell^* = 1; T, \mu) &\to \frac{1}{\exp \beta(E_q - \mu) + 1}, \\ \bar{N}(\ell, \ell^* = 1; T, \mu) &\to \frac{1}{\exp \beta(E_q + \mu) + 1}. \end{aligned}$$

Consequently, in this limit one recovers the flow equation for the chiral quark-meson model without Polyakov loops, as expected (cf. Eq. (4.34)). On the other hand, for $\ell, \ell^* \to 0$ which is expected to be the case at low temperatures, only three quark states contribute in the fermionic part of the flow.

The Polyakov loop variables appearing in Eq. (5.45) will be treated on a mean field level. Thus, in order to solve the flow equation Eq. (5.45) we first solve the mean field equations of motion Eq. (5.17) for a given temperature and chemical potential. The mean field values for ℓ and ℓ^* obtained in this way serve as input for the solution of Eq. (5.45) at the same temperature and chemical potential using the method described in Chapter 4. The initial values for the flow equation (5.45) are fixed in such a way as to obtain physical values for the pion decay constant and for the sigma, pion and constituent quark masses. Here we employ the same value for the UV cutoff as the one used in Chapter 4 in order to have a consistent picture of the FRG analysis.

In order to investigate the phase structure of the model we first calculate the order parameter $\langle\sigma\rangle$ and its derivative with respect to the temperature at vanishing chemical potential μ. The corresponding results are presented in Fig. 5.8.

As expected, the model exhibits a smooth crossover on the temperature axis for a physical pion mass as illustrated by the temperature dependence of the order parameter $\langle\sigma\rangle$ shown in Fig. 5.8-left. The pseudocritical temperature in the presence of an explicit symmetry breaking term is identified by a peak in the temperature derivative of the order parameter. However, in Fig. 5.8-right we see two pronounced peaks appearing at different temperatures. This behavior is probably a consequence of the model and the approximations used. It is related to the way the background gluon field is included in the flow equation. The first peak corresponds to the deconfinement transition in the mean field calculation. The second peak, on the other hand corresponds to the critical temperature of the chiral phase transition from the RG flow. Whether this behavior persists when also the fluctuations of the Polyakov loop are properly included remains open and calls for further RG studies. In this context it is interesting to note that a coincidence of the two transitions is not

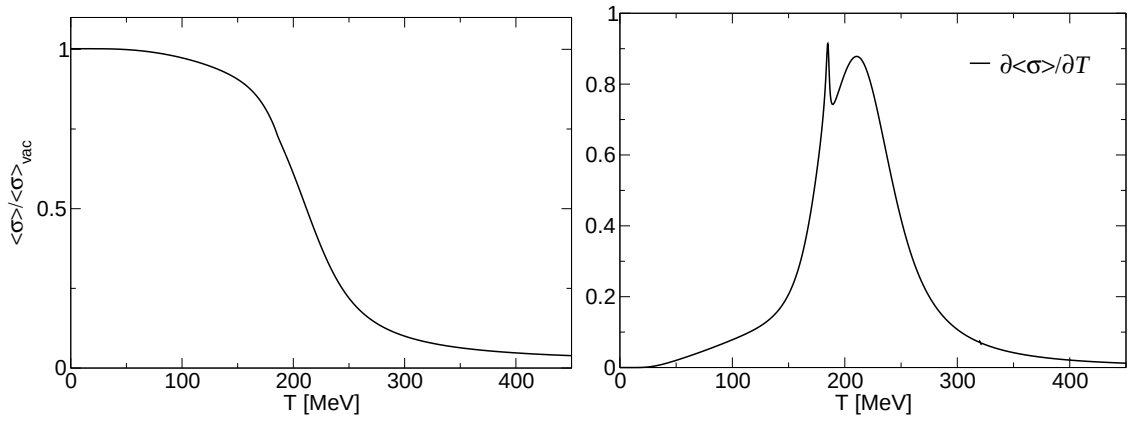

Figure 5.8: Order parameter for the chiral phase transition $\langle\sigma\rangle$ at $\mu = 0$ (left panel) and derivative $-\partial\langle\sigma\rangle/\partial T$ in FRG approach (right panel).

obtained in the present approximation by tuning the parameter T_0. In general the relation between deconfinement and chiral phase transition is not well established and at present also recent LGT calculations lead to conflicting conclusions about the relative position of these transitions at finite T [18, 19].

Our next subjects of study within the FRG formalism are the Taylor expansion coefficients c_2 and c_4. As in the mean field case, we calculate the pressure (5.19) at fixed temperature T as a function of chemical potential μ and then fit to a polynomial in μ. In this way we extract the polynomial coefficients from the fit. First, we will neglect the gluonic background and apply the FRG to the chiral quark-meson model. Here we use the flow equation (4.34) (or equivalently Eq. (5.45) with the condition $\ell, \ell^* \to 1$) and solve it with the same initial conditions that in vacuum reproduce the physical values of relevant observables (cf. Chapter 4). In Fig. 5.9 we show our results for the coefficients c_2 and c_4.

As already observed in the mean field calculation, the lack of suppression of quark degrees of freedom in the low temperature regime is clearly reflected in these results. However, at high temperatures the behavior of the coefficients c_2 and c_4 differs considerably from that seen in the mean field approximation. The application of the RG method leads to strong suppression of fluctuations just above the chiral transition due to the UV cutoff. This is also the reason why c_2 and c_4 do not converge to their ideal gas values.

The next step in the study of c_2 and c_4 within the FRG framework is the inclusion of Polyakov loops. Although we treat Polyakov loops only on a mean field level, we do expect to see a change in behavior of coefficients due to the presence of the gluonic background. Indeed, we observe the expected suppression of quark degrees of freedom at low temperatures as seen in Fig. 5.10.

The non-vanishing background field essentially modifies the properties of the

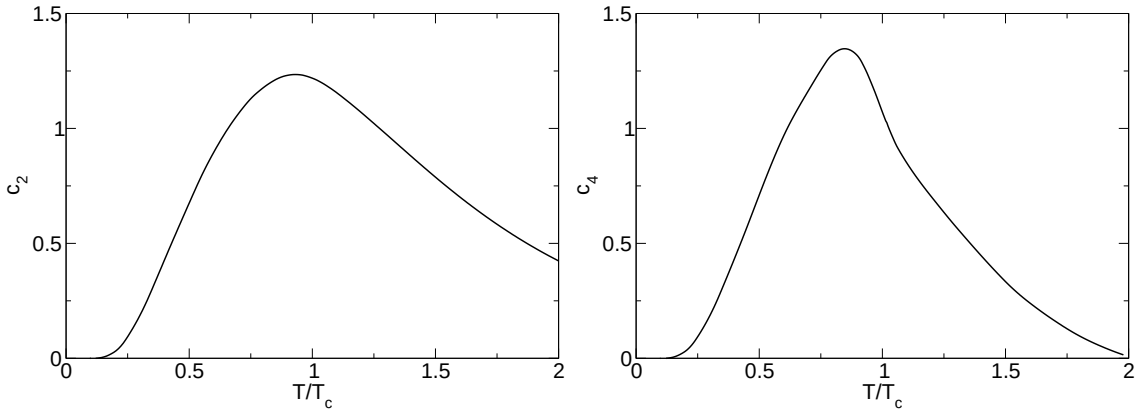

Figure 5.9: Coefficient c_2 (left panel) and coefficient c_4 (right panel) in FRG approach for the chiral quark-meson model.

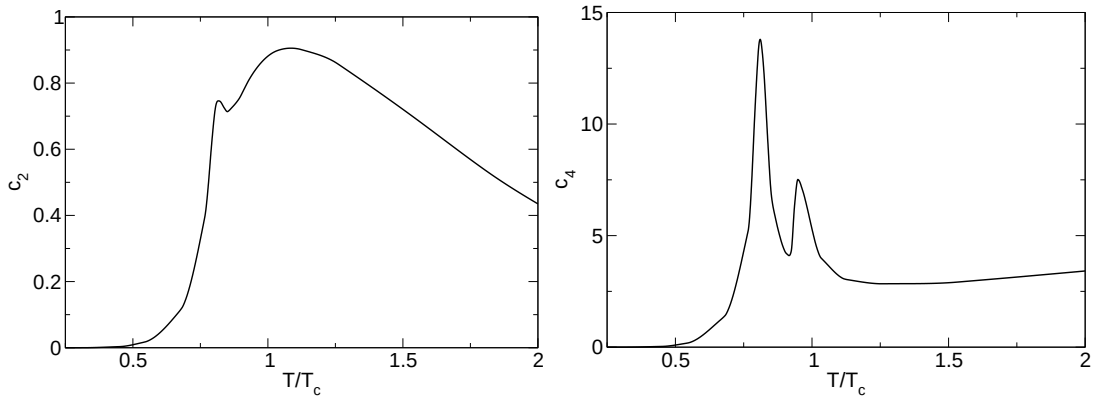

Figure 5.10: Coefficient c_2 (left panel) and coefficient c_4 (right panel) in FRG approach for the PQM model.

quark fluctuations and consequently influences the low temperature behavior of the second and fourth order coefficient. Thus, in the chirally broken phase, there is a strong suppression of the quark fluctuations due to their coupling to the Polyakov loop. This is because, as already observed under mean field dynamics, the Polyakov loop suppresses the contributions of single and double quark modes to the thermodynamic potential. Second, similarly as in the case of the order parameter $\langle\sigma\rangle$ (cf. Fig. 5.8) there is a remnant of the deconfinement transition seen as a small peak at $T = T_{dec}$. Still, the quantum fluctuations in the chiral quark-meson model, with and without Polyakov loops clearly preserve the essential, low temperature behavior of c_2 and c_4.

As in the mean field case we also investigate the behavior of the $R_{4,2}$ ratios defined as the kurtosis in Eq. (5.26). The low temperature behavior of kurtosis as the measure of the quark content of the leading particles carrying baryon number is preserved within the FRG scheme. At low temperature, the kurtosis in the FRG-PQM model equals $R_{4,2} = 9$, in agreement with the LGT and hadron resonance gas model results [80, 45]. In the absence of the Polyakov loop in the flow equation, the one- instead of three- quark states dominate the thermodynamics at low temperature. Consequently, in the FRG-QM model $R_{4,2} = 1$ is obtained instead of 9. From the above discussion it is clear that the interactions of quarks with the background Polyakov loop are essential to correctly reproduce the asymptotic behaviors of the $R_{4,2}$ found in the LGT calculations.

At high temperature, due to finite cutoff effects ($\Lambda_{UV} = 1.2$ GeV) the ratio $R_{4,2}$ calculated in the chiral quark-meson model and PQM model does not converge to the expected ideal gas value, where $R_{4,2} = 6/\pi^2$. The strong suppression of c_4 at high temperature due to the finite cutoff seen in Fig. 5.9-right implies large deviations of $R_{4,2}$ from its asymptotic, ideal gas value. The cutoff actually also affects the critical region and leads in the FRG approach to the shift of the peak position of c_4 towards $T < T_c$. This behavior is also seen in Fig. 5.9-left.

A characteristic feature of the FRG-PQM model is a remnant of the deconfinement transition that appears as a peak in the chiral susceptibility and the higher order moments of quark fluctuations. Such a behavior is also seen in Fig. 5.11-right in the $R_{4,2}$ ratio. The basic property of kurtosis as a measure of the net quark content of the baryon number carrying effective degrees of freedom is clearly related to either confinement or "statistical confinement". However, the pion mass dependence and increase of $R_{4,2}$ near T_c when approaching the chiral limit is quantitatively consistent with $O(4)$ scaling [102]. In the FRG-PQM model, the observed splitting of the "deconfinement" and "chiral" peak in $R_{4,2}$ may be a consequence of the particular truncation of the effective action in Eq. (5.45) and the fact that in the actual calculations $T_{dec} < T_c$ by construction. Nevertheless, the enhancement of the kurtosis in the critical region could be of physical importance indicating that the lattice results for the kurtosis in the critical region are due to the combination of confinement and chiral dynamics. Clearly, it would be very interesting to implement

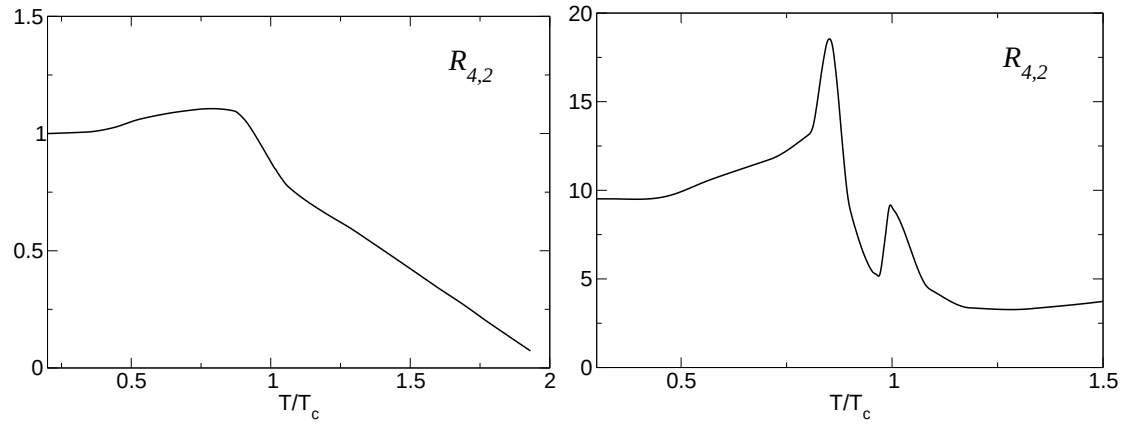

Figure 5.11: The kurtosis $R_{4,2}$ calculated within FRG scheme in the quark-meson model (left panel) and in the Polyakov loop extended quark-meson model (right panel).

the RG scheme such that it includes also fluctuations of the Polyakov loop. This would allow us to explore the relation between the confinement and chiral transition within the PQM model and study their contributions to the relative net quark number fluctuations in the critical region.

We will finish our FRG treatment of the PQM model by studying the corresponding phase diagram, which is shown for a physical pion mass in Fig. 5.12-left. Comparing the mean field results obtained previously with the RG results shown in Fig. 5.12-left it is clear that there is a significant shift in the position of the CEP towards smaller temperatures and higher chemical potential due to fluctuations. In the mean field approximation we located the CEP at $T_c = 163$ MeV and $\mu_c = 164$ MeV whereas in our RG studies we find $T_c = 98$ MeV and $\mu_c = 307$ MeV. To locate the position of the CEP in the phase diagram, we have applied the same procedure as in the mean field case. The change of fluctuations at finite chemical potential along the chiral boundary line has been calculated using the Taylor expansion (5.19) around $\mu = \mu_c$. Then, the $c_2(T_c)$ is a measure of the net quark number fluctuations at finite critical chemical potential. In Fig. 5.12-right we show the inverse c_2 along the crossover line obtained in the FRG framework. There is a clear decrease of $1/c_2$ with increasing μ. The value of $\mu = \mu_c$ where $1/c_2 \to 0$, as in the mean field case, indicates the position of the CEP. Also, there is a clear shift in the position of the chiral boundary to higher temperatures due to quantum fluctuations. Such a behavior was also observed in the chiral quark-meson model within the FRG approach [59].

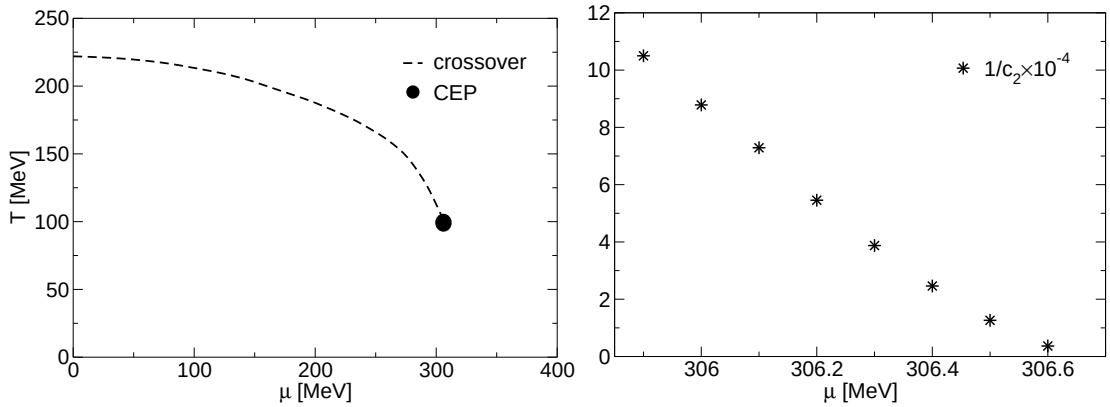

Figure 5.12: The phase diagram of the PQM model in FRG approach with the CEP located at $(T_c, \mu_c) = (98, 307)$ MeV (left panel) and inverse of the coefficient c_2 along the crossover line in the vicinity of CEP (right panel).

5.2.1 Linking with QCD

In the previous section we have analyzed several thermodynamic observables with the FRG formalism. Despite the fact that by using the RG technique one can include also meson loops (i.e. take into account quantum fluctuations), there is a significant drawback that plagues the FRG calculations. The inevitable introduction of an UV cutoff Λ_{UV}, where the initial conditions for the flow equations are given, affects the high temperature physics[6].

In order to obtain more realistic results within the RG approach, one has to carefully choose the right value for the UV cutoff Λ_{UV}. This choice can depend on the physics or the temperature region one wants to investigate. Hence, there is some temperature beyond which one cannot trust the RG results anymore. In this region the UV cutoff Λ_{UV} suppresses high momenta, which in turn influences observables that are calculated within RG approach. What happens in the high temperature region, we have already seen in Fig. 5.9. Various thermodynamic quantities decrease at high temperatures (they do not converge to the Stefan-Boltzmann limits). The coefficient c_2 obtained from the pressure, also shows this behavior. The RG calculations lead to a strong suppression of fluctuations just above the chiral transition due to the UV cutoff which is set to $\Lambda_{UV} = 1.2$ GeV. Thus, removing the cutoff Λ_{UV} and matching the low energy theory with the high temperature region is a highly non-trivial task.

Now we extend the flow equation for the grand canonical potential $\Omega(T, \mu)$ given

[6]The matter concerning the cutoff effect is a subtle issue. Still, the choice of an effective field theory can also have a considerable influence on the high (or low) energy physics. The chiral quark-meson model is a low energy model and lacks gauge degrees of freedom. This can also be a reason for obtaining results that deviate from LGT calculations.

by Eq. (5.45) in order to approach the high energy sector of QCD. The idea is to add to Eq. (5.45) a flow equation for the high-energy degrees of freedom. A first attempt in this direction has been made in Ref. [46]. According to LGT [50, 51] the equation of state of an interacting system has the properties of a free gas at high temperatures ($T \geq 200$ MeV). Thus, one can neglect the full gauge interactions of the high energy QCD and approximate the corresponding system with a free gas of quarks and gluons at some scale $k > \Lambda_{UV}$. The advantage of using this sort of an approximation is to remove the cutoff Λ_{UV} which is inevitably present during integration of Eq. (5.45).

We start with the flow equation without Polyakov loops for several reasons. First, by using the set of optimized regulators we can integrate the existing flow equation for chiral quark-meson model for the high-energy degrees of freedom analytically. The second point is that we are interested only in the high-energy part of the flow i.e. for $k > \Lambda_{UV}$. For the energy scale $k < \Lambda_{UV}$ we will switch again to Eq. (5.45). Here we use a simplified model of a gas of massless quarks and gluons to link the high-energy degrees of freedom with the chiral low-energy part.

We again use the optimized cutoff functions and neglect the current quark mass for the two light flavors. The flow equation for the high-energy part has then the following form

$$\partial_k \Omega_k^{UV}(T,\mu) = \frac{k^3}{12\pi^2}\left[16\Big(1+2n_B(k)\Big) - 2\nu_q\Big(1-n_F(k)-\bar{n}_F(k)\Big)\right]. \qquad (5.49)$$

In order to link the effective chiral quark-meson model with high-energy degrees of freedom we shall adapt the idea introduced in Ref. [46] and proceed as follows. First, we integrate Eq. (5.49) starting with some cutoff Λ_∞ which can be placed at infinity, to Λ_{UV} which is the cutoff used for integrating flow equation (5.45) or its simplified form with no Polyakov loop. At the scale $k = \Lambda_{UV}$ we switch to Eq. (5.45) or its analogue without Polyakov loop and integrate the remaining flow equation down to $k = 0$. In this way one has a smooth transition from the high energy part of the theory to the chiral low-energy part. The main goal we aim for in this approximation is to remove the dependence on the cutoff Λ_{UV}. This is easy to achieve due to the simple form of Eq. (5.49) which allows an analytic integration starting from infinity.

The integration of Eq. (5.49) yields

$$\Omega^{UV}(T,\mu) = \frac{1}{6\pi^2}\left(16N_B + 12N_F - 12\bar{N}_F\right)\Big|_\infty^{\Lambda_{UV}} \qquad (5.50)$$

where the following functions have been introduced

$$N_B = \frac{k^4}{8} - k^3 T \mathrm{Li}_1[e^{-k/T}] - 3k^2T^2\mathrm{Li}_2[e^{-k/T}] - 6kT^3\mathrm{Li}_3[e^{-k/T}] - 6T^4\mathrm{Li}_4[e^{-k/T}], \quad (5.51a)$$

$$N_F = \frac{k^4}{8} - k^3 T \mathrm{Li}_1[e^{-(k-\mu)/T}] - 3k^2T^2\mathrm{Li}_2[e^{-(k-\mu)/T}] - 6kT^3\mathrm{Li}_3[e^{-(k-\mu)/T}] - 6T^4\mathrm{Li}_4[e^{-(k-\mu)/T}], \quad (5.51b)$$

$$\bar{N_F} = \frac{k^4}{8} - k^3 T \mathrm{Li}_1[-e^{-(k+\mu)/T}] - 3k^2T^2\mathrm{Li}_2[-e^{-(k+\mu)/T}] - 6kT^3\mathrm{Li}_3[-e^{-(k+\mu)/T}] - 6T^4\mathrm{Li}_4[-e^{-(k+\mu)/T}], \quad (5.51c)$$

and $\mathrm{Li}_n[z]$ are the polylogarithmic functions given in Appendix B. The arguments of the polylogarithm functions in Eqs. (5.51a), (5.51b) and (5.51c) represent the classical Maxwell-Boltzmann distribution functions for gluons, quarks and antiquarks respectively. Using the feature that the polylogarithmic function vanishes at zero, Eq. (5.50) can further be calculated by substituting the limits of integration. Obviously, a divergent part in Eq. (5.50) will nevertheless remain. However, the vacuum part can also be easily calculated

$$\Omega_{vac}^{UV}(T,\mu) = \frac{8}{3\pi^2}\left(\frac{\Lambda_{UV}^4}{8} - \frac{\Lambda_\infty^4}{8}\right). \quad (5.52)$$

Knowing that the finite temperature part of the pressure does not depend on the vacuum energy, we can extract the high-energy contribution to the pressure, since the regularized divergent part of the potential drops out [46]. This high-energy contribution we then add to the one obtained from the RG calculation. We show our results in Fig. 5.13.

There is now a smooth transition of fluctuations from the high- to the chiral, low-energy part of the theory. Also for high temperatures we observe that both, c_2 and c_4 approach to their ideal gas value. This has not been the case where these coefficients have been calculated only within a RG method, due to a finite UV cutoff.

5.3 Conclusions

In this chapter we have investigated some thermodynamic properties as well as the phase structure of hot and dense matter. As a tool, we used both, the mean field approximation and the FRG approach. The effective model we have used was the PQM model. In order to exhibit the importance of gluonic degrees of freedom, we also used the chiral quark-meson model and compared the results obtained with this model with the ones where gluon dynamics is included via the Polyakov loop.

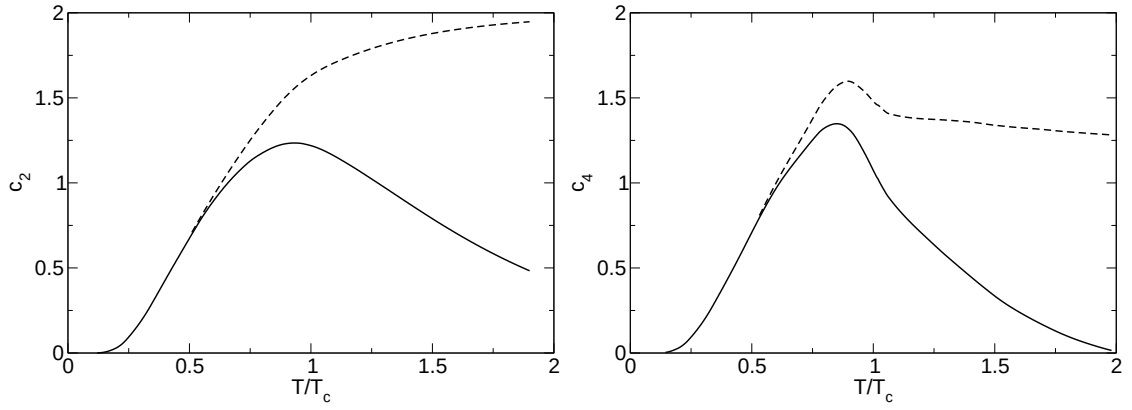

Figure 5.13: Taylor expansion coefficient c_2 (left panel) and c_4 (right panel) for the chiral quark-meson model calculated in the FRG approach with a cutoff Λ_{UV} (solid line) and after removing the cutoff by the inclusion of an additional flow for a free gas of quarks and gluons (dashed line).

The mean field investigation of the PQM model started with the exploration of the temperature dependence of the Polyakov loop at vanishing chemical potential μ. We used this behavior to determine the deconfinement transition temperature. This temperature was obtained by calculating the temperature derivative of the Polyakov loop. The position of the peak marks the deconfinement transition.

The next subject we addressed was the in-medium meson masses and the constituent quark mass. We have studied their behavior also at $\mu = 0$. Subsequent to this study, we have applied the Taylor expansion method of the pressure for vanishing μ. The reason for this was twofold. First, we wanted to emphasize the importance of gluonic degrees of freedom. Second, we used this expansion in the study of further thermodynamic observables that have proven to be valuable probes of deconfinement and chiral dynamics. We have extracted the expansion coefficients c_2 and c_4 and showed their temperature dependence. In the case where no gluonic background is present (chiral quark-meson model) we see, as expected, the absence of suppression of quark degrees of freedom at low temperatures. On the other hand, after calculating coefficient c_2 for the PQM model, the suppression in the low temperature region is present.

In the first part of the chapter, the focus of our study was also on the properties of the kurtosis $R_{4,2}$ of net quark number fluctuations and the dimensionless inverse compressibility R_κ. We have studied the behavior of these observables near the chiral transition as functions of the pion mass. We showed that it is necessary to include the coupling of the quarks to the Polyakov loop, in order to reproduce the low-temperature behavior of the kurtosis expected in QCD. We also demonstrated that near the pseudocritical temperature, both these observables are very sensitive

to the pion mass. For the physical value of m_π, the kurtosis develops a peak and the inverse compressibility a dip at the pseudocritical temperature. These structures disappear for large m_π. Our results supports the notion that, for physical quark masses, the strange quark decouples from the critical fluctuations and the scaling properties are governed by $O(4)$, the expected universality class of two flavor QCD. We also found a suppression of R_κ, as the critical end point CEP is approached. However, R_κ remains finite at the CEP, if the Taylor expansion in μ/T of the thermodynamic pressure is used.

Furthermore, we also explored the phase diagram of the PQM model, for the physical pion mass. Exploring the behavior of the coefficient c_2 along the crossover line, we located the position of the CEP. We calculated the inverse of c_2 along the crossover line from the Taylor expansion of the pressure, but now, at finite values of chemical potential μ. Consequently, as c_2 is related to the fluctuations of the net quark number, we observed a rapid decrease of the inverse of c_2 as the CEP is approached.

In the second part, we applied the FRG method to the chiral quark-meson model as well as to the PQM model. We have discussed different thermodynamic properties of the PQM model including quantum fluctuations within FRG method. In order to do so, we have introduced a suitable truncation of the PQM model that allowed us to extend the previous RG based studies of the chiral quark-meson model. This truncation consists of introducing a coupling of fermions to Polyakov loops. We have derived and subsequently solved the flow equation for the scale dependent thermodynamic potential at finite temperature and density in the presence of a background gluonic field. In our studies of thermodynamics we have discussed the role of fluctuations on the critical properties of the model. We have shown that the non-perturbative dynamics introduced within the FRG method modifies the phase diagram leading to a shift in the position of the CEP towards lower temperature. Furthermore, following the investigations in the mean field approximation we have again, now within the FRG method, analyzed the fluctuations of the net quark number density and the ratio of its fourth to second order cumulant moments (kurtosis). A comparison of the FRG approach with and without gluon background field was performed. We have shown that the FRG extended quark-meson model preserves basic properties of kurtosis obtained in the LGT calculations only if the Polyakov loop is included in the flow equation. Thus, the extension of the FRG method proposed here, that accounts for couplings of fermions to background gluon fields is of particular relevance if the quark-meson model is considered as an effective description of the QCD thermodynamics near the phase transition.

Finally, the influence of the ultraviolet cutoff effects on the thermodynamics within the FRG approach was also discussed. By means of a simple model that is represented as a free gas of massless quarks and gluons, we have introduced an additional flow equation for the high-energy degrees of freedom. Within this approximation we have undertaken a full RG study of the coefficients c_2 and c_4 for the chiral

quark-meson model. The results are in excellent agreement with the corresponding Stefan-Boltzmann limits in the high temperature region. The cutoff effect has been successfully removed, and the Taylor expansion coefficients approach their expected ideal gas values.

Chapter 6

Summary and outlook

In this thesis the main subject of investigation was the behavior of matter under extreme conditions, i.e. hot and dense matter. We have used two effective theory models (the chiral quark-meson model and the Polyakov quark-meson model) in order to assess various thermodynamic properties as well as the critical behavior of QCD at nonvanishing temperature and chemical potential. In order to obtain our results, we have used the aforementioned models as a low-energy realization of QCD. In the low-energy region QCD is highly nonperturbative (i.e. calculation based on perturbation theory fail). As a tool for performing the calculations we have employed the functional renormalization group approach to assess the role of fluctuations. Besides the RG approach, we have also used the mean field approximation. The RG approach has proven to be useful in investigating the scaling behavior of the chiral quark-meson model, whereas both, the RG and mean field calculations have been used in exploring various thermodynamic properties, the phase diagram and the phase structure of the chiral quark-meson and the PQM model. Apart from comparing the results that have been obtained within these two different approaches, we have also investigated the effects of including or excluding certain degrees of freedom present in the models. In this way we have put emphasis on the gluonic degrees of freedom and their contribution to QCD thermodynamics. The importance of having a gluonic background in effective QCD-inspired model is highlighted by our results obtained both, in the mean field as well as in the RG approach. We have also obtained the corresponding phase diagrams for both models, calculated for physical pion masses. In each case we have also located the critical endpoint at the end of the crossover line.

Summary

In the first chapter of this thesis we have given a short motivation for our study. What followed, was Chapter 2 where some basic concepts regarding (non)-Abelian gauge theories were introduced and explained. Here, we avoided going into details (especially into subtle mathematical details concerning functional methods and group theory, since they are not of crucial importance in our work) and rather tried to give an overall picture of gauge theories and especially the strong interaction. Further, in this chapter we have also introduced models used in our studies, namely the chiral quark-meson model and its extension, the Polyakov quark-meson model. For both models we have given the Lagrangians and discussed the main features. In the end, the basic concepts of chiral symmetry breaking and confinement/deconfinement were introduced and discussed.

The renormalization group approach was introduced in Chapter 3. In the first part of Chapter 3, the motivation for using the RG method was given. This particular theoretical method was the main tool in the calculations, where we explored the critical properties and the scaling behavior of the chiral quark-meson model. At the beginning of Chapter 3, we introduced the main ideas of the RG approach. Next, we also discussed the most important features of the RG and briefly discussed the problems where this method has already been successfully applied.

The focus of this presentation were the critical phenomena, as the most prominent example of the success of the RG approach in physics. Later, in the subsequent section of Chapter 3, we focused on one special RG approach, namely the functional renormalization group (FRG) approach. Before giving the main characteristics of the FRG, we also introduced the basic concepts of some important objects that appear in quantum field theory and statistical physics. The notions of the generating functional of the n-point correlation functions, (dis)connected Green functions and finally, the effective action have been introduced and briefly explained. The most important part, the flow equation for the effective average action was derived. We also discussed the most important features and properties of the flow equation, that was the starting point in all our RG investigation at nonvanishing temperature and chemical potential.

In Chapter 4 we employed the FRG method in order to explore the critical properties of the chiral-quark meson model and the $O(4)$ scaling. As a starting point for our study we used the flow equation for the scale dependent thermodynamic potential at finite temperature and density, which we derived in the presence of a symmetry-breaking external field. The main focus of our study was the universal scaling behavior of various physical quantities that are sensitive to the chiral phase transition.

We also analyzed the leading scaling behavior of the longitudinal and transverse susceptibilities as well as their ratios. In this case, the critical point was approached from the side of the symmetric and the broken phase for small, but finite values of the

external field. The notion of effective critical exponents was defined and connected with the calculated ratios of some physical quantities. The values of the critical exponents that were extracted, directly through logarithmic fits and indirectly through different ratios of corresponding observables, confirm the expectations that the chiral phase transition of the 2-flavor effective chiral quark-meson model belongs to the $O(4)$ universality class.

In Chapter 5 we considered the chiral quark-meson model and the PQM model also for finite values of the chemical potential. The first part of the analysis was done in the mean field approximation. Subjects of our study was different thermodynamic properties as well as the phase structure of these models. Here, we have focused on the behavior of the kurtosis $R_{4,2}$ of the net quark number fluctuations and the dimensionless inverse compressibility R_κ near the chiral transition as functions of the pion mass. In all these calculations, we have employed the Taylor expansion of the pressure and also extracted the expansion coefficients c_2 and c_4. By observing how these coefficients behave as functions of temperature T, we demonstrated the importance of gluonic degrees of freedom in the model. Using the same Taylor expansion, but now expanding the pressure around the non zero (critical) chemical potential, we have calculated the coefficient c_2 along the crossover line. The coefficient c_2 is related to fluctuations of net quark number and consequently, this method has been used to locate the position of the critical endpoint in the phase diagram.

In the second part of Chapter 5, the PQM model was analyzed within the FRG approach. Still, the Polyakov loop variable was treated on the mean field level. We have again in our calculations used the Taylor expansion of the pressure to calculate coefficients the c_2 and c_4. First, all calculations have been done for the chiral quark-meson model. Later, we have included Polyakov loops in order to explore the effect of having gluonic degrees of freedom in the model. As in the mean field case, we showed the corresponding phase diagram with the critical endpoint, that was determined in the same way as in the mean field approximation.

In the end we have also addressed the issue of the cutoff effect. This effect is always present in RG calculations, and here we used a simplified model to alleviate this problem. A further flow equation for the thermodynamic potential was introduced in order to link the chiral quark-meson model with the high energy sector of QCD [46]. The full gauge interactions of the high energy sector of QCD were neglected. As a consequence, the system in this regime was approximated by a free gas of quarks and gluons. We showed in the case of the coefficients c_2 and c_4 for the chiral quark-meson model how the cutoff effect can be reduced. This was achieved by integrating the flow equation for a free gas of quarks and gluons from infinity to the cutoff Λ_{UV} and then we have switched to the flow equation for the chiral quark-meson model used in our previous calculations. In this way we obtained for both coefficients c_2 and c_4 a smooth transition from the low energy (chiral) to the high energy part of the theory. Moreover, the cutoff effect was to a large extent removed and c_2 and c_4 show a nice convergence to the corresponding ideal gas values in the high temperature

limit.

Outlook

There are several possible extensions of the work and results presented in this thesis. First, regarding the mean field analysis, one could extend the results presented here by an exact mean field calculation of the dimensionless inverse compressibility R_κ. Due to the Taylor expansion, the value of R_κ is finite even as the CEP is approached. This however should not be the case, since it is expected that R_κ goes to zero. The Taylor expansion used in this work is however good enough to estimate the value of R_κ but not adequate to identify the exact location of the CEP. Thus, we expect that an exact calculation of the dimensionless inverse compressibility must give zero value for R_κ at the CEP. This calculation would then underpin the claim that the vanishing of R_κ should be treated as a signal that the CEP has been approached.

In respect of different approaches and methods used to locate the CEP (theoretically and experimentally) one particular idea has attracted a lot of attention in the heavy-ion community. It has been proposed that the so called focusing of the isentropic lines in the QCD phase diagram could indicate the position of the CEP [103]. This means that the CEP should act as an attractor for isentropic lines in hot and dense matter. Studies done recently within the mean field approximation, show that no strong focusing behavior exists near the CEP [104]. Preliminary results obtained in the mean field approximation as well as in the RG approach confirm these results [105]. Even if fluctuations are included, no focusing behavior is observed. We conclude that focusing towards the CEP is not a universal phenomenon. The work on this subject is still in progress, and the results are not presented in this thesis.

We have also addressed another subject concerning the RG treatment, namely the cutoff effect. It would be interesting to investigate this subtle issue as well as the one concerning the connection between a mean field approximation and a RG approach. In which limit is an RG calculation equivalent to a mean field approximation? Is a UV cutoff in a mean field calculation (for the chiral quark-meson model, where the Dirac see has been neglected, cf. Chapter 2) equivalent to the RG cutoff? Some of these issues are addressed in our recent work [105] that is still in progress.

One of the most challenging and interesting extensions of this work would be towards a full RG treatment of the PQM model. In this thesis, the Polyakov loop variable was studied only in the mean field approximation. A full RG treatment of the Polyakov loop would yield results beyond the usual mean field analysis, since all fluctuations would then be taken into account. In this work we have gone one step beyond the mean field analysis of the PQM model, by coupling the Polyakov loop with quarks within a truncation scheme that is then suitable for a FRG treatment. What is missing in the present approach is the RG flow of the Polyakov loop which would include all fluctuations and would consequently allow a full RG treatment of

the PQM model. In the end, in order to obtain a model that could be extended towards full QCD one would also need to include the whole gauge dynamics. It is plausible that such a full RG analysis would yield results that could give a valuable input to further theoretical and experimental studies of hot and dense QCD matter. This would bring us, at least one step, closer to the understanding of the nature of QCD phase transition(s).

Appendix A

Notations and conventions

Throughout this thesis we work in Euclidean spacetime. For the standard Dirac gamma matrices we have

$$\{\gamma_\mu, \gamma_\nu\} = -2\delta_{\mu\nu}\,. \tag{A.1}$$

Their standard representation is given by

$$\gamma_0 = \begin{pmatrix} i & 0 \\ 0 & -i \end{pmatrix}, \qquad \gamma_j = \begin{pmatrix} 0 & -\sigma_j \\ \sigma_j & 0 \end{pmatrix}, \qquad \gamma_5 = \begin{pmatrix} 0 & -1 \\ -1 & 0 \end{pmatrix}, \tag{A.2}$$

where σ_j are the Pauli matrices

$$\sigma_1 = \begin{pmatrix} 0 & 1 \\ 1 & 0 \end{pmatrix}, \qquad \sigma_2 = \begin{pmatrix} 0 & -i \\ i & 0 \end{pmatrix}, \qquad \sigma_3 = \begin{pmatrix} 1 & 0 \\ 0 & -1 \end{pmatrix}. \tag{A.3}$$

Appendix B

Temperature limits

In this Appendix we investigate more closely the temperature limits of the fermionic contribution to the pressure of the system. We also provide a bit more details concerning derivation of Eqs. (5.24) and (5.31).

Low-temperature limit

In the low-temperature limit one has $\ell, \ell^* \to 0$, which implies the suppression of the one- and two-quark states. The pressure of a system $P(T,\mu)$ is related to the grand canonical potential $\Omega(T,\mu)$ by

$$P(T,\mu) = -\frac{\Omega(T,\mu)}{V}\,. \tag{B.1}$$

Now, using Eq. (5.14) the fermion contribution to the pressure is of the form

$$P_{\bar{q}q} = \frac{N_f T}{\pi^2}\int\limits_0^\infty dp\, p^2 \left(\ln[1+e^{-3(E_p-\mu)/T}] + \ln[1+e^{-3(E_p+\mu)/T}]\right). \tag{B.2}$$

This expression can be brought in other form after integration by parts and reads

$$P_{\bar{q}q} = \frac{N_f T}{\pi^2}\int\limits_0^\infty dp \frac{p^4}{E_p}\left(\frac{1}{e^{3(E_p-\mu)/T}} + \frac{1}{e^{3(E_p+\mu)/T}}\right). \tag{B.3}$$

The next step is to change the variable $x = E_p/m_q$ that transforms (B.3) as follows

$$P_{\bar{q}q} = \frac{N_f T}{\pi^2}\int\limits_1^\infty dx\, m_q^4 \left(x^2-1\right)^{\frac{3}{2}}\left(\frac{1}{e^{3(m_q x-\mu)/T}+1} + \frac{1}{e^{3(m_q x+\mu)/T}+1}\right). \tag{B.4}$$

In order to solve the integrals present in (B.4) we have to use the Boltzmann approximation, that is valid if $3m_q/T > 1$. Thus, in this approximation the fermionic part of the pressure is

$$P_{\bar{q}q} \simeq \frac{N_f T}{\pi^2} \int_1^\infty dx\, m_q^4 \left(x^2-1\right)^{\frac{3}{2}} \left(e^{-3(m_q x-\mu)/T} + e^{-3(m_q x+\mu)/T}\right). \tag{B.5}$$

At this point we have to make a small, but inevitably mathematical detour by introducing the modified Bessel function of the second kind $K_n(z)$ that satisfies various identities[1]. We will make use of the following identity

$$K_n(z) = \frac{\sqrt{\pi}}{\left(n-\frac{1}{2}\right)!} \left(\frac{z}{2}\right)^n \int_1^\infty dx\, (x^2-1)^{n-\frac{1}{2}} e^{-zx}. \tag{B.6}$$

Now, we can represent the fermionic pressure in the low-temperature region, in the Boltzmann approximation with

$$\frac{P_{q\bar{q}}(T,\mu)}{T^4} = \frac{2N_f}{27\pi^2} \left(\frac{3m_q}{T}\right)^2 K_2\left(\frac{3m_q}{T}\right) \cosh\frac{3\mu}{T}, \tag{B.7}$$

that is nothing but Eq. (5.31).

High-temperature limit

As in the low-temperature case, we start with Eq. (5.14) that for $\ell, \ell^* \to 1$ reduces to

$$\frac{\Omega_{\bar{q}q}}{V} = -P_{\bar{q}q} = -2N_c N_f T \int \frac{d^3p}{(2\pi)^3} \left(\ln[1+e^{-(E_p-\mu)/T}] + \ln[1+e^{-(E_p+\mu)/T}]\right). \tag{B.8}$$

Further integration by parts that can be done in the same way as in the low temperature limit, yields for the pressure

$$P_{\bar{q}q} = 2N_c N_f T \frac{1}{6\pi^2} \int_0^\infty dp \frac{p^4}{E_p} \left(n_F(E_p) + \bar{n}_F(E_p)\right), \tag{B.9}$$

[1] By definition, modified Bessel functions of the second kind represent one of the solution to the modified Bessel differential equation

$$z^2 \frac{d^2y}{dz^2} + z\frac{dy}{dz} - (z^2+n^2)y = 0.$$

where $n_F(E_p)$ and $\bar{n}_F(E_p)$ are fermionic distribution functions and $E_p = \sqrt{\vec{p}^{\,2} + m_q^2}$ is the quark energy. In the case of a massless free quark/antiquark gas ($m_q \to 0$), the expression for the pressure simplifies considerably, and reads

$$P_{\bar{q}q} = 2N_c N_f \frac{1}{6\pi^2} \int_0^\infty dp\, p^3 \left(\frac{1}{e^{(p-\mu/)T} + 1} + \frac{1}{e^{(p+\mu/)T} + 1} \right). \tag{B.10}$$

Finally, the integrals appearing in (B.10) can be integrated analytically yielding

$$P_{\bar{q}q} = 2N_c N_f \frac{1}{6\pi^2} (-6T^4) \left(\mathrm{Li}_4(-e^{\mu/T}) + \mathrm{Li}_4(-e^{-\mu/T}) \right). \tag{B.11}$$

With $\mathrm{Li}_n(z)$ we have defined the polylogarithm function that is also known as de Jonquière's function. In a complex plane z it is defined through the following sum

$$\mathrm{Li}_n(z) = \sum_{k=1}^{\infty} \frac{z^k}{k^n}. \tag{B.12}$$

The integral representation of the polylogarithm function is given by

$$\mathrm{Li}_{n+1}(z) = \int_0^z \frac{\mathrm{Li}_n(t)}{t} dt. \tag{B.13}$$

For negative integer values of n the polylogarithm function $\mathrm{Li}_n(z)$ can be expressed as a ratio of polynomials. The polylogarithm functions in (B.11) are given by

$$\mathrm{Li}_4(-e^{\mu/T}) + \mathrm{Li}_4(-e^{-\mu/T}) = -\frac{7\pi^4}{360} - \frac{\pi^2}{12} \left(\frac{\mu}{T} \right)^2 - \frac{1}{24} \left(\frac{\mu}{T} \right)^4, \tag{B.14}$$

and plugging this result back into (B.11) finally gives Eq. (5.24)

$$\frac{P_{\bar{q}q}(T,\mu)}{T^4} = N_f N_c \left[\frac{1}{12\pi^2} \left(\frac{\mu}{T} \right)^4 + \frac{1}{6} \left(\frac{\mu}{T} \right)^2 + \frac{7\pi^2}{180} \right]. \tag{B.15}$$

Bibliography

[1] K. Yagi, T. Hatsuda, Y. Miake, *Quark-Gluon Plasma: From Big Bang to Little Bang*, (Cambridge University Press, Cambridge, England, 2005).

[2] P. de Forcrand, S. Kim and O. Philipsen, *A QCD chiral critical point at small chemical potential: is it there or not?*, PoS **LAT2007**, 178 (2007).

[3] http://www.star.bnl.gov/public/imagelib/collisions2001/ev2_front.jpg.

[4] H. Meyer-Ortmanns, *Phase transitions in quantum chromodynamics*, Rev. Mod. Phys. **68**, 473 (1996).

[5] http://www.gsi.de/fair/overview/research/antiprotons.html.

[6] http://www.gsi.de/fair/overview/research/nuclear-matter.html

[7] M. Gell-Mann and F. E. Low, *Quantum electrodynamics at small distances* Phys. Rev. **95**, 1300 (1954).

[8] D. J. Gross and F. Wilczek, *Ultraviolet behavior of non-Abelian gauge theories*, Phys. Rev. Lett. **30**, 1343 (1973).

[9] H. D. Politzer, *Reliable perturbative results for strong interactions?*, Phys. Rev. Lett. **30**, 1346 (1973).

[10] S. Bethke, *alpha(s) at Zinnowitz 2004*, Nucl. Phys. Proc. Suppl. **135**, 345 (2004).

[11] M. Gell-Mann and M. Levy, *The axial vector current in beta decay*, Nuovo Cimento **16**, 705 (1960).

[12] A. M. Polyakov, *Thermal Properties Of Gauge Fields And Quark Liberation*, Phys. Lett. B **72**, 477 (1978).

[13] G. 't Hooft, *On The Phase Transition Towards Permanent Quark Confinement*, Nucl. Phys. B **138**, 1 (1978).

[14] R. D. Pisarski, *Notes on the deconfining phase transition*, arXiv:hep-ph/0203271.

[15] M. E. Fisher, *The renormalization group in the theory of critical behavior*, Rev. Mod. Phys. **46**, 597 (1974).

[16] M. E. Fisher, *Renormalization group theory: Its basis and formulation in statistical physics*, Rev. Mod. Phys. **70**, 653 (1998).

[17] S. K. Ma, *Introduction to the renormalization group*, Rev. Mod. Phys. **45**, 589 (1973).

[18] M. Cheng et al., *QCD equation of state with almost physical quark masses*, Phys. Rev. D **77**, 014511 (2008).

[19] Y. Aoki, Z. Fodor, S. D. Katz and K. K. Szabo, *The QCD transition temperature: Results with physical masses in the continuum limit*, Phys. Lett. B **643**, 46 (2006).

[20] A. Gocksch and M. Ogilvie, *Finite temperature deconfinement and chiral symmetry restoration at strong coupling*, Phys. Rev. D **31**, 877 (1985).

[21] M. Buballa, *NJL model analysis of quark matter at large density*, Phys. Rept. **407**, 205 (2005).

[22] P. N. Meisinger and M. C. Ogilvie, *Chiral symmetry restoration and Z_N symmetry*, Phys. Lett. B **379**, 163 (1996).

[23] P. N. Meisinger, T. R. Miller and M. C. Ogilvie, *Phenomenological equations of state for the quark-gluon plasma*, Phys. Rev. D **65**, 034009 (2002).

[24] K. Fukushima, *Chiral effective model with the Polyakov loop*, Phys. Lett. B **591**, 277 (2004).

[25] F. Sannino, *Polyakov loops versus hadronic states*, Phys. Rev. D **66**, 034013 (2002).

[26] A. Mocsy, F. Sannino and K. Tuominen, *Confinement versus chiral symmetry*, Phys. Rev. Lett. **92**, 182302 (2004).

[27] C. Ratti, M. A. Thaler and W. Weise, *Phases of QCD: Lattice thermodynamics and a field theoretical model*, Phys. Rev. D **73**, 014019 (2006).

[28] S. Digal, E. Laermann and H. Satz, *Deconfinement through chiral symmetry restoration in two-flavour QCD*, Eur. Phys. J. C **18**, 583 (2001).

[29] E. Megias, E. Ruiz Arriola and L. L. Salcedo, *Polyakov loop in chiral quark models at finite temperature*, Phys. Rev. D **74**, 065005 (2006).

[30] E. M. Ilgenfritz and J. Kripfganz, *Dynamical fermions at nonzero chemical potential and temperature: Mean field approach*, Z. Phys. C **29**, 79 (1985).

[31] K. Fukushima, *Effects of chiral restoration on the behaviour of the Polyakov loop at strong coupling*, Phys. Lett. B **553**, 38 (2003).

[32] K. Fukushima, *Relation between the Polyakov loop and the chiral order parameter at strong coupling*, Phys. Rev. D **68**, 045004 (2003).

[33] B. J. Schaefer, J. M. Pawlowski and J. Wambach, *The phase structure of the Polyakov-quark-meson model*, Phys. Rev. D **76**, 074023 (2007).

[34] C. Wetterich, *Average action and the renormalization group equations*, Nucl. Phys. B **352**, 529 (1991).

[35] N. Tetradis and C. Wetterich, *Scale dependence of the average potential around the maximum in Phi**4 theories*, Nucl. Phys. B **383**, 197 (1992).

[36] C. Wetterich, *Exact evolution equation for the effective potential*, Phys. Lett. B **301**, 90 (1993).

[37] T. R. Morris, *The exact renormalization group and approximate solutions*, Int. J. Mod. Phys. A **9**, 2411 (1994).

[38] U. Ellwanger, *Flow equations for N point functions and bound states*, Z. Phys. C **62**, 503 (1994).

[39] J. Berges, N. Tetradis and C. Wetterich, *Non-perturbative renormalization flow in quantum field theory and statistical physics*, Phys. Rept. **363**, 223 (2002).

[40] H. Gies, *Introduction to the functional RG and applications to gauge theories*, arXiv:hep-ph/0611146.

[41] B. Delamotte, *An introduction to the nonperturbative renormalization group*, arXiv:cond-mat/0702365.

[42] C. Sasaki, B. Friman and K. Redlich, *Susceptibilities and the phase structure of a chiral model with Polyakov loops*, Phys. Rev. D **75**, 074013 (2007).

[43] C. Ratti, S. Roessner, M. A. Thaler and W. Weise, *Thermodynamics of the PNJL model*, Eur. Phys. J. C **49**, 213 (2007).

[44] S. K. Ghosh, T. K. Mukherjee, M. G. Mustafa and R. Ray, *Susceptibilities and speed of sound from PNJL model*, Phys. Rev. D **73**, 114007 (2006).

[45] S. Ejiri, F. Karsch and K. Redlich, *Hadronic fluctuations at the QCD phase transition*, Phys. Lett. B **633**, 275 (2006).

[46] J. Braun, K. Schwenzer and H. J. Pirner, *Linking the quark meson model with QCD at high temperature*, Phys. Rev. D **70**, 085016 (2004).

[47] D. F. Litim, *Optimized renormalization group flows*, Phys. Rev. D **64**, 105007 (2001).

[48] B. Stokić, B. Friman and K. Redlich, *The functional renormalization group method and $O(4)$ scaling*, (to be submitted to *Phys. Rev. D*).

[49] B. Stokić, B. Friman and K. Redlich, *Quantum fluctuations and the thermodynamics of the Polyakov loop extended quark-meson model*, (to be submitted to *Phys. Rev. D*).

[50] G. Boyd, J. Engels, F. Karsch, E. Laermann, C. Legeland, M. Lutgemeier and B. Petersson, *Thermodynamics of SU(3) Lattice Gauge Theory*, Nucl. Phys. B **469**, 419 (1996).

[51] F. Karsch, E. Laermann and A. Peikert, *The pressure in 2, 2+1 and 3 flavour QCD*, Phys. Lett. B **478**, 447 (2000).

[52] R. D. Pisarski and F. Wilczek, *Remarks on the chiral phase transition in chromodynamics*, Phys. Rev. D **29**, 338 (1984).

[53] K. Rajagopal and F. Wilczek, *Static and dynamic critical phenomena at a second order QCD phase transition*, Nucl. Phys. B **399**, 395 (1993).

[54] F. Parisen Toldin, A. Pelissetto and E. Vicari, *The 3-D $O(4)$ universality class and the phase transition in two-flavor QCD*, JHEP **0307**, 029 (2003).

[55] J. Engels, S. Holtmann, T. Mendes and T. Schulze, *Finite size scaling functions for 3-d $O(4)$ and $O(2)$ spin models and QCD*, Phys. Lett. B **514**, 299 (2001).

[56] J. Engels and T. Mendes, *Goldstone mode effects and scaling function for the three-dimensional $O(4)$ model*, Nucl. Phys. B **572**, 289 (2000).

[57] J. Engels, L. Fromme and M. Seniuch, *Correlation lengths and scaling functions in the three-dimensional $O(4)$ model*, Nucl. Phys. B **675**, 533 (2003).

[58] S. Roessner, C. Ratti and W. Weise, *Polyakov loop, diquarks and the two-flavour phase diagram*, Phys. Rev. D **75**, 034007 (2007).

[59] B. J. Schaefer and J. Wambach, *Susceptibilities near the QCD (tri)critical point*, Phys. Rev. D **75**, 085015 (2007).

[60] D. U. Jungnickel and C. Wetterich, *Effective action for the chiral quark-meson model*, Phys. Rev. D **53**, 5142 (1996).

[61] J. Berges, D. U. Jungnickel and C. Wetterich, *Two flavor chiral phase transition from nonperturbative flow equations*, Phys. Rev. D **59**, 034010 (1999).

[62] J. Berges, D. U. Jungnickel and C. Wetterich, *The chiral phase transition at high baryon density from nonperturbative flow equations*, Eur. Phys. J. C **13**, 323 (2000).

[63] B. J. Schaefer and H. J. Pirner, *The equation of state of quarks and mesons in a renormalization group flow picture*, Nucl. Phys. A **660**, 439 (1999).

[64] J. Meyer, G. Papp, H. J. Pirner and T. Kunihiro, *Renormalization group flow equation at finite density*, Phys. Rev. C **61**, 035202 (2000).

[65] N. Tetradis, *The quark-meson model and the phase diagram of two-flavour QCD*, Nucl. Phys. A **726**, 93 (2003).

[66] B. J. Schaefer and J. Wambach, *The phase diagram of the quark meson model*, Nucl. Phys. A **757**, 479 (2005).

[67] J. Braun and B. Klein, *Scaling functions for the $O(4)$-model in $d = 3$ dimensions*, Phys. Rev. D **77**, 096008 (2008).

[68] J. P. Blaizot, A. Ipp, R. Mendez-Galain and N. Wschebor, *Perturbation theory and non-perturbative renormalization flow in scalar field theory at finite temperature*, Nucl. Phys. A **784**, 376 (2007).

[69] E. K. Riedel and F. J. Wegner, *Effective critical and tricritical exponents*, Phys. Rev. B **9**, 294 (1974).

[70] D. O'Connor and C. R. Stephens, *Renormalization group theory of crossovers*, Phys. Rept. **363**, 425 (2002).

[71] G. Boyd, J. Fingberg, F. Karsch, L. Karkkainen and B. Petersson, *Critical exponents of the chiral transition in strong coupling QCD*, Nucl. Phys. B **376**, 199 (1992).

[72] F. Karsch and E. Laermann, *Susceptibilities, the specific heat and a cumulant in two flavor QCD*, Phys. Rev. D **50**, 6954 (1994).

[73] A. Kocic, J. B. Kogut and M. P. Lombardo, *Universal properties of chiral symmetry breaking*, Nucl. Phys. B **398**, 376 (1993).

[74] E. Berezin, D. J. Wallace and K. G. Wilson, *Feynman-graph expansion for the equation of state near the critical point*, Phys. Rev. B **7**, 232 (1973).

[75] A. Pelissetto and E. Vicari, *Critical phenomena and renormalization group theory*, Phys. Rept. **368**, 549 (2002).

[76] K. Kanaya and S. Kaya, *Critical exponents of a three dimensional $O(4)$ spin model*, Phys. Rev. D **51**, 2404 (1995).

[77] M. E. Fisher, V. Privman, *First-order transitions breaking $O(n)$ symmetry: Finite-size scaling*, Phys. Rev. B **32**, 447 (1985).

[78] D. J. Wallace and R. K. P. Zia, *Singularities induced by Goldstone modes*, Phys. Rev. B **12**, 5340 (1975).

[79] R. B. Griffiths, *Thermodynamic functions for fluids and ferromagnets near the critical point*, Phys. Rev. **158**, 176 (1967).

[80] C. R. Allton, S. Ejiri, S. J. Hands, O. Kaczmarek, F. Karsch, E. Laermann and C. Schmidt, *The equation of state for two flavor QCD at non-zero chemical potential*, Phys. Rev. D **68**, 014507 (2003).

[81] F. Karsch, S. Ejiri and K. Redlich, *Hadronic fluctuations in the QGP*, Nucl. Phys. A **774**, 619 (2006).

[82] S. Ejiri *et al.*, *The QCD equation of state for two flavours at non-zero chemical potential*, Nucl. Phys. A **774**, 837 (2006).

[83] Z. Fodor and S. D. Katz, *Lattice determination of the critical point of QCD at finite T and μ*, JHEP **0203**, 014 (2002).

[84] Z. Fodor and S. D. Katz, *Critical point of QCD at finite T and μ, lattice results for physical quark masses*, JHEP **0404**, 050 (2004).

[85] M. D'Elia and M. P. Lombardo, *Finite density QCD via imaginary chemical potential*, Phys. Rev. D **67**, 014505 (2003).

[86] P. de Forcrand and O. Philipsen, *The QCD phase diagram for three degenerate flavors and small baryon density*, Nucl. Phys. B **673**, 170 (2003).

[87] R. V. Gavai and S. Gupta, *Fluctuations, strangeness and quasi-quarks in heavy-ion collisions from lattice QCD*, Phys. Rev. D **73**, 014004 (2006).

[88] R. V. Gavai and S. Gupta, *Simple patterns for non-linear susceptibilities near $T(c)$*, Phys. Rev. D **72**, 054006 (2005).

[89] R. V. Gavai and S. Gupta, *Quark number susceptibilities and the Wroblewski parameter*, Eur. Phys. J. C **43**, 31 (2005).

[90] F. Karsch, *Recent lattice results on finite temperature and density QCD, part I*, PoS **CPOD07**, 026 (2007).

[91] C. Schmidt [for RBC-Bielefeld Collaboration], *Baryon number, strangeness and electric charge fluctuations at zero and non-zero chemical potential*, J. Phys. G **35**, 104093 (2008).

[92] C. Sasaki, B. Friman and K. Redlich, *Quark number fluctuations in a chiral model at finite baryon chemical potential*, Phys. Rev. D **75**, 054026 (2007).

[93] C. Sasaki, B. Friman and K. Redlich, *Chiral phase transition in the presence of spinodal decomposition*, Phys. Rev. D **77**, 034024 (2008).

[94] C. Sasaki, B. Friman and K. Redlich, *Effective chiral model with Polyakov loops and its application to hot/dense medium*, Prog. Theor. Phys. Suppl. **168**, 291 (2007).

[95] K. Redlich, B. Friman and C. Sasaki, *QCD phase diagram and charge fluctuations*, J. Phys. G **34**, S437 (2007).

[96] See e.g. Proceedings of "Quark Matter 2008".

[97] M. Le Bellac, *Thermal Field Theory*, (Cambridge University Press, Cambridge, England, 1996).

[98] J. I. Kapusta, *Finite Temperature Field Theory*, (Cambridge University Press, Cambridge, England, 1989).

[99] F. Karsch, K. Redlich and A. Tawfik, *Thermodynamics at non-zero baryon number density: A comparison of lattice and hadron resonance gas model calculations*, Phys. Lett. B **571**, 67 (2003).

[100] F. Karsch, K. Redlich and A. Tawfik, *Hadron resonance mass spectrum and lattice QCD thermodynamics*, Eur. Phys. J. C **29**, 549 (2003).

[101] K. Redlich, F. Karsch and A. Tawfik, *Heavy ion collisions and lattice QCD at finite baryon density*, J. Phys. G **30**, S1271 (2004).

[102] B. Stokić, B. Friman and K. Redlich, *Kurtosis and compressibility near the chiral phase transition*, arXiv:0809.3129 [hep-ph] (submitted to *Phys. Lett. B*).

[103] C. Nonaka and M. Asakawa, *Hydrodynamical evolution near the QCD critical end point*, Phys. Rev. C **71**, 044904 (2005).

[104] T. Kahara and K. Tuominen, *Degrees of freedom and the phase transitions of two flavor QCD*, Phys. Rev. D **78**, 034015 (2008).

[105] E. Nakano, B. Stokić, B. J. Schaefer, B. Friman and K. Redlich, (work in progress).

Acknowledgements

First of all, I would like to express my gratitude to my supervisor Professor Bengt Friman. He always had an open door and ear. I am very grateful for his patience and willingness to discuss many different topics at any time.

I am also very thankful to Professor Jochen Wambach for accepting to referee my thesis as well as for inviting me to come to Darmstadt.

I am especially indebted to Professor Krzysztof Redlich. I have had the good fortune to have the opportunity and honour to work with him on several projects during my last year of PhD studies. Further, I would also like to acknowledge many interesting and stimulating discussions with Dr. Eiji Nakano.

Thanks to all former and present colleagues from the GSI theory group for a nice working atmosphere. Also, thanks are due to my fellow PhD students from the Helmholtz Research School with whom I spent great times at many lecture weeks and workshops. Especially, I would like to thank Dr. Henner Büsching for the excellent job he did (and still is doing) as the coordinator of the Helmholtz Research School.

My family has always been on my side, in good times and in bad times. I am deeply grateful to my dear parents Vera and Branko Stokić. Their financial support made my education possible and their unlimited love and encouragement helped me out in all that I have chosen to do.

The final words go to my wife Tamara, for she was (and still is) my tower of strength. I cannot put into words all my feelings, nor can I ever make her aware of how much her love and tenderness means to me. Without her endless support and belief in me, I would never have finished this work.

Lebenslauf

Name	Borislav Stokić
Geburtsdatum	20. 05. 1975
Geburtsort	Olten (Schweiz)
Familienstand	verheiratet

09/1990–06/1994	“Uroš-Predić-Gymnasium“, Pančevo (Serbien)
10/1994–06/1996	Studium der Elektrotechnik an der Universität Belgrad (Serbien)
10/1996–10/2002	Studium der theoretischen Physik an der Universität Belgrad (Serbien)
11/2002–11/2003	Diplomarbeit an der Universität Belgrad (Serbien)
11/2003–06/2004	Aufbaustudium am Institut für Physik Belgrad (Serbien)
06/2004–12/2008	Promotion an der TU Darmstadt

Eidesstattliche Erklärung

Hiermit erkläre ich eidesstattlich, dass ich die vorliegende Dissertation selbständig verfasst, keine anderen als die angegebenen Hilfsmittel verwendet und bisher noch keinen Promotionsversuch unternommen habe.

Darmstadt, im Dezember 2008

(Unterschrift)